LASER- AND SHOCK-INDUCED DROPLET DYNAMICS: A MACHINE LEARNING BENCHMARK FOR COMPLEX MULTIPHASE FLOWS

Anonymous authors
Paper under double-blind review

ABSTRACT

Compressible multiphase flow is central to numerous engineering applications, characterized by complex wave dynamics and challenging shock-interface interactions. Despite their importance, they remain significantly missing from existing benchmarks in the Scientific Machine Learning (SciML) community, limiting progress on generalization to impactful real-world scenarios. To address this issue, we introduce two exemplary datasets from this class, Laser-Induced Droplet Explosion (LIDE) and Shock-Induced Droplet Aero-breakup (SIDA), providing researchers with valuable references to establish reliable baselines and push boundaries of SciML. Due to the high computational cost of simulating these processes with full fidelity, we explore data-driven surrogate models designed to efficiently approximate the underlying physics at reduced cost. We benchmark these datasets on diverse architectures trained autoregressively and compared across varying parameter counts. A comprehensive set of ablations is carried out to analyze the performance of the models. We identify key scenarios, such as incorporating temporal sequence information and conditioning, that enable the models to accurately capture the rich and nonlinear physics embedded in the datasets. Code and datasets will be made available upon acceptance.

1 INTRODUCTION

Modern technical applications of fluid dynamics exhibit a plethora of flow scenarios involving compressible and multiphase flows, which are characterized by discontinuities across shockwaves and phase boundaries. Gaining insights into the underlying physics of compressible flows is a cornerstone in many real-world systems. These include a wide range of scientific fields, spanning from astrophysics to engineering applications such as coating, fuel injection, biomedical treatment (Chaussy & Schmiedt, 1984), analysis of cavitation phenomena (Maeda et al., 2015), and nanoparticle synthesis (Riahi et al., 2023). Traditionally, domain experts have analyzed these phenomena through simulations and experiments. The downside of these methods is that they demand highly specialized facilities and substantial computational power.

Recent advancements in deep learning algorithms and data-driven modeling (Cai et al., 2021), (Ho et al., 2020), (Lipman et al., 2022), (Kovachki et al., 2023), (Vaswani et al., 2017)), coupled with the rapid growth of modern high-performance computing infrastructures, have accelerated discoveries in Scientific Machine Learning (SciML), enabling robust and reliable surrogate models. However, training these models requires large, multifaceted datasets that capture and correlate spatiotemporal information.

To the best of our knowledge, while datasets exist for either compressible single-phase flows (Takamoto et al., 2022), (Herde et al., 2024) or incompressible multiphase flows (Shadkhah et al., 2025), (Hassan et al., 2023), there is an absence of labeled datasets that capture the complexity of both simultaneously. We address this scarcity by providing two high-fidelity datasets pertaining to liquid droplet dynamics, called **Laser-Induced Droplet Explosion (LIDE)** and **Shock-Induced Droplet Aero-breakup (SIDA)**. This novel set of datasets involves intricate interactions of shocks with interfaces-Richtmyer-Meshkov, Rayleigh-Taylor, and Kelvin-Helmholtz instabilities. It further captures the evolution of multiscale vortical structures and wave dynamics. Therefore, it requires

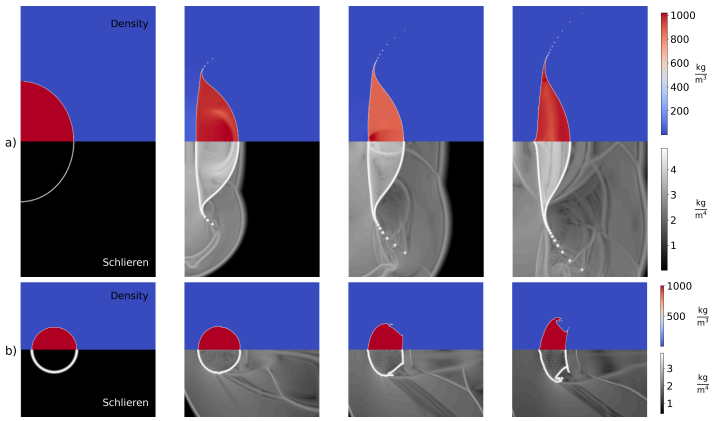

Figure 1: From left to right, Sample trajectory time-snapshots of (a) LIDE and (b) SIDA at: $\{0, \frac{T}{3}, \frac{2T}{3}, T\}$. T denotes the end time of the respective datasets. The frames of the LIDE dataset are rotated clockwise.

profound domain expertise and computational resources, and our contribution lies in introducing this valuable dataset, which paves the way for advancing research in the community. An illustration of two field variables of each dataset is depicted in Figure 1. In LIDE (Paula et al., 2019), an initial high-pressure laser cavity is generated in a micro-droplet. Initiated shock-interface interactions lead to droplet breakup and cavitation events. In SIDA (Kaiser et al., 2020), a shock wave hits a droplet and initiates aero-breakup, where triggered interfacial instabilities generate small liquid fragments through different scenarios.

We propose a many-to-many training strategy (Shadkhah et al., 2025) to benchmark our datasets on a variety of neural architectures, ranging from convolution and spectral models to attention-based approaches. Specifically, we consider UNet, Residual Network (ResNet), Fourier Neural Operator (FNO), Convolutional Neural Operator (CNO), Vision Transformer (ViT), Transolver, alongside Scalable Operator Transformer (ScOT). Furthermore, we identify key parameters and fields with the goal of designing an extensive set of ablations to experiment with the generalization capabilities of the models. Additionally, we compute the metrics over domain-specific quantities of interest on In- and Out-of-Distribution datasets to evaluate baseline models. Although training these models is computationally intensive, once trained, these models are substantially faster when used as a forward simulator. The key contributions of this work are:

- **Datasets for Complex Flow Physics.** A new high-fidelity dataset for complex flow physics involving droplet dynamics and shock-interface interactions is generated and presented.
- **Dataset Validation.** Dataset fidelity is assessed and confirmed by high-resolution simulations and independent experiments.
- **Benchmarking.** A comprehensive set of experiments is performed through side-by-side comparison with different models to gain insights into generalization capabilities.

2 Related Work

Existing benchmarks differ in scope and physical coverage. Among them, PDEBench (Takamoto et al., 2022) and the Well (Ohana et al., 2024) offer a wide variety of datasets, including single-phase compressible Navier–Stokes problems, BubbleML (Hassan et al., 2023) and MPF-Bench (Shadkhah et al., 2025) extend to multiphase problems and contribute an impressive collection of bubble and droplet datasets; however, both are limited to incompressible physics. It is noteworthy that Poseidon (Herde et al., 2024) provides an extensive set of datasets to train foundation models, although it considers only single-phase problems. Additionally, BLASTNet(Chung et al., 2023) includes compressible turbulent flow, AIRFRANS (Bonnet et al., 2022) mainly covers incompressible flow over

airfoils, FlowBench(Tali et al., 2024) incorporates fluid flow around arbitrary shapes, and CFD-Bench(Luo et al., 2023) features incompressible and single-phase CFD problems. However, there is no benchmark combining both compressible and multiphase physics in the same setting. Our work addresses this gap by integrating these two characteristics and further incorporates Symmetry, Dirichlet, and Neumann boundary conditions, thereby broadening the diversity of physical scenarios available for SciML research. A summary of the aforementioned references is presented in Table 1.

Table 1: Summary of related datasets.

Name	Dimensions	Compressible	Multiphase
PDE Bench (Takamoto et al., 2022)	2	✓	✗
Poseidon (Herde et al., 2024)	2	✓	✗
The Well (Ohana et al., 2024)	2, 3	✓	✗
BubbleML (Hassan et al., 2023)(Hassan et al., 2025)	2, 3	✗	✓
MPF-Bench (Shadkhah et al., 2025)	2, 3	✗	✓
Current study	2-Axisymmetric	✓	✓

3 DATASETS

We focus on the class of compressible multiphase problems in this paper. Breakup of liquid droplets is a significant example in this class, which can be induced by laser irradiation (LIDE) or a shock (SIDA). These two transient problems are investigated intensely through experiments and numerical simulations. The Robust Discrete Equation Method for Interface Capturing (RDEMIC) (Paula et al., 2023) is used to generate targets through solving the two-dimensional (2D) axisymmetric compressible Euler equations. Adopting an axisymmetric setup reduces computational cost compared to the full three-dimensional treatment. The set of equations, without dissipative terms in vector notation, reads

$$\partial_t \mathbf{U}_l + \nabla \cdot \mathbf{F}_l = \mathbf{B}_l \cdot \nabla \alpha_l + \mathbf{S}_l, \tag{1}$$

where subscript l denotes the index of the phase, $\mathbf{U}_l$ is the vector of conserved quantities, $\mathbf{F}_l$ is the flux tensor, $\mathbf{B}_l$ is the interaction tensor, and $\mathbf{S}_l$ is a source term to account for cylindrical symmetry,

$$\mathbf{U}_l = \begin{bmatrix} \alpha_l \\ \alpha_l \rho_l \\ \alpha_l \rho_l \mathbf{u}_l \\ \alpha_l E_l \end{bmatrix}, \quad \mathbf{F}_l = \begin{bmatrix} 0 \\ \alpha_l \rho_l \mathbf{u}_l^T \\ \alpha_l \rho_l \mathbf{u}_l \otimes \mathbf{u}_l + \alpha_l p_l \mathbf{I} \\ \alpha_l (E_l + p_l) \mathbf{u}_l^T \end{bmatrix}, \quad \mathbf{B}_l = \begin{bmatrix} -\mathbf{u}_{\text{int}}^T \\ 0 \\ p_{\text{int},l} \mathbf{I} \\ p_{\text{int},l} \mathbf{u}_{\text{int}}^T \end{bmatrix}, \quad \mathbf{S}_l = -\frac{\alpha_l u_{r,l}}{r} \begin{bmatrix} 0 \\ \rho_l \\ \rho_l \mathbf{u}_l \\ E_l + p_l \end{bmatrix}.$$

Above, α_l, ρ_l, $\mathbf{u}_l$, p_l, $u_{r,l}$, and E_l imply the volume fraction, mass density, velocity vector, pressure, velocity component in the radial direction, and total energy of phase l, respectively. Interface velocity vector and pressure are indicated by $\mathbf{u}_{\text{int}}$ and $p_{\text{int},l}$, respectively; without considering the surface tension, $p_{\text{int},l}$ is the same for all phases; r denotes the distance from the symmetry axis and $\mathbf{I}$ is the identity tensor. This method is implemented and validated extensively through the Finite Volume solver, ALPACA (Hoppe et al., 2022). In cylindrical coordinate configuration, the domain revolves around the z-axis (south, as shown in Figure 2), resulting in an axisymmetric problem. In the following sections, a brief overview of each dataset is given. For more details, refer to Appendix A.

3.1 LASER-INDUCED DROPLET EXPLOSION (LIDE)

Experimental investigations of LIDE provide a valuable insight into pure liquid states and pressure-sensitive molecular dynamics in solutions (Stan et al., 2016a). When a laser pulse hits the transparent liquid droplet, energy is deposited within nanoseconds, forming a high-pressure filament along the laser trajectory. This induces shock and expansion waves, which are reflected and subsequently generate negative pressure waves inside the droplet. Consequently, the droplet undergoes deformation

and eventually ruptures if the tension is strong enough. Notably, the negative pressure at rupture is related to the tensile strength that the liquid can sustain during decompression (Stan et al., 2016b).

This problem is also numerically addressed in literature (Paula et al., 2019). Taking advantage of the symmetries, a droplet with radius R_0 is located in the bottom left corner of a square domain with length $3R_0$, as shown in Figure 2a. The filament, heated by the laser beam along the centerline, is also illustrated. The boundary conditions (BC) are Symmetry (west) and Zero-gradient (east and north). The latter refers to a special case of Neumann BC, where the normal derivative of the field variable at the boundary is set to zero. To explore the dynamics of the explosion, we vary the values for filament pressure, ambient pressure, laser half-width, and the droplet radii along perpendicular axes, which distinguishes spherical from ellipsoidal geometries. The aforementioned parameters are subsequently used as conditioning parameters during training. More details on the initial condition values are described in Appendix A.1.

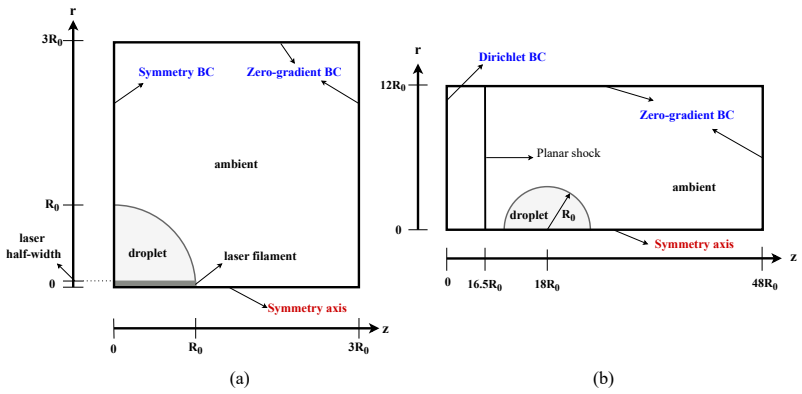

Figure 2: Initial setup for (a)LIDE and (b)SIDA.

3.2 Shock-Induced Droplet Aero-breakup (SIDA)

The droplet aero-breakup, which is caused by the sudden exposure of liquid droplets to external flow, is relevant in practical applications of fuel injection and shock-tube flow (Liang et al., 2020). The resulting shock–droplet interaction involves the evolution of reflected, transmitted, and diffracted waves, along with droplet displacement, deformation, and the development of surface instabilities. This high-speed phenomenon requires high spatiotemporal resolution to be accurately captured. Surface tension has a strong impact on the droplet breakup mode, which is characterized by the Weber number (Hinze, 1955). This non-dimensional parameter accounts for the relative dominance of aerodynamic force over surface tension. Furthermore, the external flow regime, from subsonic to supersonic, is governed by the Mach number (Kaiser et al., 2020).

Initially, we simulate the SIDA dataset in a domain of size $[48R_0, 12R_0]$, which is shown in Figure 2b. This large domain is essential to avoid undesirable boundary effects regarding wave dynamics. However, a fixed subdomain with size $[6R_0, 3R_0]$ around the droplet is saved and later used in training. This subdomain is chosen such that in the initial timestep, the shock wave is located at the west end.

Boundary conditions include Dirichlet (west) and Zero-gradient (east and north). This dataset is generated with various combinations of Mach and Weber numbers, which are later utilized as conditioning parameters in model training (Meng & Colonius, 2018), (Winter et al., 2019). More details on the initial condition values and the validation of the dataset are described in Appendix A.2.

3.3 Datasets Validation

For LIDE, we compare the expansion of the droplet outer diameter in the radial direction to validate our dataset against experiments (Stan et al., 2016b). The consistency with reference is shown in Figure 3 (a). For SIDA, the non-dimensional time (t^*) and displacement of the center of mass

(COM) in the droplet (Δz^*) are defined as $t^* = t\,\frac{u_2}{d}\sqrt{\frac{\rho_2}{\rho_{drop}}}$ and $\Delta z^* = \frac{z}{d}$, where u_2 and ρ_2 are post-shock flow velocity and density, ρ_{drop} and d are droplet density and diameter, and t is the saved timestep, respectively. The displacement of the droplet COM aligns against literature in Figure 3 (b). More details on the dataset validation are described in Appendix A.

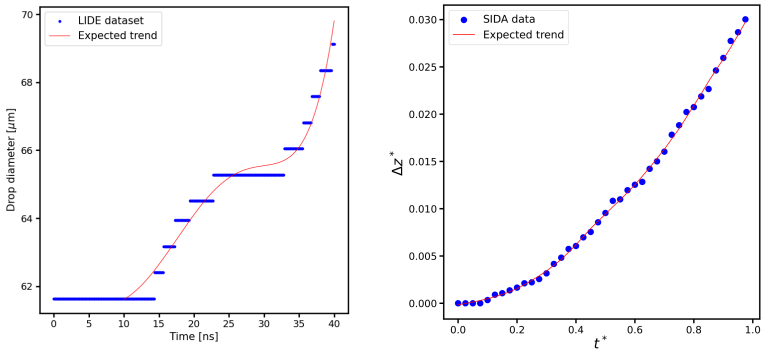

(a) (b)

Figure 3: Dataset validation of (a) LIDE (Stan et al., 2016b) (b) SIDA (Winter et al., 2019).

3.4 METADATA

Each dataset[1] includes 128 trajectories, and the splitting for training/validation/inference is 86/10/32. In total, 6 fields are made available for each dataset, where density, pressure, X-velocity, Y-velocity, and schlieren are common in both datasets. The remaining channel is the total energy for LIDE, and vorticity for SIDA. The spatiotemporal parameters used in the numerical solver are presented in Table 2. The datasets are stored as HDF5 files, with sizes of 75 GB and 12 GB for LIDE and SIDA, respectively, and the shapes for both are **[num_of_trajectories][num_of_timesteps][fields][X-resolution][Y-resolution]**. Each trajectory in the dataset file is assigned a unique group name based on its corresponding conditioning parameters. Sample Out-of-Distribution (OOD) datasets with a similar size to the test part of the In-Distribution (ID) data are considered to assess the generalisation capabilities of trained ML models. For OOD LIDE, higher pressures within the laser width, and for OOD SIDA, higher shock Mach numbers are considered. Details on the parameter ranges considered to generate ID and OOD datasets are provided in Appendix A.

Table 2: Metadata for LIDE and SIDA datasets

Dataset	**Resolution** [X, Y]	**End time [s]**	**CFL**[2]	$\boldsymbol{\Delta t}_{\text{solver}}$ **[s]**[3]	$\boldsymbol{\Delta x}$ **[m]**	**# trajectories**	**# timesteps**
LIDE	[256, 256]	20×10^{-9}	0.35	6.80×10^{-12}	1.25×10^{-7}	128	201
SIDA	[256, 128]	15×10^{-6}	0.50	1.95×10^{-9}	1.17×10^{-5}	128	61

[1]The uploaded supplementary material as a .zip file includes metadata.json files for each LIDE and SIDA dataset. Also, sample video files for ID and OOD datasets are provided for visualization.

[2]CFL refers to Courant-Friedrichs-Lewy criterion.

[3]This is the average solver timestep among all trajectories.

4 EXPERIMENTS

4.1 DESIGN OF EXPERIMENTS

This section outlines the Design of Experiments (DOE). Each experiment is assigned a unique tag for easier identification and comparison. We use **'P'** for Pressure, **'D'** for Density, **'U'** for X-Velocity, **'V'** for Y-Velocity, **'E'** for Energy, **'S'** for Schlieren, and **'Vo'** for Vorticity. For example, an experiment with a tag 'PDUV[ES]_T_(3,2)' implies the input channels are Pressure (P), Density (D), X-Velocity (U), Y-Velocity (V), Energy (E), and Schlieren (S). '[ES]' shows that Energy and Schlieren are counted as conditioning fields and are not predicted in the output. Furthermore, 'T' indicates that the conditioning parameters are included in the experiment. Finally, '(3,2)' corresponds to 3 consecutive inputs and 2 consecutive predicted frames. The complete DOE table is provided in the Appendix B.1.

4.2 BASELINE MODELS

We investigate the performance of the datasets on a variety of neural architecture baselines, The models under consideration are: UNet (Ronneberger et al., 2015), ResNet (He et al., 2016), FNO (Li et al., 2020), CNO (Raonic et al., 2023), ViT (Dosovitskiy et al., 2020), Transolver (Wu et al., 2024), and ScOT (Herde et al., 2024). Each model was trained from scratch on two parameter categories, i.e., 1M and 50M. However, ResNet and Transolver are trained only with 1M model parameters due to their high computational requirements for the 50M size. For more details on model hyperparameters, refer to Appendix B.2.

4.3 INVESTIGATION SCENARIOS

We analyze our results by categorizing the experiments into three distinct scenarios. Each scenario addresses a certain learning problem, and experiments are grouped by altering only the learning parameter while holding all other parameters fixed. The following subsections give a brief overview of these learning problems.

4.3.1 TEMPORAL CONTEXT

Historic information, provided through additional temporal inputs (frames), has proved its efficacy (Hassan et al., 2023), (Shadkhah et al., 2025). In some experiments, to facilitate the understanding of the patterns, we incorporate multiple frames into the model. This provision is effective in learning transient trajectories. For both datasets, we experiment with either 1 input or including a sequence of 3 historic inputs. We also define a stride parameter during dataloading, which skips a fixed number of timesteps. In the LIDE and SIDA datasets, strides of 10 and 5 timesteps are employed, respectively.

4.3.2 CONDITIONING PARAMETERS

In many fluid dynamic problems, the physics are fundamentally characterized by non-dimensional and domain parameters, which influence the system's evolution. These provide crucial information as they dictate the governing dynamics, leading to distinct flow regimes. Conditioning the model with such parameters improves generalization (Kohl et al., 2023), (Peebles & Xie, 2023). The conditioning parameters for the LIDE and SIDA datasets are mentioned in section 3. These are injected into the models through the normalization layers (Herde et al., 2024). More details on the implementation are provided in Appendix B.3.

4.3.3 CONDITIONING FIELDS

In this experimental scenario, additional channels are appended to the inputs before passing them to the model. These extra channels are called conditioning fields, which are derived quantities from existing inputs. For the LIDE dataset, we incorporate energy and schlieren as the conditioning fields, whereas for the SIDA dataset, vorticity and schlieren are used. We aim to test the hypothesis that this type of conditioning guides the model towards generalization.

4.4 TRAINING AUTOREGRESSIVE MODELS

In this work, we use a many-to-many training style to train each of our baselines, $\mathcal{M}_\theta$. The dataset is a discrete spatiotemporal system, containing c channels. For a particular trajectory, the mapping is given by $\mathbf{X}_t : \Omega \times [0, T] \to \mathbb{R}^c$, where $\Omega \subset \mathbb{R}^2$ and T represents the last timestep of the trajectory.

During training, we split each of the training trajectories into M windows. The length of each window is determined by the number of input and output sequences, denoted by l_1 and l_2, respectively, and s denotes the stride, which are all hyperparameters of the temporal context study as mentioned in section 4.3.1.

The input sequence of the m^{th} window is given by $\mathbf{X}_m = [\mathbf{X}_m, \dots \mathbf{X}_{m+(l_1 \times s)]} \in \mathbb{R}^{l_1 \times c}$ and the corresponding target is $\mathbf{Y}_m = [\mathbf{X}_{m+((l_1+1)\times s)]} \dots \mathbf{X}_{m+((l_1+l_2)\times s)}] \in \mathbb{R}^{l_2 \times c}$. The training loss reads:

$$\text{MSE} := \frac{1}{M} \sum_{m=1}^{M} \left\| \mathcal{M}_\theta \left(\mathbf{X}_m \right) - \mathbf{Y}_m \right\|^2, \tag{2}$$

After each training epoch, the validation loss is computed by rolling out the model autoregressively for 5 steps and then computing the Root Mean Square Error (RMSE) over the output channels.

4.5 INFERENCE METRICS

During inference, we start from the initial condition of each trajectory and rollout the model in an autoregressive fashion to reach the final frame. The predictions across trajectories are accumulated into a tensor ($\hat{Y}$), and normalized with the target (Y). The normalized Root Mean Square Error (nRMSE) metric is obtained as shown in Equation 3. **This metric is referred to as error-type 1.**

$$\text{nRMSE} = \sqrt{\frac{\sum_{\text{all dims}} (Y - \hat{Y})^2}{\sum_{\text{all dims}} Y^2 + \epsilon}} \tag{3}$$

We define an **error-type 2** starting from the initial frame and performing rollout until the end of the sequence. The model prediction and target tensors are of shape (N, R, T, C, spatial-dims), where N is the number of test trajectories, R is the number of rollout steps, T is the number of output timesteps per rollout step, C is the number of output channels, and spatial-dims is the resolution of the dataset. The error aggregation is performed in four stages:

1. In each trajectory, we first compute nRMSE between the prediction and the target tensor over the T, C, and spatial-dims, resulting in an overall tensor with shape (N, R).
2. We compute the cumulative summation along the rollout dimension, retaining the shape (N, R).
3. We compute mean and standard deviation across trajectories (N), which results in a tensor of shape (R).
4. Finally, we reduce across the rollout dimension to obtain the overall mean and standard deviation. **We denote this metric as error-type 2**.

In addition to the metrics over the output channels, the aforementioned error types are computed for the domain-specific quantities of interest (QoI) to better understand the underlying physics of the problem, namely, evolution of Kinetic Energy (KE) and Vorticity Production (VP). These QoIs are defined in Appendix B.5. Dataset-specific QoIs over the rollout for LIDE and SIDA are the change of droplet outer radius (OR) and the displacement of droplet center of mass (COM), respectively, over time.

5 RESULTS

5.1 EFFECT OF SEQUENCE INFORMATION

Within the many-to-many autoregressive training framework, we evaluate three configurations of sequence information: (1,1), (3,1), and (3,2), corresponding to one input–one prediction, three in-

puts–one prediction, and three inputs–two predictions, respectively. For both the LIDE and the SIDA datasets, we observe a consistent performance improvement across all models trained with three historical timesteps, with the single-prediction models having a slight metric advantage over the two-consecutive-prediction models. A further gain in accuracy is obtained upon increasing the parameter count, with UNet performing the best. These results for the SIDA are tabulated in Table 32. The results for the LIDE are shown in Table 19 and 20 in the Appendix C. As expected, the model's performance degrades on the OOD datasets; however, including temporal context improves its performance compared to single-frame inputs. The complete set of tables for both datasets and for all QoIs is presented in Appendix C. Moreover, Appendix D presents the cumulative nRMSE trends for both in-distribution and out-of-distribution datasets. Over longer rollouts, UNet consistently outperforms the other models for most QoIs, establishing itself as a robust baseline.

Table 3: Effect of sequence information for SIDA In-Distribution (ID) and Out-of-Distribution (OOD) datasets. Error-type 2 over output channels from section 4.5 is presented.

MODEL	TAG	1M		50M	
		ID	OOD	ID	OOD
UNet	PDUV_F_(1,1)	3.5661±2.4696	5.9914±3.2792	3.4983±2.5270	5.9438±3.2522
	PDUV_F_(3,1)	**0.3383±0.2089**	2.2998±1.7754	**0.1356±0.0976**	1.9424±1.5948
	PDUV_F_(3,2)	0.4406±0.2437	**2.1979±1.6703**	0.1785±0.1080	**1.8812±1.4977**
FNO	PDUV_F_(1,1)	3.5224±2.5528	6.0820±3.2896	3.4720±2.5577	5.9768±3.2572
	PDUV_F_(3,1)	**0.5333±0.2829**	**2.1215±1.5319**	**0.2498±0.1387**	**2.0963±1.5242**
	PDUV_F_(3,2)	0.7123±0.3624	2.1449±1.5747	0.3389±0.1827	2.0990±1.5458
ViT	PDUV_F_(1,1)	4.4758±2.8750	5.8219±3.1222	3.5527±2.7160	5.7645±3.1503
	PDUV_F_(3,1)	1.5891±0.9548	3.4253±2.4145	**0.4430±0.2336**	**1.8428±1.3876**
	PDUV_F_(3,2)	**1.3832±0.7495**	**2.4443±1.6647**	0.5441±0.2699	1.8678±1.3767
ScOT	PDUV_F_(1,1)	3.5764±2.5158	5.8985±3.2421	3.5173±2.6462	5.8306±3.1826
	PDUV_F_(3,1)	**0.6884±0.4222**	**1.9005±1.3770**	**0.2059±0.1199**	1.6318±1.3494
	PDUV_F_(3,2)	0.7995±0.4265	1.9084±1.3867	0.2639±0.1459	**1.5164±1.2414**
CNO	PDUV_F_(1,1)	3.9955±2.6786	5.8508±3.1777	3.5025±2.5455	5.9444±3.2344
	PDUV_F_(3,1)	**0.6943±0.4235**	2.1707±1.8099	**0.1621±0.1032**	1.8159±1.4794
	PDUV_F_(3,2)	0.8584±0.4459	**1.8360±1.3758**	0.2210±0.1248	**1.7634±1.3875**
ResNet	PDUV_F_(1,1)	3.7260±2.4574	6.0844±3.3406		
	PDUV_F_(3,1)	**0.5570±0.3461**	2.3042±1.7139		
	PDUV_F_(3,2)	0.6356±0.3669	**2.3012±1.6856**		
Transolver	PDUV_F_(1,1)	5.7995±3.4502	6.9499±3.7154		
	PDUV_F_(3,1)	**4.7065±2.6888**	**4.8852±2.7289**		
	PDUV_F_(3,2)	5.2026±2.7770	5.1580±2.7698		

5.2 Effect of conditioning parameters

We conduct several studies to assess if including conditioning parameters as described in section 4.3.2 has a pronounced influence on the inference metrics. For the LIDE dataset, we observe that embedding these parameters into the baselines generally has a positive impact, whereas metrics deteriorate for the SIDA dataset, as shown in Table 4 and Table 36, respectively. It is worth noting that the characteristics of the conditioning parameters in the SIDA dataset are different from those of the LIDE dataset. In the former, the parameters are geometry-based, and for the latter, these are flow properties. Furthermore, we observe that conditioning parameters substantially enhance the prediction in the single-input single-output experiments, motivating their adoption in scenarios where generating temporal context windows poses challenges. The complete set of tables for both datasets and for all QoIs is presented in Appendix C.

Table 4: Effect of conditioning parameters for LIDE In-Distribution (ID) and Out-of-Distribution (OOD) datasets. Error-type 2 over output channels from section 4.5 is presented.

MODEL	TAG	1M		50M	
		ID	OOD	ID	OOD
UNet	PDUV_F_(1,1)	2.9972±2.4755	**9.0795±5.9229**	2.1209±1.8598	**8.0827±5.3407**
	PDUV_T_(1,1)	**2.9636±2.5183**	10.1979±7.5259	**1.2553±1.1437**	8.1129±5.4866
	PDUV_F_(3,1)	**1.5341±1.2526**	**6.0177±5.0873**	**1.0029±0.8511**	**5.0866±4.2680**
	PDUV_T_(3,1)	2.6413±2.3683	9.6531±7.8398	1.0383±0.9354	6.6239±5.2895
FNO	PDUV_F_(1,1)	3.6399±3.1425	**7.8868±5.3663**	2.5836±2.2495	**7.2695±5.3881**
	PDUV_T_(1,1)	**2.7562±2.4957**	9.1299±6.1320	**1.6632±1.4450**	8.7610±6.3761
	PDUV_F_(3,1)	2.4656±2.4281	**5.9441±4.8157**	1.6334±1.4492	**6.4107±5.4997**
	PDUV_T_(3,1)	**2.1101±2.2230**	6.4283±5.1802	**1.5349±1.2236**	7.3136±5.1163
ViT	PDUV_F_(1,1)	6.7641±4.8388	**8.5556±5.3823**	2.1804±1.7873	6.3454±4.3554
	PDUV_T_(1,1)	**4.6571±3.6689**	11.1820±12.6204	**1.0744±0.7655**	**6.0053±5.3625**
	PDUV_F_(3,1)	4.1118±3.0304	**6.4825±5.1926**	1.4109±1.1031	**3.9230±3.2763**
	PDUV_T_(3,1)	**3.4518±2.4023**	10.4698±11.1001	**1.0612±0.7537**	4.4118±4.0008
ScOT	PDUV_F_(1,1)	2.8022±2.2122	**7.4147±4.9714**	2.2992±1.8961	**7.0310±4.6946**
	PDUV_T_(1,1)	**2.1729±1.6478**	15.8824±16.0901	**1.0326±0.8473**	10.2492±10.8710
	PDUV_F_(3,1)	**1.7180±1.3379**	**6.4316±7.3418**	1.1854±0.9577	**5.1242±5.4815**
	PDUV_T_(3,1)	1.7619±1.3709	8.0149±6.9873	**0.8772±0.6840**	7.8435±7.3701
CNO	PDUV_F_(1,1)	**2.1786±1.7884**	**7.7764±6.8129**	2.1271±1.7921	**6.7606±4.9076**
	PDUV_T_(1,1)	2.6620±2.2500	10.6073±7.5735	**2.0716±1.8737**	9.5014±6.0985
	PDUV_F_(3,1)	**1.2258±0.9966**	**6.4241±6.3085**	**1.1850±0.9985**	**4.7852±3.9415**
	PDUV_T_(3,1)	2.6061±2.4252	9.0774±6.4503	1.8087±1.6317	8.0127±5.4545
ResNet	PDUV_F_(1,1)	7.1277±5.7086	9.8022±6.0704		
	PDUV_T_(1,1)	**4.8602±3.8324**	**9.1651±5.5656**		
	PDUV_F_(3,1)	5.0517±4.3040	**6.4456±4.5672**		
	PDUV_T_(3,1)	**3.3461±2.5509**	8.8525±6.2045		
Transolver	PDUV_F_(1,1)	**4.9459±3.6294**	**8.3506±5.2692**		
	PDUV_T_(1,1)	8.3954±5.2724	8.7039±5.2462		
	PDUV_F_(3,1)	**3.4782±2.3452**	**5.5601±4.1509**		
	PDUV_T_(3,1)	4.9456±3.2063	8.5088±5.8755		

5.3 Effect of conditioning fields

Considering the selected conditioning fields for each dataset, as described in Section 4.3.3, we conclude that, across all models and parameter counts, incorporating these fields, in general, degrades the predictions, resulting in increased errors during inference. The complete set of tables for both datasets and for all QoIs is presented in Appendix C.

5.4 Baseline model performance study

We investigate error-type 1 (section 4.5) in baseline models on an identical experiment for each dataset. As a sample experiment, we present Table 5, which shows that a higher parameter count improves the prediction accuracy across all models. UNet consistently achieves superior performance compared to all the other baselines in both the 1M and 50M categories. Remaining tables for In-Distribution (ID) and Out-of-Distribution (OOD) datasets are available in Appendix E.

5.5 Comparison between error types

We compare the two error types, **defined in section 4.5**, to correlate the metrics with the predicted rollout. It is worth emphasizing that from our ablations, error-type 2 demonstrates better coherence

Table 5: Error-type 1 from section 4.5 for experiment PDUV_F_(3,1) for the LIDE In-Distribution (ID) dataset across all 1M and 50M models.

MODEL	1M				50M			
	output channels	OR	KE	VP	output channels	OR	KE	VP
CNO	0.1641	0.7208	0.1182	0.2360	0.1658	0.7696	0.0995	0.1413
FNO	0.3814	0.7405	1.5689	2.0840	0.2538	0.7069	0.7270	0.9354
ScOT	0.2234	0.4091	0.3476	0.3303	0.1570	0.8316	0.1831	0.1294
UNet	0.2140	0.3373	0.1471	0.1766	0.1383	0.3408	0.0601	0.0677
ViT	0.5237	0.8853	1.5604	1.3256	0.1792	0.8206	0.2179	0.1896
ResNet	0.7244	1.0878	0.2947	1.4805	–	–	–	–
Transolver	0.4091	1.2833	0.7547	0.4055	–	–	–	–

with predicted rollouts in some cases. For example, as shown in Table 6, UNet-50M achieves higher accuracy according to error-type 2 compared to ViT-50M; UNet captures the droplet interface more precisely, indicating better performance as a surrogate relative to ViT. The corresponding plot is available in Figure 54 in Appendix F. In contrast, error-type 1 suggests that ViT predicts better. This discrepancy highlights the importance of selecting an error metric that aligns with the qualitative behavior observed in rollout plots (Luo et al., 2023). Sample rollout prediction plots, during inference, for the LIDE-ID and the SIDA-ID datasets are shown in Appendix F.

Table 6: Error-type 1 and 2 over output channels from section 4.5 for the experiment PDUV_T_(3,1) for the LIDE In-Distribution (ID) dataset across models with 50M parameters.

MODEL	Error type 1	Error type 2
UNet	0.1407	1.0383
FNO	0.1969	1.5349
ViT	0.1293	1.0612
ScOT	0.1111	0.8772
CNO	0.2463	1.8087

6 Conclusion

This study presents two novel datasets in the domain of compressible multiphase fluid dynamics. We benchmarked seven baseline models on these datasets with varying parameter counts. Domain-specific quantities of interest (QoIs) are considered, and our study scenarios explore the influence of historical information, conditioning parameters, and fields on all QoIs. The inference results of the trained baseline models on both the LIDE and SIDA datasets showed superior prediction accuracy upon incorporating additional temporal context. Subsequently, introducing additional channels as conditioning fields to the input degraded the prediction accuracy during inference on both datasets. Furthermore, injecting conditional parameters into the baselines yielded bifurcating results for the datasets. Despite poor performance on the SIDA dataset, models show better accuracy on the LIDE dataset. Finally, we examined the interpretation of two error types and their correlation with the rollout plots, which illustrates the importance of selecting a suitable error metric in choosing an appropriate surrogate. In conclusion, it is essential to highlight that representing the complex physics and patterns through the current datasets by surrogates still poses a challenge. This observation motivates the integration of such datasets in the SciML community to further the development of data-driven surrogates.

Limitations and Future works. Extending the dataset diversity to include multi-droplet and bubble scenarios, analyzing different combinations of conditioning fields and parameters, and advancing toward more effective conditioning algorithms are promising future directions.

7 REPRODUCIBILITY STATEMENT

We introduce two datasets in this paper, which are reproducible based on our description in the main text (section 3) and supplements in the Appendix A. These explanations include the referenced Finite Volume solver, numerical setup, and initial conditions. More details on the solver code and generator scripts for creating datasets are provided in the HuggingFace repository. In addition, for reproducing model evaluations, we will provide the datasets, the benchmarking code, and the trained model weights upon acceptance.

REFERENCES

John David Anderson. Modern compressible flow: with historical perspective. *(No Title)*, 1990.

Jimmy Lei Ba, Jamie Ryan Kiros, and Geoffrey E Hinton. Layer normalization. *arXiv preprint arXiv:1607.06450*, 2016.

Florent Bonnet, Jocelyn Mazari, Paola Cinnella, and Patrick Gallinari. Airfrans: High fidelity computational fluid dynamics dataset for approximating reynolds-averaged navier–stokes solutions. *Advances in Neural Information Processing Systems*, 35:23463–23478, 2022.

Shengze Cai, Zhiping Mao, Zhicheng Wang, Minglang Yin, and George Em Karniadakis. Physics-informed neural networks (pinns) for fluid mechanics: A review. *Acta Mechanica Sinica*, 37(12): 1727–1738, 2021.

Christian Chaussy and Egbert Schmiedt. Extracorporeal shock wave lithotripsy (eswl) for kidney stones. an alternative to surgery? *Urologic radiology*, 6(1):80–87, 1984.

Wai Tong Chung, Bassem Akoush, Pushan Sharma, Alex Tamkin, Ki Sung Jung, Jacqueline Chen, Jack Guo, Davy Brouzet, Mohsen Talei, Bruno Savard, et al. Turbulence in focus: Benchmarking scaling behavior of 3d volumetric super-resolution with blastnet 2.0 data. *Advances in Neural Information Processing Systems*, 36:77430–77484, 2023.

PhysicsNeMo Contributors. Nvidia physicsnemo: An open-source framework for physics-based deep learning in science and engineering. `https://github.com/NVIDIA/physicsnemo`, February 2023. Software release.

Alexey Dosovitskiy, Lucas Beyer, Alexander Kolesnikov, Dirk Weissenborn, Xiaohua Zhai, Thomas Unterthiner, Mostafa Dehghani, Matthias Minderer, Georg Heigold, Sylvain Gelly, et al. An image is worth 16x16 words: Transformers for image recognition at scale. *arXiv preprint arXiv:2010.11929*, 2020.

Sigal Gottlieb and Chi-Wang Shu. Total variation diminishing runge-kutta schemes. *Mathematics of computation*, 67(221):73–85, 1998.

Jayesh K Gupta and Johannes Brandstetter. Towards multi-spatiotemporal-scale generalized pde modeling. *arXiv preprint arXiv:2209.15616*, 2022.

Sheikh Md Shakeel Hassan, Arthur Feeney, Akash Dhruv, Jihoon Kim, Youngjoon Suh, Jaiyoung Ryu, Yoonjin Won, and Aparna Chandramowlishwaran. Bubbleml: A multi-physics dataset and benchmarks for machine learning. *arXiv preprint arXiv:2307.14623*, 2023.

Sheikh Md Shakeel Hassan, Xianwei Zou, Akash Dhruv, and Aparna Chandramowlishwaran. Bubbleformer: Forecasting boiling with transformers. In *The Thirty-ninth Annual Conference on Neural Information Processing Systems Datasets and Benchmarks Track*, 2025.

Kaiming He, Xiangyu Zhang, Shaoqing Ren, and Jian Sun. Deep residual learning for image recognition. In *Proceedings of the IEEE conference on computer vision and pattern recognition*, pp. 770–778, 2016.

Maximilian Herde, Bogdan Raonic, Tobias Rohner, Roger Käppeli, Roberto Molinaro, Emmanuel de Bézenac, and Siddhartha Mishra. Poseidon: Efficient foundation models for pdes. *Advances in Neural Information Processing Systems*, 37:72525–72624, 2024.

Julius O Hinze. Fundamentals of the hydrodynamic mechanism of splitting in dispersion processes. *AIChE journal*, 1(3):289–295, 1955.

Jonathan Ho, Ajay Jain, and Pieter Abbeel. Denoising diffusion probabilistic models. *Advances in neural information processing systems*, 33:6840–6851, 2020.

Nils Hoppe, Josef M Winter, Stefan Adami, and Nikolaus A Adams. Alpaca-a level-set based sharp-interface multiresolution solver for conservation laws. *Computer Physics Communications*, 272: 108246, 2022.

Guang-Shan Jiang and Chi-Wang Shu. Efficient implementation of weighted eno schemes. *Journal of computational physics*, 126(1):202–228, 1996.

JWJ Kaiser, JM Winter, S Adami, and NA Adams. Investigation of interface deformation dynamics during high-weber number cylindrical droplet breakup. *International Journal of Multiphase Flow*, 132:103409, 2020.

Georg Kohl, Li-Wei Chen, and Nils Thuerey. Benchmarking autoregressive conditional diffusion models for turbulent flow simulation. *arXiv preprint arXiv:2309.01745*, 2023.

Nikola Kovachki, Zongyi Li, Burigede Liu, Kamyar Azizzadenesheli, Kaushik Bhattacharya, Andrew Stuart, and Anima Anandkumar. Neural operator: Learning maps between function spaces with applications to pdes. *Journal of Machine Learning Research*, 24(89):1–97, 2023.

Zongyi Li, Nikola Kovachki, Kamyar Azizzadenesheli, Burigede Liu, Kaushik Bhattacharya, Andrew Stuart, and Anima Anandkumar. Fourier neural operator for parametric partial differential equations. *arXiv preprint arXiv:2010.08895*, 2020.

Yu Liang, Yazhong Jiang, Chih-Yung Wen, and Yao Liu. Interaction of a planar shock wave and a water droplet embedded with a vapour cavity. *Journal of Fluid Mechanics*, 885:R6, 2020.

Yaron Lipman, Ricky TQ Chen, Heli Ben-Hamu, Maximilian Nickel, and Matt Le. Flow matching for generative modeling. *arXiv preprint arXiv:2210.02747*, 2022.

Ze Liu, Han Hu, Yutong Lin, Zhuliang Yao, Zhenda Xie, Yixuan Wei, Jia Ning, Yue Cao, Zheng Zhang, Li Dong, et al. Swin transformer v2: Scaling up capacity and resolution. 2022 ieee. In *CVF Conference on Computer Vision and Pattern Recognition (CVPR)*, pp. 11999–12009, 2021.

Zhuang Liu, Hanzi Mao, Chao-Yuan Wu, Christoph Feichtenhofer, Trevor Darrell, and Saining Xie. A convnet for the 2020s. In *Proceedings of the IEEE/CVF conference on computer vision and pattern recognition*, pp. 11976–11986, 2022.

Yining Luo, Yingfa Chen, and Zhen Zhang. Cfdbench: A large-scale benchmark for machine learning methods in fluid dynamics. *arXiv preprint arXiv:2310.05963*, 2023.

Kazuki Maeda, Wayne Kreider, Adam Maxwell, Bryan Cunitz, Tim Colonius, and Michael Bailey. Modeling and experimental analysis of acoustic cavitation bubbles for burst wave lithotripsy. In *Journal of Physics: Conference Series*, volume 656, pp. 012027. IOP Publishing, 2015.

Jomela C Meng and Tim Colonius. Numerical simulation of the aerobreakup of a water droplet. *Journal of Fluid Mechanics*, 835:1108–1135, 2018.

Ruben Ohana, Michael McCabe, Lucas Meyer, Rudy Morel, Fruzsina Agocs, Miguel Beneitez, Marsha Berger, Blakesly Burkhart, Stuart Dalziel, Drummond Fielding, et al. The well: a large-scale collection of diverse physics simulations for machine learning. *Advances in Neural Information Processing Systems*, 37:44989–45037, 2024.

Thomas Paula, Stefan Adami, and Nikolaus A Adams. Analysis of the early stages of liquid-water-drop explosion by numerical simulation. *Physical Review Fluids*, 4(4):044003, 2019.

Thomas Paula, Stefan Adami, and Nikolaus A Adams. A robust high-resolution discrete-equations method for compressible multi-phase flow with accurate interface capturing. *Journal of Computational Physics*, 491:112371, 2023.

William Peebles and Saining Xie. Scalable diffusion models with transformers. In *Proceedings of the IEEE/CVF international conference on computer vision*, pp. 4195–4205, 2023.

Bogdan Raonic, Roberto Molinaro, Tobias Rohner, Siddhartha Mishra, and Emmanuel de Bezenac. Convolutional neural operators. In *ICLR 2023 workshop on physics for machine learning*, 2023.

Farbod Riahi, Alexander Bußmann, Carlos Doñate-Buendia, Stefan Adami, Nicolaus A Adams, Stephan Barcikowski, and Bilal Gökce. Characterizing bubble interaction effects in synchronous-double-pulse laser ablation for enhanced nanoparticle synthesis. *Photonics Research*, 11(12): 2054–2071, 2023.

Olaf Ronneberger, Philipp Fischer, and Thomas Brox. U-net: Convolutional networks for biomedical image segmentation. In *International Conference on Medical image computing and computer-assisted intervention*, pp. 234–241. Springer, 2015.

Mehdi Shadkhah, Ronak Tali, Ali Rabeh, Cheng-Hau Yang, Ethan Herron, Abhisek Upadhyaya, Adarsh Krishnamurthy, Chinmay Hegde, Aditya Balu, and Baskar Ganapathysubramanian. Mpf-bench: A large scale dataset for sciml of multi-phase-flows: Droplet and bubble dynamics. *arXiv preprint arXiv:2502.07080*, 2025.

Shubham Sharma, Awanish Pratap Singh, S Srinivas Rao, Aloke Kumar, and Saptarshi Basu. Shock induced aerobreakup of a droplet. *Journal of Fluid Mechanics*, 929:A27, 2021.

Claudiu A Stan, Despina Milathianaki, Hartawan Laksmono, Raymond G Sierra, Trevor A McQueen, Marc Messerschmidt, Garth J Williams, Jason E Koglin, Thomas J Lane, Matt J Hayes, et al. Liquid explosions induced by x-ray laser pulses. *Nature Physics*, 12(10):966–971, 2016a.

Claudiu A Stan, Philip R Willmott, Howard A Stone, Jason E Koglin, Mengning Liang, Andrew L Aquila, Joseph S Robinson, Karl L Gumerlock, Gabriel Blaj, Raymond G Sierra, et al. Negative pressures and spallation in water drops subjected to nanosecond shock waves. *The journal of physical chemistry letters*, 7(11):2055–2062, 2016b.

Makoto Takamoto, Timothy Praditia, Raphael Leiteritz, Daniel MacKinlay, Francesco Alesiani, Dirk Pflüger, and Mathias Niepert. Pdebench: An extensive benchmark for scientific machine learning. *Advances in Neural Information Processing Systems*, 35:1596–1611, 2022.

Ronak Tali, Ali Rabeh, Cheng-Hau Yang, Mehdi Shadkhah, Samundra Karki, Abhisek Upadhyaya, Suriya Dhakshinamoorthy, Marjan Saadati, Soumik Sarkar, Adarsh Krishnamurthy, et al. Flowbench: A large scale benchmark for flow simulation over complex geometries. *arXiv preprint arXiv:2409.18032*, 2024.

TG Theofanous and GJ Li. On the physics of aerobreakup. *Physics of fluids*, 20(5), 2008.

Ashish Vaswani, Noam Shazeer, Niki Parmar, Jakob Uszkoreit, Llion Jones, Aidan N Gomez, Łukasz Kaiser, and Illia Polosukhin. Attention is all you need. *Advances in neural information processing systems*, 30, 2017.

Josef Winter, Jakob Kaiser, Stefan Adami, and Nikolaus Adams. Numerical investigation of 3d drop-breakup mechanisms using a sharp interface level-set method. In *11th International Symposium on Turbulence and Shear Flow Phenomena, TSFP 2019*, 2019.

Haixu Wu, Huakun Luo, Haowen Wang, Jianmin Wang, and Mingsheng Long. Transolver: A fast transformer solver for pdes on general geometries. *arXiv preprint arXiv:2402.02366*, 2024.

A DATASETS

As mentioned in the main text, we solve the compressible multiphase Euler equations (Equation 1) with the RDEMIC, which captures the interface as a diffuse zone on a Cartesian grid. This method combines the solutions of pairwise Riemann problems to obtain the finite-volume flux. By a modified partitioning of the Riemann solutions and a specific combination of fluxes and non-conservative terms, the method is made practically applicable for high-resolution shock-interface problems (Paula et al., 2023). We use this method in ALPACA (Hoppe et al., 2022), which is a well-suited environment for compressible single-phase simulations and other multi-phase methods, although originally developed as a level-set-based sharp-interface solver. Its standout features include a wide variety of Riemann solvers, high-resolution reconstruction schemes, and a state-of-the-art multiresolution algorithm for high computational efficiency. In both datasets in this study, the cell face fluxes are reconstructed with the fifth-order WENO scheme (Jiang & Shu, 1996). Furthermore, a third-order Runge-Kutta Total Variation Diminishing scheme is applied for time discretization (Gottlieb & Shu, 1998).

To close the governing equation (Equation 1), an Equation of State (EOS) is used, which relates pressure to density and internal energy. We adopt the stiffened-gas EOS to generate both datasets, which reads

$$p(\rho, e) = (\gamma - 1)\rho e - \gamma p_{\text{stiff}} \quad \Longleftrightarrow \quad e(\rho, p) = \frac{p + \gamma p_{\text{stiff}}}{(\gamma - 1)\rho}, \tag{4}$$

with p being the pressure of the fluid, ρ the mass density, e the internal energy, γ the model constant. In addition, p_{stiff} accounts for a pre-compression of the fluid. To degenerate the aforementioned equation to an ideal-gas EOS for air, we adopt $\gamma = 1.4$ and $p_{\text{stiff}} = 0$. The total energy density, $E[\frac{J}{m^3}]$, is obtained by considering internal energy from Equation 4 and kinetic energy, as shown in Equation 5:

$$E = \rho e + 1/2\rho(u_r^2 + u_z^2) \tag{5}$$

Here, u_r and u_z are the velocity components in the r and z directions, respectively. Schlieren $[\frac{kg}{m^4}]$ is computed in the solver by Equation 6:

$$\text{schlieren} = \nabla\rho \tag{6}$$

Additionally, vorticity $[s^{-1}]$ is defined in Equation 7:

$$\text{vorticity} = \nabla \times \mathbf{u} \tag{7}$$

A.1 THE LIDE DATASET

To simulate this problem, careful considerations must be taken into account. The filament along the centerline, which is heated by a laser in a very short time, is pre-initialized with vapor instead of liquid water. However, it is important to note that the density of the vapor in this zone remains equal to that of liquid water, since the laser energy heats the liquid rapidly. A summary of initial condition values is presented in Table 7.

Table 7: Initial conditions for the LIDE dataset

Phase-l	ρ_l [$\mathrm{kg\,m^{-3}}$]	$\{u_{r,l}, u_{z,l}\}$ [$\mathrm{m\,s^{-1}}$]	p_l [Pa]	
1 (Ambient air)	0.74	0.0, 0.0	p_{ambient}	
2 (Liquid droplet)	998.2	0.0, 0.0	p_{ambient}	$z >$ laser half-width
	998.2	0.0, 0.0	p_{filament}	$z <$ laser half-width

Validation. We compare the evolution of the droplet diameter in the radial direction to validate our dataset against experiments (Stan et al., 2016b). According to experimental observations, the droplet starts to expand upon the arrival of the radial shock wave, which is induced by high pressure in the filament. Due to the wave interactions, a decrease in the expansion rate is observed, which is again followed by an increase. This trend is depicted in Figure 4 and is in good agreement with experiments.

In this problem, it is crucial to analyze and understand the wave interactions inside the droplet. After rapid energy deposition along the centerline, the main shock spreads radially, approaching the droplet surface. The corresponding reflection results in a curved negative-pressure wave, which increases the tension. Shortly after, this wave collapses toward the z-axis and impacts the motion of the droplet's surface (Paula et al., 2019). These phenomena are depicted step-by-step from top to bottom in Figure 5.

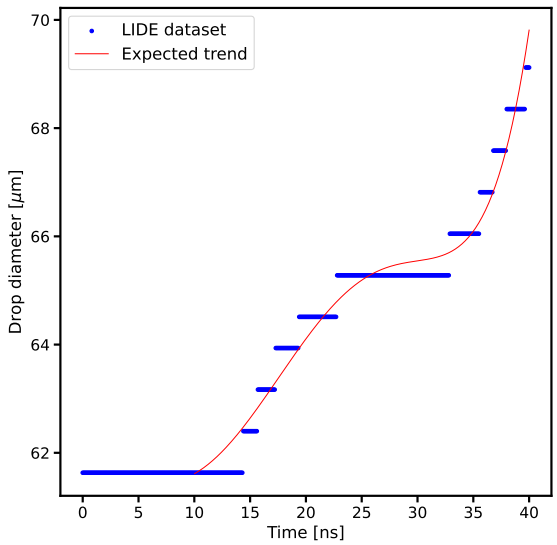

Figure 4: Validation of the LIDE data compared to the expected trend (Stan et al., 2016b).

Parameter Range. Considering that different laser pulse energies result in different pressures in the filament ($p_{filament}$), we cover a range from 10^8 to 10^{10} [Pa] in our dataset. Alongside the high-pressure, the ambient pressure ($p_{ambient}$) varies between 10^5 and 10^6 [Pa]. In addition, the laser half-width changes in the range of 2×10^{-7} to 1.5×10^{-6} [m]. The droplet radius along the r and z axes varies from 1×10^{-5} to 1.6×10^{-5} [m]. For Out-of-Distribution (OOD) trajectories, we increase the high pressure to a higher range: 10^{10} - 8×10^{10} [Pa].

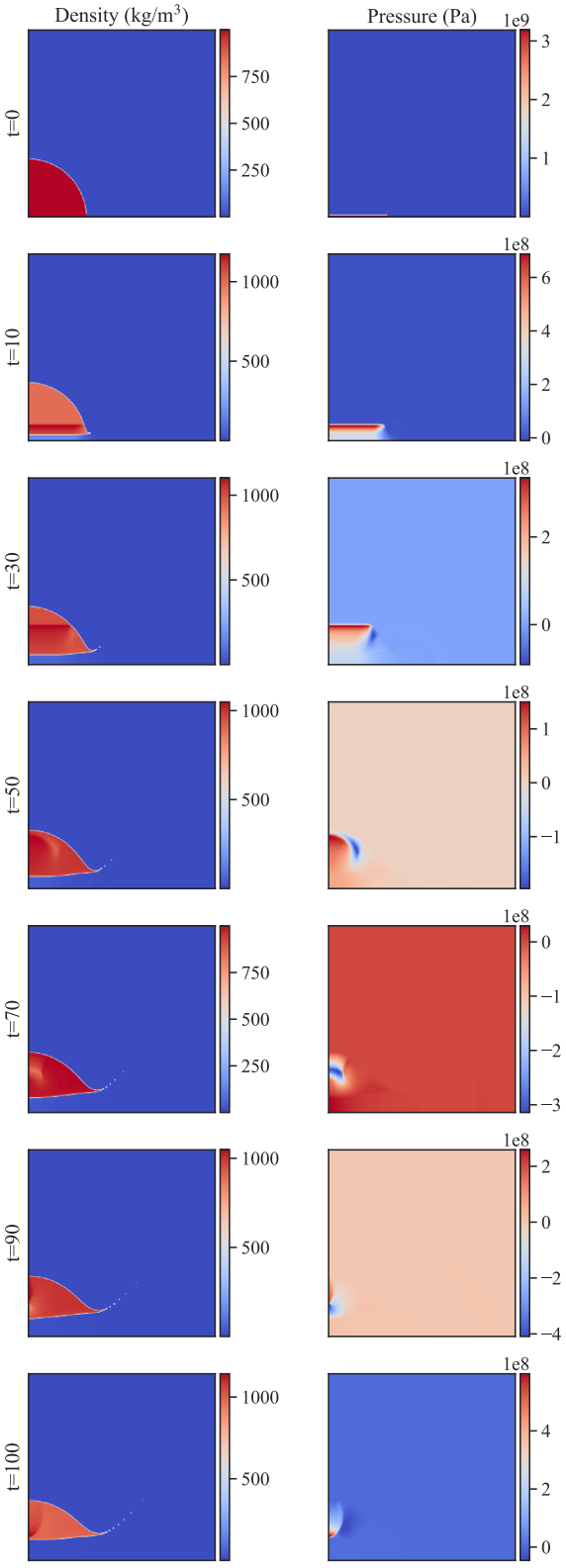

Figure 5: Visualization of droplet's motion and deformation in the LIDE dataset.

A.2 THE SIDA DATASET

To get a better understanding of this problem, both wave dynamics and droplet breakup modes are studied extensively in the literature (Sharma et al., 2021), (Theofanous & Li, 2008). Breakup modes are characterized by the Weber number (Hinze, 1955), which is defined as follows:

$$We = \frac{\rho_2 u_2^2 d}{\sigma} \tag{8}$$

In this definition, ρ_2 and u_2 refer to post-shock density and velocity of the external flow, respectively. Additionally, d is the droplet diameter and σ denotes the surface tension coefficient. For droplet aero-breakup, two major breakup modes are introduced: Rayleigh-Taylor Piercing (RTP) and shear-induced entrainment (SIE). RTP is the main instability mode for small Weber numbers (starting at $We \approx 28$), and SIE is the terminal instability mode for increasing Weber numbers ($We > 10^3$) (Theofanous & Li, 2008). For this study, we cover the Weber number in the range [530, 40000], which corresponds to the transition regions from RTP to SIE and also the SIE region itself.

After the shock impact, the post-shock flow plays a significant role in droplet deformation and breakup. The post-shock flow regime is identified by the Mach number, which is a non-dimensional parameter that relates flow velocity to the speed of sound. We compute the post-shock flow properties using the normal shock relation. These relations are given by (Anderson, 1990):

$$u_s = M_s \cdot c_1 \tag{9}$$

$$u_{1,\text{rel}} = -u_s \tag{10}$$

$$u_1 = u_{1,\text{rel}} + u_s \tag{11}$$

$$T_2 = T_1 \left(1 + \frac{2\gamma\left(M_s^2 - 1\right)}{\gamma + 1}\right)\left(\frac{2 + (\gamma - 1)M_s^2}{(\gamma + 1)M_s^2}\right) \tag{12}$$

$$c_2 = \sqrt{\gamma \cdot R_1 \cdot T_2} \tag{13}$$

$$M_{f2,\text{rel}} = \sqrt{\frac{1 + \frac{\gamma-1}{2}M_s^2}{\gamma M_s^2 - \frac{\gamma-1}{2}}} \tag{14}$$

$$u_{2,\text{rel}} = M_{f2,\text{rel}} \cdot c_2 \tag{15}$$

$$u_2 = u_s - u_{2,\text{rel}} \tag{16}$$

$$\rho_2 = \rho_1 \cdot \frac{(\gamma + 1)M_s^2}{2 + (\gamma - 1)M_s^2} \tag{17}$$

$$p_2 = p_1 \left(1 + \frac{2\gamma\left(M_s^2 - 1\right)}{\gamma + 1}\right) \tag{18}$$

We use M_s for the shock and M_f for the post-shock flow Mach number. The flow states before and after the shock wave are referred to with subscripts 1 and 2, respectively. Furthermore, T is the temperature, c is the speed of sound, $\gamma = \frac{c_p}{c_v}$ is the ratio of specific heat, and R is the specific gas constant. We consider shock Mach numbers spanning from 1.2 to 3.5. Then, based on the selected shock Mach number, we calculate ρ_2, u_2, and p_2 for the west Dirichlet boundary condition. Next, the surface tension coefficient is computed from the Weber number. A summary of initial condition values is presented in Table 8. It should be noted that the value $16.5R_0$ in the table, shows the location of the shock wave in the initial setup (refer to Figure 2).

Table 8: Initial conditions for the SIDA dataset

l	ρ_l [kg m^{-3}]	$\{u_{r,l}, u_{z,l}\}$ [m s^{-1}]	p_l [Pa] $\mathbf{p_l}$ [Pa]	
1 (Ambient air)	ρ_2	0.0, u_2	p_2	$z < 16.5R_0$
	1.2	0.0, 0.0	101325.0	$z > 16.5R_0$
2 (Liquid droplet)	998.2	0.0, 0.0	101325.0	

Parameter Range. As mentioned above, we adopt shock Mach numbers spanning from 1.2 to 3.5, and Weber numbers between 530 and 40000. For the Out-of-Distribution (OOD) dataset, we extend the shock Mach number to range between 3.5 to 5.

Validation. We compare the SIDA dataset against numerical studies. Since we employ an axisymmetric setup in our simulation, a full three-dimensional study is referenced for validation (Winter et al., 2019), (Meng & Colonius, 2018). For this purpose, the non-dimensional time (t^*) and displacement of the center of mass (COM) in the droplet (Δz^*) are defined as

$$t^* = t\,\frac{u_2}{d}\sqrt{\frac{\rho_2}{\rho_{drop}}}, \tag{19}$$

and

$$\Delta z^* = \frac{z}{d}, \tag{20}$$

where t is the saved timestep, and ρ_{drop} is density of the liquid droplet. Upon shock and post-shock flow impact, the droplet COM accelerates. This trend is clearly observable in our dataset, which aligns with results from the literature. In Figure 7, the flattening of the droplet surface and the hat-shaped deformation are shown in order from top to bottom. Noteworthy, the perturbations on the surface of the droplet are related to shear-induced instabilities (Sharma et al., 2021).

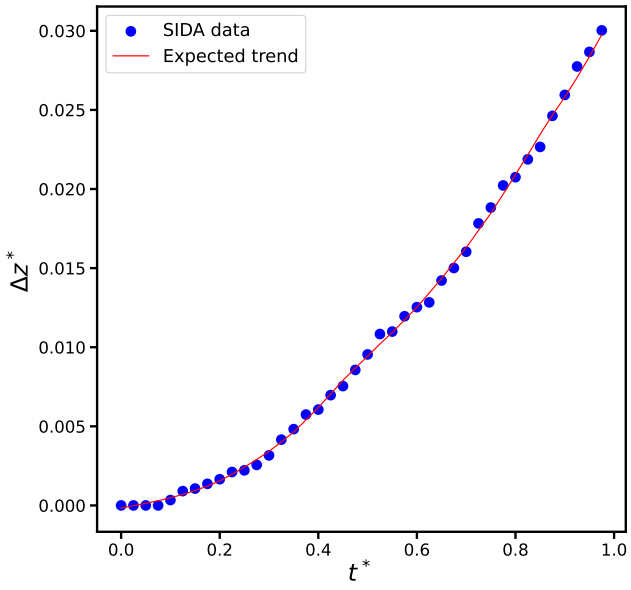

Figure 6: Validation of SIDA data against numerical studies (Winter et al., 2019),(Meng & Colonius, 2018).

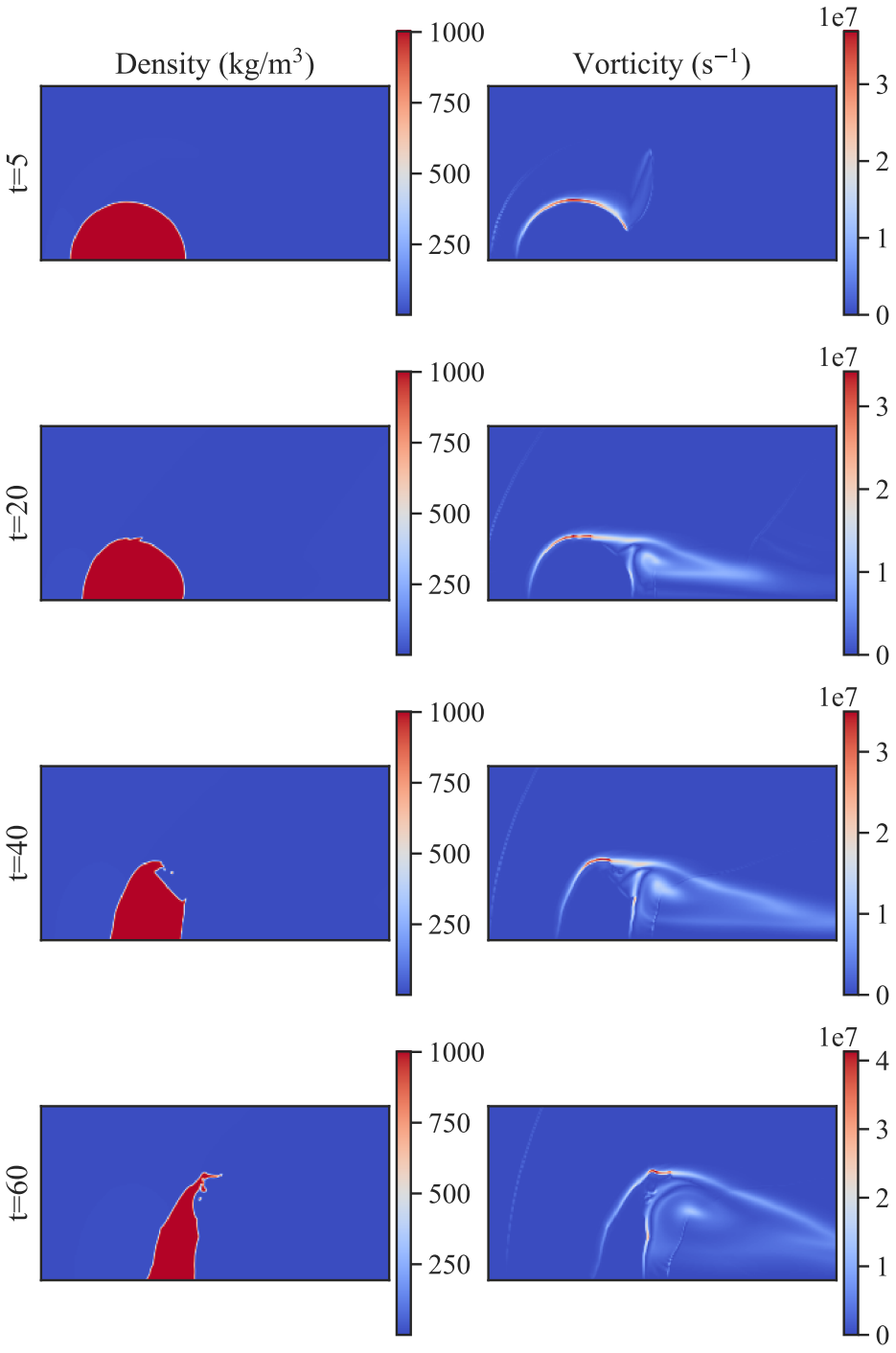

Figure 7: Visualization of droplet's motion and deformation in the SIDA dataset.

B EXPERIMENT DETAILS

B.1 DESIGN OF EXPERIMENTS

The complete set of experiments for the SIDA and the LIDE datasets is shown in Tables 9 and 10, respectively. We experiment with a variety of input, conditioning, and output channels, along with the combinations of sequence info and conditioning parameters.

Table 9: SIDA (PDUVVoS) experiments with Tag identifiers.

# Expt	Tag	Input Channels	Output Channels	Cond[4]	Seq Info [5]
1	PDUV_F_(1,1)	Pressure, Density X-velocity, Y-Velocity	Pressure, Density X-Velocity, Y-Velocity	F	1, 1, 5
2	PDUV_F_(3,1)	Pressure, Density X-velocity, Y-velocity	Pressure, Density Velocity_x, Velocity_y	F	3, 1, 5
3	PDUV_T_(3,1)	Pressure, Density X-velocity, Y-velocity	Pressure, Density X-velocity, Y-velocity	T	3, 1, 5
4	PDUV[VoS]_F_(1,1)	Pressure, Density X-velocity, Y-velocity [Vorticity, Schlieren]	Pressure, Density X-velocity, Y-velocity	F	1, 1, 5
5	PDUV[VoS]_F_(3,1)	Pressure, Density X-velocity, Y-velocity [Vorticity, Schlieren]	Pressure, Density X-velocity, Y-velocity	F	3, 1, 5
6	PDUV[VoS]_T_(3,1)	Pressure, Density X-velocity, Y-velocity [Vorticity, Schlieren]	Pressure, Density X-velocity, Y-velocity	T	3, 1, 5
7	PDUV_F_(3,2)	Pressure, Density X-velocity, Y-velocity	Pressure, Density X-velocity, Y-velocity	F	3, 2, 5
8	PDUV[VoS]_F_(3,2)	Pressure, Density X-velocity, Y-velocity [Vorticity, Schlieren]	Pressure, Density X-velocity, Y-velocity	F	3, 2, 5

[4]refers to the boolean flag indicating whether conditioning parameters are injected into the normalization layer.

[5]refers to the sequence information: [number of historic inputs, number of bundled predictions, stride between timesteps].

Table 10: LIDE (PDUVES) experiments with Tag identifiers.

# Expt	Tag	Input Channels	Output Channels	Cond	Seq Info
1	P_F_(1,1)	Pressure	Pressure	F	1, 1, 10
2	P_F_(3,1)	Pressure	Pressure	F	3, 1, 10
3	P_T_(1,1)	Pressure	Pressure	T	1, 1, 10
4	P_T_(3,1)	Pressure	Pressure	T	3, 1, 10
5	PDUV_F_(1,1)	Pressure, Density X-velocity, Y-velocity	Pressure, Density X-velocity, Y-velocity	F	1, 1, 10
6	PDUV_F_(3,1)	Pressure, Density X-velocity, Y-velocity	Pressure, Density X-velocity, Y-velocity	F	3, 1, 10
7	P[ES]_F_(1,1)	Pressure, [Energy, Schlieren]	Pressure	F	1, 1, 10
8	P[ES]_F_(3,1)	Pressure [Energy, Schlieren]	Pressure	F	3, 1, 10
9	PDUV[ES]_F_(1,1)	Pressure, Density X-velocity, Y-velocity [Energy, Schlieren]	Pressure, Density X-velocity, Y-velocity	F	1, 1, 10
10	PDUV[ES]_F_(3,1)	Pressure, Density X-velocity, Y-velocity [Energy, Schlieren]	Pressure, Density X-velocity, Y-velocity	F	3, 1, 10
11	P_F_(3,2)	Pressure	Pressure	F	3, 2, 10
12	PDUV_F_(3,2)	Pressure, Density X-velocity, Y-velocity	Pressure, Density X-velocity, Y-velocity	F	3, 2, 10
13	PDUV_T_(1,1)	Pressure, Density X-velocity, Y-velocity	Pressure, Density X-velocity, Y-velocity	T	1, 1, 10
14	PDUV_T_(3,1)	Pressure, Density X-velocity, Y-velocity	Pressure, Density X-velocity, Y-velocity	T	3, 1, 10

B.2 Baseline Model Details

In this section, we provide a brief overview of all the models used as baselines. In all the models described in this section, the LayerNorm (Ba et al., 2016) is used as the default choice of normalization layer, and the normalized grid X- and Y-coordinates are appended as additional channels with the input channels.

1. **UNet:** We implement the UNet variant as described in Gupta & Brandstetter (2022). UNets follow a structure that first performs spatial downsampling and then spatial upsampling, with each block composed of multiple convolutional layers. A distinctive feature of UNet is the inclusion of skip connections that link activations from the downsampling path to their corresponding upsampling layers. Table 11 shows the hyperparameters chosen for the two model parameter categories. The number of latent channels corresponds to the feature dimension produced after the first convolutional layer. Along the downsampling path, the base latent channel dimension is adjusted according to a channel multiplier list, with each element specifying the factor used to increase the number of channels at successive levels of the model.

Table 11: UNet hyperparameters.

Hyperparameters	**1M**	**50M**
Latent channels	28	48
Channel Multiplier	[1,4]	[1,2,2,4]
Activation	GELU	GELU

2. **Residual Network (ResNet):** The baseline ResNet is implemented as described in Gupta & Brandstetter (2022), where no up- or down-projection techniques have been used. The input channels are projected to the latent channels by a convolutional layer and subsequently passed through four ResNet blocks. Each block consists of two 3x3 convolutional layers, each followed by an activation function and a norm layer. The convolutional layers employ a stride and padding of 1, preserving the spatial resolution of the feature maps. The final output is then obtained by adding the original input to the convolutional output. Refer to Table 12 for the hyperparameters.

Table 12: ResNet hyperparameters.

Hyperparameters	**1M**
Latent channels	112
# residual blocks	[1, 1, 1, 1]
Activation	GELU

3. **Fourier Neural Operator (FNO):** The FNO is designed to approximate mappings between function spaces by performing computations directly in the Fourier domain. Its architecture can be divided into three main components: a lifting network, a sequence of Fourier layers, and a decoder network. We adopt the implementation described in Contributors (2023) and use the hyperparameters as shown in Table 13 for our experiments.

   The lifting network first maps the input channels into a higher-dimensional latent space using pointwise convolutions. The dimension of this latent space is described by the latent channels. The core of the model is composed of Fourier layers that have spectral convolution with a point-wise linear convolution layer acting as a skip connection. The activation is applied to the summation of the spectral convolutions and this convolutional skip layer. In each spectral convolution, the input is transformed into the Fourier domain using Fast Fourier Transform (FFT), where a specified number of modes are retained and updated with

learned complex weights, and the result is projected back to the spatial domain through the decoder network.

Table 13: FNO hyperparameters.

Hyperparameters	1M	50M
Latent channels	16	32
FNO Layers	4	6
Modes	16	45
Padding	8	8
Padding Type	constant	constant
Activation in Fourier Layers	GELU	GELU
Decoder layers	2	2
Decoder layers size	128	256
Decoder activation	SiLU	SiLU

4. **Vision Transformer (ViT):** A modified ViT (Dosovitskiy et al., 2020) architecture was adopted. The implementation follows the general ViT paradigm, splitting the image into square patches of size 8, embedding and passing them through a transformer encoder, and reconstructing the spatial output from the resulting latent representations with the additional capability to handle non-square inputs. The ViT model consists of a patch-based embedding, an encoder, and a decoder. Passing the input through the embedding-encoder-decoder pipeline results in a reconstruction of the original input shape. The Embedding divides the image into non-overlapping patches, embeds them via a linear projection, and adds positional encodings. For each patch, this results in a sequence of token vectors, each with dimensions specified by the latent channels. The transformer encoder processes this sequence using standard Multi-Head Self-Attention (MHSA) and feedforward layers, with the hidden size denoted by the intermediate size variable. The number of the hidden layers determines the number of the encoder layers. The number of MHSA in each layer is specified by the number of attention heads. This attention stage allows global spatial interactions across the patch grid, enabling the model to learn long-range dependencies. Table 14 shows the hyperparameters for the two learnable parameter categories.

Table 14: ViT hyperparameters.

Hyperparameters	1M	50M
Latent channels	128	504
Patch size	8	8
# hidden layers	2	12
# attention heads	4	14
intermediate size	512	1024
Activation	GELU	GELU

5. **Scalable Operator Transformer (ScOT):** The ScOT model is based on the Poseidon framework (Herde et al., 2024). At its core, ScOT adopts a hierarchical transformer architecture inspired by vision transformers with a window-based approach. The input is partitioned into a uniform grid of non-overlapping patches. We implement an additional capability to process non-square inputs. Each patch undergoes an averaging operation using a shared spatial weight matrix, followed by a linear projection into a latent embedding space, whose size is described by the latent channels. This procedure produces a piecewise-constant latent function representation over the domain, which serves as the input to the

transformer backbone. The motivation for this patch-based embedding is to reduce the computational complexity associated with global attention while preserving essential local information about the input field.

Once embedded, the representation is processed through a series of hierarchical SwinV2 Transformer blocks (Liu et al., 2021), arranged in multiple stages that progressively downsample and subsequently upsample the latent feature maps, forming a UNet-like architecture. The number of blocks per stage is defined by the variable 'depths' in Table 15. Each stage applies windowed MHSA, where attention computations are restricted to local windows rather than the entire spatial domain, significantly reducing the quadratic cost of global attention. The number of parallel MHSA per stage is determined by the number of attention heads. To ensure information exchange across windows and avoid locality bias, the attention windows are shifted between consecutive layers, enabling effective global context modeling over multiple layers.

The hierarchical design incorporates patch merging operations during the encoder phase to reduce spatial resolution and increase the feature dimension, thereby allowing deeper layers to capture global structures. Conversely, the decoder phase employs patch expansion to restore resolution, and skip connections in the form of ConvNext blocks (Liu et al., 2022), bridging the corresponding encoder and decoder stages. The number of blocks per stage in the ConvNext blocks is specified by the hyperparameter 'skip-connections'.

Table 15: ScOT hyperparameters.

Hyperparameters	**1M**	**50M**
Latent channels	27	150
Patch size	4	4
Depths	[3,3,3]	[4,4,4]
# attention heads	[3,6,12]	[6,12,24]
Skip connections	[2,2,0]	[3,3,0]
Window size	16	16
MLP ratio	2.0	4.0
Activation	GELU	GELU

6. **Convolutional Neural Operator (CNO):** A CNO, similar to a UNet, processes an input function by first feeding it into a series of encoder layers, which progressively reduce the spatial resolution while increasing the number of channels. The representation is then passed through decoder layers, which perform the opposite operation: they restore spatial resolution while compressing the channel dimension. In parallel, the encoder and decoder stages, operating at the same spatial scale or spectral band, are linked through ResNet-style skip connections.

   The key idea lies in the model's upsampling and downsampling strategy, where a low-pass filter is applied to prevent the introduction of new high-frequency noise during the sampling process. This design complies with the Shannon sampling theorem, allowing the discrete data points to remain consistent with their corresponding continuous functions. Refer to Table 16 for the hyperparameters.

7. **Transolver** It is a transformer-based model designed to learn how physical fields evolve according to PDEs. Instead of treating the input like an image, it views the spatial grid as a set of points and learns how information should flow between them using attention. The model embeds the input fields, applies transformer layers that capture both local interactions and long-range dependencies, and then reconstructs the output field. Its design includes spatially meaningful positional encodings and mechanisms to compare points across a reference grid, enabling it to generalize across various resolutions and geometries. Refer to Table 17 for the hyperparameters.

Table 16: CNO hyperparameters.

Hyperparameters	1M	50M
Latent channels	32	64
Depth	4	5
# blocks (except at neck)	2	6
# blocks (at neck)	2	7
Channel multiplier	16	32
Activation	custom LeakyReLU	custom LeakyReLU

Table 17: Transolver hyperparameters.

Hyperparameters	1M
Latent channels	112
# layers	4
# attention heads	8
Dropout	0.0
# slices	32
reference grid resolution	12
MLP ratio	1.0
Activation	GELU

B.3 CONDITIONING

In this section, we describe the formulation of the strategy used to integrate conditioning parameters into the model (Herde et al., 2024). For an input $x \in \mathbb{R}^d$, and k being the conditioning parameters, the conditional layer norm formulation is given by Equation 21. Figure 8 illustrates this injection of conditioning parameters into the layer norm. Here γ and β are simple linear layers and $\hat{\gamma}$ and $\hat{\beta}$ are learnable affine transform parameters of the layer norm, respectively.

$$\begin{aligned} \hat{\mathbf{x}} &= \gamma(k) \odot \mathbf{x} + \beta(k) \\ LayerNorm(\mathbf{x}) &= \hat{\gamma} \odot \frac{\hat{\mathbf{x}} - \mu(\hat{\mathbf{x}})}{\sqrt{\sigma^2(\hat{\mathbf{x}}) + \epsilon}} + \hat{\beta}, \\ \mu(\hat{\mathbf{x}}) &= \frac{1}{d}\sum_{j=1}^{d} \hat{x}_j, \quad \sigma^2(\hat{\mathbf{x}}) = \frac{1}{d}\sum_{j=1}^{d} \big(\hat{x}_j - \mu(\hat{\mathbf{x}})\big)^2. \end{aligned} \tag{21}$$

B.4 TRAINING HYPERPARAMETERS

Table 18 shows the training hyperparameters that are common for all the models. Each model has its own specific hyperparameters, which are described in Appendix B.2. All models were trained on NVIDIA RTX A6000 48GB GPU with bf16 mixed-precision, except for the FNO and CNO, which were trained on fp32.

B.5 ERROR METRICS

To compute the Kinetic Energy (KE) of the domain comprising N cells for each rollout step, we employ Equation 22.

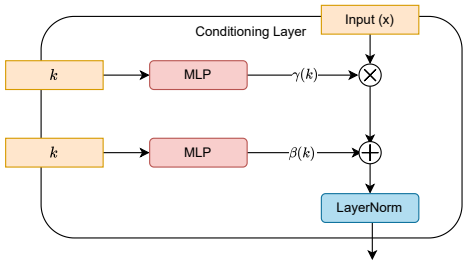

Figure 8: Conditional LayerNorm.

Table 18: Training hyperparameters.

Hyperparameter	**Value**
Number of Epochs	128
Batch Size	32
Optimizer	AdamW
Weight Decay	0.000001
Learning Rate(LR)	0.00005
LR Scheduler	Cosine
Warmup Ratio	0.0
Mix-precision	bf16 (except FNO: fp32)

$$\text{KE} = \Sigma_{i=0}^{N} \frac{1}{2} \rho_i ({u_r}_i^2 + {u_z}_i^2) \Delta V_i \tag{22}$$

Similarly, for Vorticity Production (VP) for N cells, we use Equation 23.

$$\text{VP} = \Sigma_{i=0}^{N} \left(\frac{\partial u_{z\,i}}{\partial r} - \frac{\partial u_{r\,i}}{\partial z} \right)^2 \tag{23}$$

Here, u_r and u_z are the velocity components in the r and z directions, respectively. We compute the square to avoid negative vorticity values.

C RESULTS

The complete set of tables, including the evaluation results on both LIDE and SIDA, is shown in this section. These tables cover three scenarios, which are already discussed in the main text, section 5. These scenarios are the effect of sequence information, conditioning parameters, and fields. Moreover, we introduced two error types, 1 and 2, in section 4.5. For each experiment, we compute error type 2 over **output channels, the evolution of Kinetic Energy (KE), and Vorticity Production (VP)**. In addition, for each dataset, we introduce a quantity of interest (QoI) and repeat the computation over this Dataset-specific QoI. These are **the change of droplet outer radius (OR) and displacement of droplet center of mass (COM)** for LIDE and SIDA, respectively.

C.1 ERROR-TYPE 2 METRICS FOR THE LIDE DATASET

Table 19: Effect of sequence information for LIDE In-Distribution (ID) and Out-of-Distribution (OOD) datasets. Error-type 2 over output channels from section 4.5 is presented. MODELS: UNet, FNO, ViT, ScOT, CNO

MODEL	TAG	1M		50M	
		ID	OOD	ID	OOD
UNet	P_F_(1,1)	9.1478±8.0895	13.0943±8.7709	5.3090±6.7340	11.9953±7.5931
	P_F_(3,1)	3.4922±3.9388	9.1548±6.0536	1.9950±2.6557	7.8092±7.1191
	P_F_(3,2)	3.9751±3.7768	9.0973±5.7687	2.1201±2.8103	7.2636±5.6294
	P_T_(1,1)	5.3515±4.9418	17.8080±15.0191	2.3514±2.6213	9.0930±6.1429
	P_T_(3,1)	4.3477±3.9575	12.7650±9.2722	1.6726±2.1158	7.5000±5.2114
	PDUV_F_(1,1)	2.9972±2.4756	9.0796±5.9230	2.1210±1.8598	8.0828±5.3407
	PDUV_F_(3,1)	1.5341±1.2526	6.0177±5.0874	1.0030±0.8511	5.0866±4.2680
	PDUV_F_(3,2)	1.8878±1.4960	5.1885±3.9663	1.0518±0.8712	5.4376±4.7212
	P[ES]_F_(1,1)	23.0535±18.8769	16.0039±11.8845	29.6090±24.6381	36.0516±30.8501
	P[ES]_F_(3,1)	13.0605±13.3488	20.2864±17.7559	11.1466±10.3795	19.2790±16.1179
	PDUV[ES]_F_(1,1)	7.5569±6.2939	10.5505±6.1862	9.9430±8.6244	11.4681±7.2812
	PDUV[ES]_F_(3,1)	5.1957±4.6966	9.3330±7.0384	4.4018±3.7968	8.5123±6.5495
FNO	P_F_(1,1)	6.3022±5.1934	10.3828±7.0152	5.2016±5.4331	12.0931±7.6183
	P_F_(3,1)	4.6875±4.6579	9.5000±6.8683	3.6339±4.4195	8.7828±6.6895
	P_F_(3,2)	4.9082±4.6673	8.6019±5.6522	3.4477±4.2682	8.0590±5.7641
	P_T_(1,1)	6.0708±5.0622	9.8894±6.0049	4.3767±4.2430	18.1397±15.7189
	P_T_(3,1)	3.9302±3.4157	8.7390±5.2368	2.8506±3.0168	8.6539±5.2262
	PDUV_F_(1,1)	3.6399±3.1425	7.8868±5.3663	2.5836±2.2495	7.2695±5.3881
	PDUV_F_(3,1)	2.4656±2.4281	5.9441±4.8157	1.6334±1.4492	6.4107±5.4997
	PDUV_F_(3,2)	2.0686±1.6025	5.8610±4.4382	1.5864±1.2262	6.3866±5.0470
	P[ES]_F_(1,1)	27.6326±22.1648	26.2085±20.8494	32.7032±25.4675	27.6014±23.5059
	P[ES]_F_(3,1)	10.8859±8.1119	14.1592±10.4569	14.2710±10.8054	14.5738±10.2457
	PDUV[ES]_F_(1,1)	8.6627±6.7686	12.3647±8.0489	8.9522±7.0050	11.1104±6.8842
	PDUV[ES]_F_(3,1)	6.6485±5.3640	9.6179±6.0460	5.0849±4.2891	8.7880±5.6131
ViT	P_F_(1,1)	9.1603±5.5769	10.2389±5.8189	6.2536±7.1400	10.8063±7.6196
	P_F_(3,1)	8.6900±5.5057	10.2917±6.1372	4.1896±4.9856	7.6857±6.3458
	P_F_(3,2)	7.6380±5.2494	10.4696±6.9706	4.4838±5.4155	7.6581±5.9456
	P_T_(1,1)	7.4830±5.7665	11.5443±7.7521	1.7560±2.0376	8.9017±6.6578
	P_T_(3,1)	5.0959±3.8155	10.5010±7.0844	1.5175±1.4244	7.7419±5.9593
	PDUV_F_(1,1)	6.7641±4.8388	8.5556±5.3823	2.1804±1.7873	6.3454±4.3554
	PDUV_F_(3,1)	4.1118±3.0304	6.4825±5.1926	1.4109±1.1031	3.9230±3.2763
	PDUV_F_(3,2)	3.3079±2.3757	6.0555±5.4917	1.3113±0.9807	4.1262±3.6042
	P[ES]_F_(1,1)	19.4751±19.8881	17.3331±13.6654	12.7624±10.7407	15.7572±12.5764
	P[ES]_F_(3,1)	9.2608±7.0138	11.8868±9.0272	7.3133±5.8014	10.2300±8.2406
	PDUV[ES]_F_(1,1)	9.2205±8.8594	11.4403±9.2148	4.3167±3.4105	7.1662±4.9084
	PDUV[ES]_F_(3,1)	5.4353±4.1444	7.7203±6.2456	3.8999±3.2830	5.4419±4.3560
ScOT	P_F_(1,1)	8.2057±6.9389	11.6114±7.4053	5.1421±6.1064	11.3345±7.6428
	P_F_(3,1)	4.8706±4.7652	7.0995±5.8052	3.1855±4.2143	6.1995±5.6304
	P_F_(3,2)	4.4133±4.2731	7.0349±6.0759	3.4873±4.3623	6.4399±5.7289
	P_T_(1,1)	7.8716±19.5111	77.7586±85.1101	2.2581±2.5968	11.4039±8.8884
	P_T_(3,1)	4.8011±4.6080	41.1675±43.1742	1.8432±2.0658	23.1959±25.7497
	PDUV_F_(1,1)	2.8022±2.2122	7.4147±4.9714	2.2992±1.8961	7.0310±4.6946
	PDUV_F_(3,1)	1.7180±1.3379	6.4316±7.3418	1.1854±0.9577	5.1242±5.4815
	PDUV_F_(3,2)	1.6306±1.1924	4.5044±4.0265	1.2412±0.9675	4.3705±3.9198
	P[ES]_F_(1,1)	21.4050±22.1739	22.0405±17.6376	16.8751±13.1522	15.5203±9.7885
	P[ES]_F_(3,1)	6.2541±5.3469	7.7537±5.7890	6.0439±4.9679	8.0174±5.8438
	PDUV[ES]_F_(1,1)	8.5861±7.6685	8.7523±6.9290	6.4329±6.2919	10.0934±7.6721
	PDUV[ES]_F_(3,1)	4.2951±4.1789	9.7228±10.4728	4.2373±4.2770	8.4763±8.7977
CNO	P_F_(1,1)	5.8675±6.4694	28.5730±20.1015	5.5428±6.2562	35.9518±35.2050
	P_F_(3,1)	2.1754±2.6216	10.0666±8.6685	2.3462±3.2362	7.4284±6.6611
	P_F_(3,2)	2.6451±2.9804	7.2544±6.5288	2.2003±2.9196	10.2079±9.7935
	P_T_(1,1)	5.7219±5.7462	16.1748±13.3171	3.7626±4.6015	11.5224±7.8040
	P_T_(3,1)	4.2187±4.2207	10.7036±7.3115	3.1813±3.2968	8.9759±5.4488
	PDUV_F_(1,1)	2.1786±1.7884	7.7764±6.8129	2.1271±1.7921	6.7606±4.9076
	PDUV_F_(3,1)	1.2258±0.9966	6.4241±6.3085	1.1850±0.9985	4.7852±3.9415
	PDUV_F_(3,2)	1.3169±1.0001	4.1531±3.4367	1.3296±1.0634	4.6685±3.9123
	P[ES]_F_(1,1)	26.0960±22.0672	39.5163±34.1637	27.8891±22.8285	33.5685±28.1269
	P[ES]_F_(3,1)	8.6612±7.3315	10.0280±7.1972	8.4329±7.1614	14.1459±12.8208
	PDUV[ES]_F_(1,1)	8.7094±7.9076	13.4745±9.9670	7.5888±6.7066	11.8868±9.0768
	PDUV[ES]_F_(3,1)	4.9778±4.7576	7.3581±6.0097	4.7545±4.2252	7.9192±6.5797

Table 20: Effect of sequence information for LIDE In-Distribution (ID) and Out-of-Distribution (OOD) datasets. Error-type 2 over output channels from section 4.5 is presented. MODELS: ResNet and Transolver

MODEL	TAG	1M	
		ID	OOD
ResNet	P_F_(1,1)	15.8603±14.2650	14.5966±10.5899
	P_F_(3,1)	9.7710±7.7492	10.9950±7.2943
	P_F_(3,2)	6.3019±5.0498	9.5956±5.5532
	P_T_(1,1)	8.4347±6.6584	18.5181±14.7422
	P_T_(3,1)	6.2434±5.2237	20.0036±15.6632
	PDUV_F_(1,1)	7.1277±5.7086	9.8022±6.0704
	PDUV_F_(3,1)	5.0517±4.3040	6.4456±4.5672
	PDUV_F_(3,2)	2.6025±1.9887	5.3443±3.8090
	P[ES]_F_(1,1)	22.7663±16.9184	30.5975±25.0920
	P[ES]_F_(3,1)	10.6258±7.4852	14.4755±10.1972
	PDUV[ES]_F_(1,1)	6.5783±4.6303	10.2784±6.3609
	PDUV[ES]_F_(3,1)	6.3316±4.7105	8.5529±5.2428
Transolver	P_F_(1,1)	7.7697±6.8997	11.3624±7.4919
	P_F_(3,1)	3.7175±3.7892	6.7653±5.1699
	P_F_(3,2)	4.6809±4.1168	8.7001±6.3872
	P_T_(1,1)	3.8780±3.8781	9.3457±6.6854
	P_T_(3,1)	3.0103±2.9045	7.5745±5.2939
	PDUV_F_(1,1)	4.9459±3.6294	8.3506±5.2692
	PDUV_F_(3,1)	3.4782±2.3452	5.5601±4.1509
	PDUV_F_(3,2)	5.8298±3.8836	6.7510±4.4488
	P[ES]_F_(1,1)	16.7733±12.4990	14.5373±9.9606
	P[ES]_F_(3,1)	9.6835±7.1451	10.8923±8.3330
	PDUV[ES]_F_(1,1)	9.1508±7.5811	9.7693±7.6113
	PDUV[ES]_F_(3,1)	6.0474±4.3954	7.4736±5.4511

Table 21: Effect of sequence information for LIDE In-Distribution (ID) and Out-of-Distribution (OOD) datasets. Error-type 2 over KE from section 4.5 is presented.

MODEL	TAG	1M		50M	
		ID	OOD	ID	OOD
UNet	PDUV_F_(1,1)	2.9558±3.4607	7.4869±9.0017	0.7912±0.9653	8.0747±7.5999
	PDUV_F_(3,1)	1.5158±1.7694	5.8522±5.8268	0.6309±0.9576	4.6977±3.9619
	PDUV_F_(3,2)	2.0264±2.2633	7.9273±6.9269	1.1124±1.2723	5.7533±5.6323
	PDUV[ES]_F_(1,1)	20.3706±34.1137	10.1271±15.9696	85.3670±95.5683	153.1264±176.1153
	PDUV[ES]_F_(3,1)	16.7911±23.1446	106.7279±127.6807	7.1791±9.1559	38.0896±41.2699
FNO	PDUV_F_(1,1)	17.3105±56.5599	10.9310±16.6896	7.7942±39.8016	20.4284±40.8841
	PDUV_F_(3,1)	9.4252±25.9660	13.1689±17.0462	5.0986±27.2035	5.3432±9.4238
	PDUV_F_(3,2)	3.5499±5.2362	7.0161±4.5337	1.4311±1.4455	5.6575±4.4884
	PDUV[ES]_F_(1,1)	25.1967±25.9655	28.1146±31.9155	20.8824±31.6092	9.1176±11.8356
	PDUV[ES]_F_(3,1)	11.2583±9.6838	4.7826±3.8797	6.1821±7.2471	21.7777±30.0173
ViT	PDUV_F_(1,1)	30.7485±75.0957	13.4051±28.2157	1.9576±1.9775	2.7012±2.0355
	PDUV_F_(3,1)	8.4927±9.5889	21.5649±28.8912	2.0578±1.8248	11.1058±6.4700
	PDUV_F_(3,2)	5.8635±4.6720	42.0109±101.9154	3.1128±2.6023	14.1639±8.6045
	PDUV[ES]_F_(1,1)	241.4799±870.9689	145.0038±397.7887	16.0164±19.8772	6.9168±8.2187
	PDUV[ES]_F_(3,1)	27.0586±39.7306	25.4535±23.4193	9.8028±13.6173	14.4241±9.5125
ScOT	PDUV_F_(1,1)	3.3588±3.5977	3.6852±3.2128	1.5700±1.4611	3.0450±2.3063
	PDUV_F_(3,1)	3.4918±4.2602	22.0304±39.1454	1.8417±1.7165	7.0220±18.5086
	PDUV_F_(3,2)	4.6926±4.0309	14.9502±8.3347	2.1463±1.7221	5.9104±4.1972
	PDUV[ES]_F_(1,1)	62.5426±145.8651	25.8621±39.7799	43.8361±70.6359	27.6410±45.7599
	PDUV[ES]_F_(3,1)	10.6228±13.9594	46.5500±63.7638	15.5375±19.7119	40.3355±42.3768
CNO	PDUV_F_(1,1)	2.4282±2.7867	14.8098±19.7260	1.6192±1.9654	7.1715±7.9620
	PDUV_F_(3,1)	1.6514±1.7726	31.4155±37.0237	1.2797±1.4745	4.4545±4.1664
	PDUV_F_(3,2)	2.4189±2.1014	6.7205±5.8820	1.8983±1.6440	4.5032±4.4261
	PDUV[ES]_F_(1,1)	42.3454±45.6934	147.1579±157.3773	21.5265±26.4024	99.8242±121.7740
	PDUV[ES]_F_(3,1)	14.6887±19.6394	41.0990±52.3916	2.7269±3.3062	6.9642±9.2008
ResNet	PDUV_F_(1,1)	72.0392±186.8011	21.9601±35.3048		
	PDUV_F_(3,1)	5.2020±11.0591	5.9362±3.9994		
	PDUV_F_(3,2)	3.2099±4.3074	8.1963±5.5746		
	PDUV[ES]_F_(1,1)	30.4190±41.2347	64.9705±64.7465		
	PDUV[ES]_F_(3,1)	26.2392±33.9826	25.1360±32.8936		
Transolver	PDUV_F_(1,1)	5.6585±6.2504	5.4874±3.5771		
	PDUV_F_(3,1)	8.2177±8.3123	31.5978±26.8641		
	PDUV_F_(3,2)	19.5804±13.9786	37.3732±20.2799		
	PDUV[ES]_F_(1,1)	72.7505±228.9720	27.5679±43.1728		
	PDUV[ES]_F_(3,1)	38.8649±37.2626	72.0413±61.4863		

Table 22: Effect of sequence information for LIDE In-Distribution (ID) and Out-of-Distribution (OOD) datasets. Error-type 2 over VP from section 4.5 is presented.

MODEL	TAG	1M		50M	
		ID	OOD	ID	OOD
UNet	PDUV_F_(1,1)	2.2364±1.8249	7.6716±4.9818	1.1246±1.3118	6.6250±4.5504
	PDUV_F_(3,1)	1.4657±1.3658	4.2129±2.3582	0.5786±0.6629	4.8546±3.6289
	PDUV_F_(3,2)	2.8379±1.8601	5.5938±3.3693	0.8377±0.7912	4.2676±2.6929
	PDUV[ES]_F_(1,1)	5.9239±6.3310	6.2247±4.3015	9.2649±8.3096	15.2664±17.0709
	PDUV[ES]_F_(3,1)	3.7189±4.2770	18.7705±29.1679	2.3040±2.8389	8.0838±8.7216
FNO	PDUV_F_(1,1)	15.4477±38.8379	10.0575±11.7609	8.1643±39.6190	10.5453±15.8533
	PDUV_F_(3,1)	8.7514±19.1512	10.0428±11.7263	4.8705±22.6135	5.1937±3.2168
	PDUV_F_(3,2)	4.7165±3.5565	6.9232±4.4139	2.6684±2.0407	5.2543±3.3209
	PDUV[ES]_F_(1,1)	7.6566±9.2270	6.3084±3.6235	6.2573±7.7260	6.8818±7.8352
	PDUV[ES]_F_(3,1)	4.1110±4.3578	4.6076±3.7051	2.6139±2.7369	20.8548±24.9235
ViT	PDUV_F_(1,1)	35.9765±50.1389	10.7088±14.2735	2.1195±1.7062	6.0996±3.5933
	PDUV_F_(3,1)	13.7822±15.4450	11.8592±20.5723	1.7101±1.8497	3.5671±2.1539
	PDUV_F_(3,2)	3.7469±4.5967	5.0032±5.8750	2.0180±1.3555	4.2558±2.5245
	PDUV[ES]_F_(1,1)	116.2920±166.9602	51.8742±99.6273	5.3122±6.8443	5.0159±5.2584
	PDUV[ES]_F_(3,1)	31.3124±44.7175	21.5597±25.9508	5.0579±7.6161	5.0811±7.9904
ScOT	PDUV_F_(1,1)	3.2438±2.3717	7.2868±3.9963	1.4184±1.3680	5.8183±3.3720
	PDUV_F_(3,1)	2.7103±2.0030	6.1239±5.2132	0.8984±0.8154	4.7614±3.2915
	PDUV_F_(3,2)	3.3650±2.1891	5.9972±3.2918	1.3082±0.9690	4.8981±2.9342
	PDUV[ES]_F_(1,1)	6.2914±11.0882	6.8750±4.1989	8.1067±12.0643	7.6245±5.7289
	PDUV[ES]_F_(3,1)	2.9604±3.3728	6.7903±6.5895	2.5907±3.6683	4.8924±3.7627
CNO	PDUV_F_(1,1)	2.3980±1.9352	5.0360±2.8973	1.4503±1.5786	5.6487±3.7962
	PDUV_F_(3,1)	1.9368±1.4496	4.8935±2.9276	1.1844±1.1809	5.1373±3.3016
	PDUV_F_(3,2)	2.7687±1.7760	5.9649±3.6874	1.7443±1.3692	5.1603±3.1993
	PDUV[ES]_F_(1,1)	5.6469±6.5604	7.1679±7.5588	4.5431±5.7530	6.5345±7.5133
	PDUV[ES]_F_(3,1)	2.5447±2.8231	4.2803±2.7221	2.1570±2.6265	4.6820±3.2973
ResNet	PDUV_F_(1,1)	35.3231±75.9315	5.7896±4.4612		
	PDUV_F_(3,1)	28.5191±65.6205	6.3865±7.7030		
	PDUV_F_(3,2)	17.1056±37.6935	6.7059±5.9792		
	PDUV[ES]_F_(1,1)	66.6398±120.4167	21.7128±30.8889		
	PDUV[ES]_F_(3,1)	29.7433±46.1951	7.7186±9.6800		
Transolver	PDUV_F_(1,1)	3.7311±4.9342	6.1950±3.9039		
	PDUV_F_(3,1)	3.2161±4.3176	6.8555±5.0112		
	PDUV_F_(3,2)	11.5979±11.1597	13.8273±10.7180		
	PDUV[ES]_F_(1,1)	48.7057±82.3430	19.3961±24.8031		
	PDUV[ES]_F_(3,1)	6.6554±8.8829	8.8493±14.1979		

Table 23: Effect of sequence information for LIDE In-Distribution (ID) and Out-of-Distribution (OOD) datasets. Error-type 2 over OR from section 4.5 is presented.

MODEL	TAG	1M		50M	
		ID	OOD	ID	OOD
UNet	PDUV_F_(1,1)	27.6161±83.5283	288.1661±361.6815	25.9451±78.9227	336.0100±416.4188
	PDUV_F_(3,1)	22.5440±64.7437	360.2897±422.2532	21.6422±62.6203	325.0154±380.1980
	PDUV_F_(3,2)	25.2007±72.3719	304.1421±357.8917	11.5376±35.9400	246.6969±285.4076
	PDUV[ES]_F_(1,1)	10.1121±13.9343	12.7286±27.3411	19.4516±58.1035	27.6148±52.5871
	PDUV[ES]_F_(3,1)	21.5989±67.8911	68.7352±141.6686	18.9192±53.5520	74.0707±178.7413
FNO	PDUV_F_(1,1)	29.6074±93.7013	313.8395±437.8267	9.9817±46.2403	320.7908±453.1373
	PDUV_F_(3,1)	37.0998±106.2921	413.0769±490.3942	26.7387±80.1169	331.4658±421.8210
	PDUV_F_(3,2)	29.6000±82.8274	343.0459±387.5149	29.7442±83.5604	278.5166±342.8986
	PDUV[ES]_F_(1,1)	42.1162±111.6572	389.1060±525.8061	13.9013±41.0257	100.3914±190.0753
	PDUV[ES]_F_(3,1)	11.3997±36.5709	65.5979±245.8531	17.4764±49.3967	227.7179±364.7697
ViT	PDUV_F_(1,1)	28.3570±84.8627	316.4301±381.2929	7.3652±28.7282	154.0128±218.9231
	PDUV_F_(3,1)	26.6128±87.9115	106.3928±240.9438	16.3596±58.4039	108.5414±239.3181
	PDUV_F_(3,2)	31.4939±89.9586	403.3719±457.6138	39.1299±108.5654	395.2225±461.4427
	PDUV[ES]_F_(1,1)	24.9565±69.7981	240.2715±326.7355	19.9529±60.1380	212.9958±261.6513
	PDUV[ES]_F_(3,1)	11.2870±38.3220	171.8278±256.1028	6.3234±11.7187	105.0288±216.5524
ScOT	PDUV_F_(1,1)	19.0514±57.4875	213.0902±263.9498	29.8124±91.7401	360.4875±460.3578
	PDUV_F_(3,1)	25.3996±76.6864	361.9640±412.0892	8.1928±41.8663	176.1184±329.3044
	PDUV_F_(3,2)	25.3838±74.0512	370.2090±439.8857	16.7229±61.8938	238.5913±329.3854
	PDUV[ES]_F_(1,1)	28.4080±86.3271	297.9673±404.0781	19.1925±58.2088	216.5683±272.0256
	PDUV[ES]_F_(3,1)	33.4385±101.7622	333.1158±415.8457	21.1220±59.9334	271.1644±309.5756
CNO	PDUV_F_(1,1)	20.3428±62.2283	407.2689±527.2424	19.7226±60.0229	261.2177±332.9367
	PDUV_F_(3,1)	22.7767±66.8182	163.3376±283.7012	19.7672±71.7488	91.9920±200.5455
	PDUV_F_(3,2)	15.4841±49.3636	144.9798±221.2885	35.2070±104.4445	407.2021±461.4344
	PDUV[ES]_F_(1,1)	34.5318±101.6591	298.9503±438.7167	16.0693±48.4838	71.8442±107.9373
	PDUV[ES]_F_(3,1)	7.3676±11.9052	9.7813±5.3788	17.2166±48.6478	207.3200±232.2929
ResNet	PDUV_F_(1,1)	48.2119±127.4267	443.6026±559.3933		
	PDUV_F_(3,1)	50.6830±131.6622	507.9845±594.5909		
	PDUV_F_(3,2)	43.3286±119.8816	285.9452±379.6090		
	PDUV[ES]_F_(1,1)	20.2926±66.2371	74.7534±168.2826		
	PDUV[ES]_F_(3,1)	5.0466±4.8902	8.6086±7.1586		
Transolver	PDUV_F_(1,1)	50.4440±122.6158	479.4698±587.8039		
	PDUV_F_(3,1)	54.6837±128.0420	312.8717±446.2977		
	PDUV_F_(3,2)	28.0606±64.1206	222.4606±249.9115		
	PDUV[ES]_F_(1,1)	11.5269±6.4621	315.8390±533.3240		
	PDUV[ES]_F_(3,1)	15.6974±29.7730	306.3072±530.8621		

Table 24: Effect of conditioning parameters for LIDE In-Distribution (ID) and Out-of-Distribution (OOD) datasets. Error-type 2 over output channels from section 4.5 is presented.

MODEL	TAG	1M		50M	
		ID	OOD	ID	OOD
UNet	P_F_(1,1)	9.1478±8.0895	13.0942±8.7709	5.3089±6.7339	11.9953±7.5931
	P_T_(1,1)	5.3515±4.9417	17.8080±15.0190	2.3513±2.6213	9.0930±6.1429
	P_F_(3,1)	3.4922±3.9388	9.1547±6.0535	1.9950±2.6556	7.8092±7.1190
	P_T_(3,1)	4.3477±3.9574	12.7650±9.2722	1.6726±2.1157	7.4999±5.2113
	PDUV_F_(1,1)	2.9972±2.4755	9.0795±5.9229	2.1209±1.8598	8.0827±5.3407
	PDUV_T_(1,1)	2.9636±2.5183	10.1979±7.5259	1.2553±1.1437	8.1129±5.4866
	PDUV_F_(3,1)	1.5341±1.2526	6.0177±5.0873	1.0029±0.8511	5.0866±4.2680
	PDUV_T_(3,1)	2.6413±2.3683	9.6531±7.8398	1.0383±0.9354	6.6239±5.2895
FNO	P_F_(1,1)	6.3022±5.1934	10.3828±7.0152	5.2016±5.4331	12.0931±7.6183
	P_T_(1,1)	6.0708±5.0622	9.8894±6.0049	4.3767±4.2430	18.1397±15.7189
	P_F_(3,1)	4.6875±4.6579	9.5000±6.8683	3.6339±4.4195	8.7828±6.6895
	P_T_(3,1)	3.9302±3.4157	8.7390±5.2368	2.8506±3.0168	8.6539±5.2262
	PDUV_F_(1,1)	3.6399±3.1425	7.8868±5.3663	2.5836±2.2495	7.2695±5.3881
	PDUV_T_(1,1)	2.7562±2.4957	9.1299±6.1320	1.6632±1.4450	8.7610±6.3761
	PDUV_F_(3,1)	2.4656±2.4281	5.9441±4.8157	1.6334±1.4492	6.4107±5.4997
	PDUV_T_(3,1)	2.1101±2.2230	6.4283±5.1802	1.5349±1.2236	7.3136±5.1163
ViT	P_F_(1,1)	9.1603±5.5769	10.2389±5.8189	6.2536±7.1400	10.8063±7.6196
	P_T_(1,1)	7.4830±5.7665	11.5443±7.7521	1.7560±2.0376	8.9017±6.6578
	P_F_(3,1)	8.6900±5.5057	10.2917±6.1372	4.1896±4.9856	7.6857±6.3458
	P_T_(3,1)	5.0959±3.8155	10.5010±7.0844	1.5175±1.4244	7.7419±5.9593
	PDUV_F_(1,1)	6.7641±4.8388	8.5556±5.3823	2.1804±1.7873	6.3454±4.3554
	PDUV_T_(1,1)	4.6571±3.6689	11.1820±12.6204	1.0744±0.7655	6.0053±5.3625
	PDUV_F_(3,1)	4.1118±3.0304	6.4825±5.1926	1.4109±1.1031	3.9230±3.2763
	PDUV_T_(3,1)	3.4518±2.4023	10.4698±11.1001	1.0612±0.7537	4.4118±4.0008
ScOT	P_F_(1,1)	8.2057±6.9389	11.6114±7.4053	5.1421±6.1064	11.3345±7.6428
	P_T_(1,1)	7.8716±19.5111	77.7586±85.1101	2.2581±2.5968	11.4039±8.8884
	P_F_(3,1)	4.8706±4.7652	7.0995±5.8052	3.1855±4.2143	6.1995±5.6304
	P_T_(3,1)	4.8011±4.6080	41.1675±43.1742	1.8432±2.0658	23.1959±25.7497
	PDUV_F_(1,1)	2.8022±2.2122	7.4147±4.9714	2.2992±1.8961	7.0310±4.6946
	PDUV_T_(1,1)	2.1729±1.6478	15.8824±16.0901	1.0326±0.8473	10.2492±10.8710
	PDUV_F_(3,1)	1.7180±1.3379	6.4316±7.3418	1.1854±0.9577	5.1242±5.4815
	PDUV_T_(3,1)	1.7619±1.3709	8.0149±6.9873	0.8772±0.6840	7.8435±7.3701
CNO	P_F_(1,1)	5.8675±6.4694	28.5730±20.1015	5.5428±6.2562	35.9518±35.2050
	P_T_(1,1)	5.7219±5.7462	16.1748±13.3171	3.7626±4.6015	11.5224±7.8040
	P_F_(3,1)	2.1754±2.6216	10.0666±8.6685	2.3462±3.2362	7.4284±6.6611
	P_T_(3,1)	4.2187±4.2207	10.7036±7.3115	3.1813±3.2968	8.9760±5.4488
	PDUV_F_(1,1)	2.1786±1.7884	7.7764±6.8129	2.1271±1.7921	6.7606±4.9076
	PDUV_T_(1,1)	2.6620±2.2500	10.6073±7.5735	2.0716±1.8737	9.5014±6.0985
	PDUV_F_(3,1)	1.2258±0.9966	6.4241±6.3085	1.1850±0.9985	4.7852±3.9415
	PDUV_T_(3,1)	2.6061±2.4252	9.0774±6.4503	1.8087±1.6317	8.0127±5.4545
ResNet	P_F_(1,1)	15.8603±14.2650	14.5966±10.5899		
	P_T_(1,1)	8.4347±6.6584	18.5181±14.7422		
	P_F_(3,1)	9.7710±7.7492	10.9950±7.2943		
	P_T_(3,1)	6.2434±5.2237	20.0036±15.6632		
	PDUV_F_(1,1)	7.1277±5.7086	9.8022±6.0704		
	PDUV_T_(1,1)	4.8602±3.8324	9.1651±5.5656		
	PDUV_F_(3,1)	5.0517±4.3040	6.4456±4.5672		
	PDUV_T_(3,1)	3.3461±2.5509	8.8525±6.2045		
Transolver	P_F_(1,1)	7.7697±6.8997	11.3624±7.4919		
	P_T_(1,1)	3.8780±3.8781	9.3457±6.6854		
	P_F_(3,1)	3.7175±3.7892	6.7653±5.1699		
	P_T_(3,1)	3.0103±2.9045	7.5745±5.2939		
	PDUV_F_(1,1)	4.9459±3.6294	8.3506±5.2692		
	PDUV_T_(1,1)	8.3954±5.2724	8.7039±5.2462		
	PDUV_F_(3,1)	3.4782±2.3452	5.5601±4.1509		
	PDUV_T_(3,1)	4.9456±3.2063	8.5088±5.8755		

Table 25: Effect of conditioning parameters for LIDE In-Distribution (ID) and Out-of-Distribution (OOD) datasets. Error-type 2 over KE from section 4.5 is presented.

MODEL	TAG	1M		50M	
		ID	OOD	ID	OOD
UNet	PDUV_F_(1,1)	2.9558±3.4607	7.4869±9.0017	0.7912±0.9653	8.0747±7.5999
	PDUV_T_(1,1)	5.8103±14.5419	44.3624±67.1609	1.8841±2.2318	21.0380±39.8297
	PDUV_F_(3,1)	1.5158±1.7694	5.8522±5.8268	0.6309±0.9576	4.6977±3.9619
	PDUV_T_(3,1)	5.9552±13.5994	178.5762±265.3987	2.0062±6.6965	65.4653±124.1800
FNO	PDUV_F_(1,1)	17.3105±56.5599	10.9310±16.6896	7.7942±39.8016	20.4284±40.8841
	PDUV_T_(1,1)	3.5652±5.4341	9.1283±13.5591	2.3204±8.9024	30.3218±54.8095
	PDUV_F_(3,1)	9.4252±25.9660	13.1689±17.0462	5.0986±27.2035	5.3432±9.4238
	PDUV_T_(3,1)	2.6480±5.6620	25.1748±42.5476	0.9550±1.2139	9.1987±11.1568
ViT	PDUV_F_(1,1)	30.7485±75.0957	13.4051±28.2157	1.9576±1.9775	2.7012±2.0355
	PDUV_T_(1,1)	13.7787±15.8051	206.6721±490.4529	1.8299±1.7364	17.8208±22.1968
	PDUV_F_(3,1)	8.4927±9.5889	21.5649±28.8912	2.0578±1.8248	11.1058±6.4700
	PDUV_T_(3,1)	8.7343±10.8018	101.8180±153.4608	1.9404±1.7064	10.8021±11.9168
ScOT	PDUV_F_(1,1)	3.3588±3.5977	3.6852±3.2128	1.5700±1.4611	3.0450±2.3063
	PDUV_T_(1,1)	6.8205±8.3661	169.6440±370.9922	2.1943±2.2499	672.6685±1149.7342
	PDUV_F_(3,1)	3.4918±4.2602	22.0304±39.1454	1.8417±1.7165	7.0220±18.5086
	PDUV_T_(3,1)	5.2982±6.3912	322.9135±558.6424	2.3892±2.2477	101.1714±152.1318
CNO	PDUV_F_(1,1)	2.4282±2.7867	14.8098±19.7260	1.6192±1.9654	7.1715±7.9620
	PDUV_T_(1,1)	4.9821±11.5265	281.5538±507.0057	4.5075±7.8777	49.5062±65.8603
	PDUV_F_(3,1)	1.6514±1.7726	31.4155±37.0237	1.2797±1.4745	4.4545±4.1664
	PDUV_T_(3,1)	3.1501±4.0803	18.7740±44.7674	2.6809±4.0172	42.1340±79.9313
ResNet	PDUV_F_(1,1)	72.0392±186.8011	21.9601±35.3048		
	PDUV_T_(1,1)	11.2374±19.0098	38.5417±50.4448		
	PDUV_F_(3,1)	5.2020±11.0591	5.9362±3.9994		
	PDUV_T_(3,1)	6.0783±8.6927	12.5039±20.1806		
Transolver	PDUV_F_(1,1)	5.6585±6.2504	5.4874±3.5771		
	PDUV_T_(1,1)	27.3894±25.6446	12.6030±15.6500		
	PDUV_F_(3,1)	8.2177±8.3123	31.5978±26.8641		
	PDUV_T_(3,1)	23.1919±17.7832	25.8517±31.2784		

Table 26: Effect of conditioning parameters for LIDE In-Distribution (ID) and Out-of-Distribution (OOD) datasets. Error-type 2 over VP from section 4.5 is presented.

MODEL	TAG	1M		50M	
		ID	OOD	ID	OOD d
UNet	PDUV_F_(1,1)	2.2364±1.8249	7.6716±4.9818	1.1246±1.3118	6.6250±4.5504
	PDUV_T_(1,1)	2.6919±1.9304	6.7822±3.8915	1.0655±1.4727	8.4409±5.2510
	PDUV_F_(3,1)	1.4657±1.3658	4.2129±2.3582	0.5786±0.6629	4.8546±3.6289
	PDUV_T_(3,1)	2.0459±2.2480	6.5417±3.4596	0.9025±1.1001	7.4573±4.5266
FNO	PDUV_F_(1,1)	15.4477±38.8379	10.0575±11.7609	8.1643±39.6190	10.5453±15.8533
	PDUV_T_(1,1)	6.9028±11.2910	21.9416±30.2423	3.4257±8.3260	28.1019±38.8927
	PDUV_F_(3,1)	8.7514±19.1512	10.0428±11.7263	4.8705±22.6135	5.1937±3.2168
	PDUV_T_(3,1)	5.3098±8.0500	8.4202±10.7254	2.4009±1.7602	9.3546±9.0295
ViT	PDUV_F_(1,1)	35.9765±50.1389	10.7088±14.2735	2.1195±1.7062	6.0996±3.5933
	PDUV_T_(1,1)	12.1881±18.9528	64.7967±102.2082	1.7690±1.5420	7.8840±10.1525
	PDUV_F_(3,1)	13.7822±15.4450	11.8592±20.5723	1.7101±1.8497	3.5671±2.1539
	PDUV_T_(3,1)	12.6794±18.8376	82.6483±125.2612	1.5897±1.7060	3.8315±4.8235
ScOT	PDUV_F_(1,1)	3.2438±2.3717	7.2868±3.9963	1.4184±1.3680	5.8183±3.3720
	PDUV_T_(1,1)	4.4437±3.0729	10.4074±11.7337	1.3951±1.3767	24.3249±38.3291
	PDUV_F_(3,1)	2.7103±2.0030	6.1239±5.2132	0.8984±0.8154	4.7614±3.2915
	PDUV_T_(3,1)	3.2888±2.5007	4.6767±2.4503	1.3000±0.9832	9.1858±11.4396
CNO	PDUV_F_(1,1)	2.3980±1.9352	5.0360±2.8973	1.4503±1.5786	5.6487±3.7962
	PDUV_T_(1,1)	3.6897±3.5841	8.5344±9.0559	2.2872±2.1839	7.4226±4.2026
	PDUV_F_(3,1)	1.9368±1.4496	4.8935±2.9276	1.1844±1.1809	5.1373±3.3016
	PDUV_T_(3,1)	3.4163±3.1853	5.5930±3.7933	2.2287±2.5476	5.6225±3.0315
ResNet	PDUV_F_(1,1)	35.3231±75.9315	5.7896±4.4612		
	PDUV_T_(1,1)	18.5294±30.0486	10.7451±8.9306		
	PDUV_F_(3,1)	28.5191±65.6205	6.3865±7.7030		
	PDUV_T_(3,1)	11.3432±14.3506	8.8084±6.2336		
Transolver	PDUV_F_(1,1)	3.7311±4.9342	6.1950±3.9039		
	PDUV_T_(1,1)	74.0015±271.6266	18.6063±27.1426		
	PDUV_F_(3,1)	3.2161±4.3176	6.8555±5.0112		
	PDUV_T_(3,1)	10.9489±11.6813	9.6702±11.7623		

Table 27: Effect of conditioning parameters for LIDE In-Distribution (ID) and Out-of-Distribution (OOD) datasets. Error-type 2 over OR from section 4.5 is presented.

MODEL	TAG	1M		50M	
		ID	OOD	ID	OOD
UNet	PDUV_F_(1,1)	27.6161±83.5283	288.1661±361.6815	25.9451±78.9227	336.0100±416.4188
	PDUV_T_(1,1)	24.3380±73.8961	131.6247±268.9813	17.2210±58.2018	79.1639±218.8088
	PDUV_F_(3,1)	22.5440±64.7437	360.2897±422.2532	21.6422±62.6203	325.0154±380.1980
	PDUV_T_(3,1)	26.7619±76.1744	78.3667±208.0575	28.4698±82.3074	26.1189±97.2739
FNO	PDUV_F_(1,1)	29.6074±93.7013	313.8395±437.8267	9.9817±46.2403	320.7908±453.1373
	PDUV_T_(1,1)	32.7552±98.8249	426.3703±548.5769	30.9927±94.9173	374.0674±491.5785
	PDUV_F_(3,1)	37.0998±106.2921	413.0769±490.3942	26.7387±80.1169	331.4658±421.8210
	PDUV_T_(3,1)	38.9718±112.4069	415.5112±491.0000	27.6664±83.7146	170.6939±302.2608
ViT	PDUV_F_(1,1)	28.3570±84.8627	316.4301±381.2929	7.3652±28.7282	154.0128±218.9231
	PDUV_T_(1,1)	34.7868±106.0204	42.1618±147.9682	12.5737±41.5759	400.0511±491.7083
	PDUV_F_(3,1)	26.6128±87.9115	106.3928±240.9438	16.3596±58.4039	108.5414±239.3181
	PDUV_T_(3,1)	38.9649±110.5403	396.1875±465.9020	27.1187±87.2383	163.6112±277.0810
ScOT	PDUV_F_(1,1)	19.0514±57.4875	213.0902±263.9498	29.8124±91.7401	360.4875±460.3578
	PDUV_T_(1,1)	43.7381±125.7196	89.7623±238.1051	23.4326±79.5363	472.5784±600.7889
	PDUV_F_(3,1)	25.3996±76.6864	361.9640±412.0892	8.1928±41.8663	176.1184±329.3044
	PDUV_T_(3,1)	27.3812±81.1700	159.3863±310.1257	9.5601±40.0058	140.4161±333.8770
CNO	PDUV_F_(1,1)	20.3428±62.2283	407.2689±527.2424	19.7226±60.0229	261.2177±332.9367
	PDUV_T_(1,1)	19.5992±59.2119	170.7035±352.2779	12.9402±48.1851	28.8141±91.3571
	PDUV_F_(3,1)	22.7767±66.8182	163.3376±283.7012	19.7672±71.7488	91.9920±200.5455
	PDUV_T_(3,1)	21.2636±59.1526	159.2449±359.0494	11.8448±45.1271	147.4758±372.0305
ResNet	PDUV_F_(1,1)	48.2119±127.4267	443.6026±559.3933		
	PDUV_T_(1,1)	7.3037±25.1349	190.7057±284.2230		
	PDUV_F_(3,1)	50.6830±131.6622	507.9845±594.5909		
	PDUV_T_(3,1)	23.5701±83.5540	71.7497±176.7698		
Transolver	PDUV_F_(1,1)	50.4440±122.6158	479.4698±587.8039		
	PDUV_T_(1,1)	26.2207±79.1707	317.7513±430.3635		
	PDUV_F_(3,1)	54.6837±128.0420	312.8717±446.2977		
	PDUV_T_(3,1)	9.0898±5.5820	9.7856±5.3570		

Table 28: Effect of conditioning fields for LIDE In-Distribution (ID) and Out-of-Distribution (OOD) datasets. Error-type 2 over output channels from section 4.5 is presented.

MODEL	TAG	1M		50M	
		ID	OOD	ID	OOD
UNet	P_F_(1,1)	9.1478±8.0895	13.0943±8.7709	5.3090±6.7340	11.9953±7.5931
	P[ES]_F_(1,1)	23.0535±18.8769	16.0039±11.8845	29.6090±24.6381	36.0516±30.8501
	P_F_(3,1)	3.4922±3.9388	9.1548±6.0536	1.9950±2.6557	7.8092±7.1191
	P[ES]_F_(3,1)	13.0605±13.3488	20.2864±17.7559	11.1466±10.3795	19.2790±16.1179
	PDUV_F_(1,1)	2.9972±2.4756	9.0796±5.9230	2.1210±1.8598	8.0828±5.3407
	PDUV[ES]_F_(1,1)	7.5569±6.2939	10.5505±6.1862	9.9430±8.6244	11.4681±7.2812
	PDUV_F_(3,1)	1.5341±1.2526	6.0177±5.0874	1.0030±0.8511	5.0866±4.2680
	PDUV[ES]_F_(3,1)	5.1957±4.6966	9.3330±7.0384	4.4018±3.7968	8.5123±6.5495
FNO	P_F_(1,1)	6.3022±5.1934	10.3828±7.0152	5.2016±5.4331	12.0931±7.6183
	P[ES]_F_(1,1)	27.6326±22.1648	26.2085±20.8494	32.7032±25.4675	27.6014±23.5059
	P_F_(3,1)	4.6875±4.6579	9.5000±6.8683	3.6339±4.4195	8.7828±6.6895
	P[ES]_F_(3,1)	10.8859±8.1119	14.1592±10.4569	14.2710±10.8054	14.5738±10.2457
	PDUV_F_(1,1)	3.6399±3.1425	7.8868±5.3663	2.5836±2.2495	7.2695±5.3881
	PDUV[ES]_F_(1,1)	8.6627±6.7686	12.3647±8.0489	8.9522±7.0050	11.1104±6.8842
	PDUV_F_(3,1)	2.4656±2.4281	5.9441±4.8157	1.6334±1.4492	6.4107±5.4997
	PDUV[ES]_F_(3,1)	6.6485±5.3640	9.6179±6.0460	5.0849±4.2891	8.7880±5.6131
ViT	P_F_(1,1)	9.1603±5.5769	10.2389±5.8189	6.2536±7.1400	10.8063±7.6196
	P[ES]_F_(1,1)	19.4751±19.8881	17.3331±13.6654	12.7624±10.7407	15.7572±12.5764
	P_F_(3,1)	8.6900±5.5057	10.2917±6.1372	4.1896±4.9856	7.6857±6.3458
	P[ES]_F_(3,1)	9.2608±7.0138	11.8868±9.0272	7.3133±5.8014	10.2299±8.2406
	PDUV_F_(1,1)	6.7641±4.8388	8.5556±5.3823	2.1804±1.7873	6.3454±4.3554
	PDUV[ES]_F_(1,1)	9.2205±8.8594	11.4403±9.2148	4.3167±3.4105	7.1662±4.9084
	PDUV_F_(3,1)	4.1118±3.0304	6.4825±5.1926	1.4109±1.1031	3.9230±3.2763
	PDUV[ES]_F_(3,1)	5.4353±4.1444	7.7203±6.2456	3.8999±3.2830	5.4419±4.3560
ScOT	P_F_(1,1)	8.2057±6.9389	11.6114±7.4053	5.1421±6.1064	11.3345±7.6428
	P[ES]_F_(1,1)	21.4050±22.1739	22.0405±17.6376	16.8751±13.1522	15.5203±9.7885
	P_F_(3,1)	4.8706±4.7652	7.0995±5.8052	3.1855±4.2143	6.1995±5.6304
	P[ES]_F_(3,1)	6.2541±5.3469	7.7537±5.7890	6.0439±4.9679	8.0174±5.8438
	PDUV_F_(1,1)	2.8022±2.2122	7.4147±4.9714	2.2992±1.8961	7.0310±4.6946
	PDUV[ES]_F_(1,1)	8.5861±7.6685	8.7523±6.9290	6.4329±6.2919	10.0934±7.6721
	PDUV_F_(3,1)	1.7180±1.3379	6.4316±7.3418	1.1854±0.9577	5.1242±5.4815
	PDUV[ES]_F_(3,1)	4.2951±4.1789	9.7228±10.4728	4.2373±4.2770	8.4763±8.7977
CNO	P_F_(1,1)	5.8675±6.4694	28.5730±20.1015	5.5428±6.2562	35.9518±35.2050
	P[ES]_F_(1,1)	26.0960±22.0672	39.5163±34.1637	27.8891±22.8285	33.5685±28.1269
	P_F_(3,1)	2.1754±2.6216	10.0666±8.6685	2.3462±3.2362	7.4284±6.6611
	P[ES]_F_(3,1)	8.6612±7.3315	10.0280±7.1972	8.4329±7.1614	14.1459±12.8208
	PDUV_F_(1,1)	2.1786±1.7884	7.7764±6.8129	2.1271±1.7921	6.7606±4.9076
	PDUV[ES]_F_(1,1)	8.7094±7.9076	13.4745±9.9670	7.5888±6.7066	11.8868±9.0768
	PDUV_F_(3,1)	1.2258±0.9966	6.4241±6.3085	1.1850±0.9985	4.7852±3.9415
	PDUV[ES]_F_(3,1)	4.9778±4.7576	7.3581±6.0097	4.7545±4.2252	7.9192±6.5797
ResNet	P_F_(1,1)	15.8603±14.2650	14.5966±10.5899		
	P[ES]_F_(1,1)	22.7663±16.9184	30.5975±25.0920		
	P_F_(3,1)	9.7710±7.7492	10.9950±7.2943		
	P[ES]_F_(3,1)	10.6258±7.4852	14.4755±10.1972		
	PDUV_F_(1,1)	7.1277±5.7086	9.8022±6.0704		
	PDUV[ES]_F_(1,1)	6.5783±4.6303	10.2784±6.3609		
	PDUV_F_(3,1)	5.0517±4.3040	6.4456±4.5672		
	PDUV[ES]_F_(3,1)	6.3316±4.7105	8.5529±5.2428		
Transolver	P_F_(1,1)	7.7697±6.8997	11.3624±7.4919		
	P[ES]_F_(1,1)	16.7733±12.4990	14.5373±9.9606		
	P_F_(3,1)	3.7175±3.7892	6.7653±5.1699		
	P[ES]_F_(3,1)	9.6835±7.1451	10.8923±8.3330		
	PDUV_F_(1,1)	4.9459±3.6294	8.3506±5.2692		
	PDUV[ES]_F_(1,1)	9.1508±7.5811	9.7693±7.6113		
	PDUV_F_(3,1)	3.4782±2.3452	5.5601±4.1509		
	PDUV[ES]_F_(3,1)	6.0474±4.3954	7.4736±5.4511		

Table 29: Effect of conditioning fields for LIDE In-Distribution (ID) and Out-of-Distribution (OOD) datasets. Error-type 2 over KE from section 4.5 is presented.

MODEL	TAG	1M		50M	
		ID	OOD	ID	OOD
UNet	PDUV_F_(1,1)	2.9558±3.4607	7.4869±9.0017	0.7912±0.9653	8.0747±7.5999
	PDUV[ES]_F_(1,1)	20.3706±34.1137	10.1271±15.9696	85.3670±95.5683	153.1264±176.1153
	PDUV_F_(3,1)	1.5158±1.7694	5.8522±5.8268	0.6309±0.9576	4.6977±3.9619
	PDUV[ES]_F_(3,1)	16.7911±23.1446	106.7279±127.6807	7.1791±9.1559	38.0896±41.2699
FNO	PDUV_F_(1,1)	17.3105±56.5599	10.9310±16.6896	7.7942±39.8016	20.4284±40.8841
	PDUV[ES]_F_(1,1)	25.1967±25.9655	28.1146±31.9155	20.8824±31.6092	9.1176±11.8356
	PDUV_F_(3,1)	9.4252±25.9660	13.1689±17.0462	5.0986±27.2035	5.3432±9.4238
	PDUV[ES]_F_(3,1)	11.2583±9.6838	4.7826±3.8797	6.1821±7.2471	21.7777±30.0173
ViT	PDUV_F_(1,1)	30.7485±75.0957	13.4051±28.2157	1.9576±1.9775	2.7012±2.0355
	PDUV[ES]_F_(1,1)	241.4799±870.9689	145.0038±397.7887	16.0164±19.8772	6.9168±8.2187
	PDUV_F_(3,1)	8.4927±9.5889	21.5649±28.8912	2.0578±1.8248	11.1058±6.4700
	PDUV[ES]_F_(3,1)	27.0586±39.7306	25.4535±23.4193	9.8028±13.6173	14.4241±9.5125
ScOT	PDUV_F_(1,1)	3.3588±3.5977	3.6852±3.2128	1.5700±1.4611	3.0450±2.3063
	PDUV[ES]_F_(1,1)	62.5426±145.8651	25.8621±39.7799	43.8361±70.6359	27.6410±45.7599
	PDUV_F_(3,1)	3.4918±4.2602	22.0304±39.1454	1.8417±1.7165	7.0220±18.5086
	PDUV[ES]_F_(3,1)	10.6228±13.9594	46.5500±63.7638	15.5375±19.7119	40.3355±42.3768
CNO	PDUV_F_(1,1)	2.4282±2.7867	14.8098±19.7260	1.6192±1.9654	7.1715±7.9620
	PDUV[ES]_F_(1,1)	42.3454±45.6934	147.1579±157.3773	21.5265±26.4024	99.8242±121.7740
	PDUV_F_(3,1)	1.6514±1.7726	31.4155±37.0237	1.2797±1.4745	4.4545±4.1664
	PDUV[ES]_F_(3,1)	14.6887±19.6394	41.0990±52.3916	2.7269±3.3062	6.9642±9.2008
ResNet	PDUV_F_(1,1)	72.0392±186.8011	21.9601±35.3048		
	PDUV[ES]_F_(1,1)	30.4190±41.2347	64.9705±64.7465		
	PDUV_F_(3,1)	5.2020±11.0591	5.9362±3.9994		
	PDUV[ES]_F_(3,1)	26.2392±33.9826	25.1360±32.8936		
Transolver	PDUV_F_(1,1)	5.6585±6.2504	5.4874±3.5771		
	PDUV[ES]_F_(1,1)	72.7505±228.9720	27.5679±43.1728		
	PDUV_F_(3,1)	8.2177±8.3123	31.5978±26.8641		
	PDUV[ES]_F_(3,1)	38.8649±37.2626	72.0413±61.4863		

Table 30: Effect of conditioning fields for LIDE In-Distribution (ID) and Out-of-Distribution (OOD) datasets. Error-type 2 over VP from section 4.5 is presented.

MODEL	TAG	1M		50M	
		ID	OOD	ID	OOD
UNet	PDUV_F_(1,1)	2.2364±1.8249	7.6716±4.9818	1.1246±1.3118	6.6250±4.5504
	PDUV[ES]_F_(1,1)	5.9239±6.3310	6.2247±4.3015	9.2649±8.3096	15.2664±17.0709
	PDUV_F_(3,1)	1.4657±1.3658	4.2129±2.3582	0.5786±0.6629	4.8546±3.6289
	PDUV[ES]_F_(3,1)	3.7189±4.2770	18.7705±29.1679	2.3040±2.8389	8.0838±8.7216
FNO	PDUV_F_(1,1)	15.4477±38.8379	10.0575±11.7609	8.1643±39.6190	10.5453±15.8533
	PDUV[ES]_F_(1,1)	7.6566±9.2270	6.3084±3.6235	6.2573±7.7260	6.8818±7.8352
	PDUV_F_(3,1)	8.7514±19.1512	10.0428±11.7263	4.8705±22.6135	5.1937±3.2168
	PDUV[ES]_F_(3,1)	4.1110±4.3578	4.6076±3.7051	2.6139±2.7369	20.8548±24.9235
ViT	PDUV_F_(1,1)	35.9765±50.1389	10.7088±14.2735	2.1195±1.7062	6.0996±3.5933
	PDUV[ES]_F_(1,1)	116.2920±166.9602	51.8742±99.6273	5.3122±6.8443	5.0159±5.2584
	PDUV_F_(3,1)	13.7822±15.4450	11.8592±20.5723	1.7101±1.8497	3.5671±2.1539
	PDUV[ES]_F_(3,1)	31.3124±44.7175	21.5597±25.9508	5.0579±7.6161	5.0811±7.9904
ScOT	PDUV_F_(1,1)	3.2438±2.3717	7.2868±3.9963	1.4184±1.3680	5.8183±3.3720
	PDUV[ES]_F_(1,1)	6.2914±11.0882	6.8750±4.1989	8.1067±12.0643	7.6245±5.7289
	PDUV_F_(3,1)	2.7103±2.0030	6.1239±5.2132	0.8984±0.8154	4.7614±3.2915
	PDUV[ES]_F_(3,1)	2.9604±3.3728	6.7903±6.5895	2.5907±3.6683	4.8924±3.7627
CNO	PDUV_F_(1,1)	2.3980±1.9352	5.0360±2.8973	1.4503±1.5786	5.6487±3.7962
	PDUV[ES]_F_(1,1)	5.6469±6.5604	7.1679±7.5588	4.5431±5.7530	6.5345±7.5133
	PDUV_F_(3,1)	1.9368±1.4496	4.8935±2.9276	1.1844±1.1809	5.1373±3.3016
	PDUV[ES]_F_(3,1)	2.5447±2.8231	4.2803±2.7221	2.1570±2.6265	4.6820±3.2973
ResNet	PDUV_F_(1,1)	35.3231±75.9315	5.7896±4.4612		
	PDUV[ES]_F_(1,1)	66.6398±120.4167	21.7128±30.8889		
	PDUV_F_(3,1)	28.5191±65.6205	6.3865±7.7030		
	PDUV[ES]_F_(3,1)	29.7433±46.1951	7.7186±9.6800		
Transolver	PDUV_F_(1,1)	3.7311±4.9342	6.1950±3.9039		
	PDUV[ES]_F_(1,1)	48.7057±82.3430	19.3961±24.8031		
	PDUV_F_(3,1)	3.2161±4.3176	6.8555±5.0112		
	PDUV[ES]_F_(3,1)	6.6554±8.8829	8.8493±14.1979		

Table 31: Effect of conditioning fields for LIDE In-Distribution (ID) and Out-of-Distribution (OOD) datasets. Error-type 2 over OR from section 4.5 is presented.

MODEL	TAG	1M		50M	
		ID	OOD	ID	OOD
UNet	PDUV_F_(1,1)	27.6161±83.5283	288.1661±361.6815	25.9451±78.9227	336.0100±416.4188
	PDUV[ES]_F_(1,1)	10.1121±13.9343	12.7286±27.3411	19.4516±58.1035	27.6148±52.5871
	PDUV_F_(3,1)	22.5440±64.7437	360.2897±422.2532	21.6422±62.6203	325.0154±380.1980
	PDUV[ES]_F_(3,1)	21.5989±67.8911	68.7352±141.6686	18.9192±53.5520	74.0707±178.7413
FNO	PDUV_F_(1,1)	29.6074±93.7013	313.8395±437.8267	9.9817±46.2403	320.7908±453.1373
	PDUV[ES]_F_(1,1)	42.1162±111.6572	389.1060±525.8061	13.9013±41.0257	100.3914±190.0753
	PDUV_F_(3,1)	37.0998±106.2921	413.0769±490.3942	26.7387±80.1169	331.4658±421.8210
	PDUV[ES]_F_(3,1)	11.3997±36.5709	65.5979±245.8531	17.4764±49.3967	227.7179±364.7697
ViT	PDUV_F_(1,1)	28.3570±84.8627	316.4301±381.2929	7.3652±28.7282	154.0128±218.9231
	PDUV[ES]_F_(1,1)	24.9565±69.7981	240.2715±326.7355	19.9529±60.1380	212.9958±261.6513
	PDUV_F_(3,1)	26.6128±87.9115	106.3928±240.9438	16.3596±58.4039	108.5414±239.3181
	PDUV[ES]_F_(3,1)	11.2870±38.3220	171.8278±256.1028	6.3234±11.7187	105.0288±216.5524
ScOT	PDUV_F_(1,1)	19.0514±57.4875	213.0902±263.9498	29.8124±91.7401	360.4875±460.3578
	PDUV[ES]_F_(1,1)	28.4080±86.3271	297.9673±404.0781	19.1925±58.2088	216.5683±272.0256
	PDUV_F_(3,1)	25.3996±76.6864	361.9640±412.0892	8.1928±41.8663	176.1184±329.3044
	PDUV[ES]_F_(3,1)	33.4385±101.7622	333.1158±415.8457	21.1220±59.9334	271.1644±309.5756
CNO	PDUV_F_(1,1)	20.3428±62.2283	407.2689±527.2424	19.7226±60.0229	261.2177±332.9367
	PDUV[ES]_F_(1,1)	34.5318±101.6591	298.9503±438.7167	16.0693±48.4838	71.8442±107.9373
	PDUV_F_(3,1)	22.7767±66.8182	163.3376±283.7012	19.7672±71.7488	91.9920±200.5455
	PDUV[ES]_F_(3,1)	7.3676±11.9052	9.7813±5.3788	17.2166±48.6478	207.3200±232.2929
ResNet	PDUV_F_(1,1)	48.2119±127.4267	443.6026±559.3933		
	PDUV[ES]_F_(1,1)	20.2926±66.2371	74.7534±168.2826		
	PDUV_F_(3,1)	50.6830±131.6622	507.9845±594.5909		
	PDUV[ES]_F_(3,1)	5.0466±4.8902	8.6086±7.1586		
Transolver	PDUV_F_(1,1)	50.4440±122.6158	479.4698±587.8039		
	PDUV[ES]_F_(1,1)	11.5269±6.4621	315.8390±533.3240		
	PDUV_F_(3,1)	54.6837±128.0420	312.8717±446.2977		
	PDUV[ES]_F_(3,1)	15.6974±29.7730	306.3072±530.8621		

C.2 Error-type 2 metrics for The SIDA Dataset

Table 32: Effect of sequence information for SIDA In-Distribution (ID) and Out-of-Distribution (OOD) datasets. Error-type 2 over output channels from section 4.5 is presented.

MODEL	TAG	1M		50M	
		ID	OOD	ID	OOD
UNet	PDUV_F_(1,1)	3.5661±2.4696	5.9914±3.2792	3.4983±2.5270	5.9438±3.2522
	PDUV_F_(3,1)	**0.3383±0.2089**	2.2998±1.7754	**0.1356±0.0976**	1.9424±1.5948
	PDUV_F_(3,2)	0.4406±0.2437	**2.1979±1.6703**	0.1785±0.1080	**1.8812±1.4977**
FNO	PDUV_F_(1,1)	3.5224±2.5528	6.0820±3.2896	3.4720±2.5577	5.9768±3.2572
	PDUV_F_(3,1)	**0.5333±0.2829**	**2.1215±1.5319**	**0.2498±0.1387**	**2.0963±1.5242**
	PDUV_F_(3,2)	0.7123±0.3624	2.1449±1.5747	0.3389±0.1827	2.0990±1.5458
ViT	PDUV_F_(1,1)	4.4758±2.8750	5.8219±3.1222	3.5527±2.7160	5.7645±3.1503
	PDUV_F_(3,1)	1.5891±0.9548	3.4253±2.4145	**0.4430±0.2336**	**1.8428±1.3876**
	PDUV_F_(3,2)	**1.3832±0.7495**	**2.4443±1.6647**	0.5441±0.2699	1.8678±1.3767
ScOT	PDUV_F_(1,1)	3.5764±2.5158	5.8985±3.2421	3.5173±2.6462	5.8306±3.1826
	PDUV_F_(3,1)	**0.6884±0.4222**	**1.9005±1.3770**	**0.2059±0.1199**	1.6318±1.3494
	PDUV_F_(3,2)	0.7995±0.4265	1.9084±1.3867	0.2639±0.1459	**1.5164±1.2414**
CNO	PDUV_F_(1,1)	3.9955±2.6786	5.8508±3.1777	3.5025±2.5455	5.9444±3.2344
	PDUV_F_(3,1)	**0.6943±0.4235**	2.1707±1.8099	**0.1621±0.1032**	1.8159±1.4794
	PDUV_F_(3,2)	0.8584±0.4459	**1.8360±1.3758**	0.2210±0.1248	**1.7634±1.3875**
ResNet	PDUV_F_(1,1)	3.7260±2.4574	6.0844±3.3406		
	PDUV_F_(3,1)	**0.5570±0.3461**	2.3042±1.7139		
	PDUV_F_(3,2)	0.6356±0.3669	**2.3012±1.6856**		
Transolver	PDUV_F_(1,1)	5.7995±3.4502	6.9499±3.7154		
	PDUV_F_(3,1)	**4.7065±2.6888**	**4.8852±2.7289**		
	PDUV_F_(3,2)	5.2026±2.7770	5.1580±2.7698		

Table 33: Effect of sequence information for SIDA In-Distribution (ID) and Out-of-Distribution (OOD) datasets. Error-type 2 over KE from section 4.5 is presented.

MODEL	TAG	1M		50M	
		ID	OOD	ID	OOD
UNet	PDUV_F_(1,1)	11.2017±29.5656	5.6983±3.0230	11.7372±31.0932	5.6613±2.9967
	PDUV_F_(3,1)	0.5052±0.2615	2.5368±1.0710	0.1532±0.0897	1.4758±0.8257
	PDUV_F_(3,2)	0.9620±0.6433	9.6801±5.2064	0.4389±0.2677	2.2230±1.1932
FNO	PDUV_F_(1,1)	10.8110±27.7074	5.7480±3.0231	10.7965±28.7023	5.6957±2.9859
	PDUV_F_(3,1)	0.7682±0.5172	1.9919±1.3654	0.2823±0.1765	1.5754±1.9135
	PDUV_F_(3,2)	1.2933±0.6185	1.5242±0.8227	0.5000±0.3997	2.7004±1.5806
ViT	PDUV_F_(1,1)	31.9704±87.7762	4.0911±2.0809	15.7706±44.1921	5.3135±2.7717
	PDUV_F_(3,1)	6.6527±8.3450	32.5122±28.4652	0.9694±0.6501	3.3619±1.4849
	PDUV_F_(3,2)	5.3889±3.2322	5.4872±2.9669	1.9649±1.1585	2.7149±1.9905
ScOT	PDUV_F_(1,1)	16.2807±44.8844	5.3495±2.8561	15.2877±42.6846	5.3579±2.8067
	PDUV_F_(3,1)	2.6928±1.9141	2.5941±1.1618	1.0306±0.6112	2.1724±0.9115
	PDUV_F_(3,2)	4.2225±2.2977	9.6165±5.0281	1.7483±0.9528	5.3631±2.7718
CNO	PDUV_F_(1,1)	17.6490±49.1966	5.0935±2.5799	12.7633±35.2539	5.5010±2.8628
	PDUV_F_(3,1)	3.9209±2.3251	10.1072±9.3279	0.4011±0.2343	1.3602±0.6405
	PDUV_F_(3,2)	4.9192±3.6170	20.5139±13.7615	0.8113±0.5196	1.3482±0.7874
ResNet	PDUV_F_(1,1)	10.9262±28.4670	5.7403±3.0356		
	PDUV_F_(3,1)	0.8521±0.5177	1.9815±0.8412		
	PDUV_F_(3,2)	1.4069±0.6998	5.6830±3.2346		
Transolver	PDUV_F_(1,1)	21.6155±58.9766	5.0188±2.6784		
	PDUV_F_(3,1)	67.9430±41.9429	59.5887±20.7706		
	PDUV_F_(3,2)	181.1406±151.2849	96.0656±48.8018		

Table 34: Effect of sequence information for SIDA In-Distribution (ID) and Out-of-Distribution (OOD) datasets. Error-type 2 over VP from section 4.5 is presented.

MODEL	TAG	1M		50M	
		ID	OOD	ID	OOD
UNet	PDUV_F_(1,1)	4.8548±9.7684	5.1872±2.8746	5.1272±10.2187	5.1860±2.8710
	PDUV_F_(3,1)	0.4678±0.5580	1.9011±1.4640	0.1094±0.1362	2.0724±1.6647
	PDUV_F_(3,2)	0.7461±1.0477	2.4576±1.7732	0.3118±0.3532	2.1101±1.7997
FNO	PDUV_F_(1,1)	4.6886±8.4082	5.4445±2.9026	4.7255±9.1404	5.3154±2.8825
	PDUV_F_(3,1)	0.9580±0.6336	2.1666±1.2573	0.4874±0.4576	1.7614±1.5075
	PDUV_F_(3,2)	1.1520±0.7034	2.7981±1.6515	0.6015±0.4159	1.3866±0.9442
ViT	PDUV_F_(1,1)	28.3750±59.3870	2.6103±1.1959	5.4192±11.6520	5.0160±2.7830
	PDUV_F_(3,1)	13.1278±16.1199	4.9536±5.5894	0.5882±0.9129	1.4598±2.5938
	PDUV_F_(3,2)	4.1804±4.5308	2.1003±1.7241	0.8756±1.1214	1.7605±2.6311
ScOT	PDUV_F_(1,1)	5.0246±10.1023	5.1421±2.8596	5.4551±12.0375	4.9934±2.7667
	PDUV_F_(3,1)	1.6140±2.9631	1.4442±0.6758	0.4774±0.8474	1.1108±0.9826
	PDUV_F_(3,2)	1.3736±2.0323	0.7779±0.5431	0.8046±1.0890	0.7494±0.6484
CNO	PDUV_F_(1,1)	5.0839±10.2831	5.0351±2.8432	5.0165±10.3994	5.0809±2.8365
	PDUV_F_(3,1)	1.9935±6.3802	0.9771±0.7020	0.2560±0.2127	2.0421±1.5173
	PDUV_F_(3,2)	3.4611±6.6855	2.8181±1.6026	0.5898±0.4428	2.1937±1.6745
ResNet	PDUV_F_(1,1)	5.1266±10.6196	5.1755±2.8330		
	PDUV_F_(3,1)	0.5801±0.4023	1.6962±1.3323		
	PDUV_F_(3,2)	0.6297±0.4655	2.2821±1.5949		
Transolver	PDUV_F_(1,1)	6.9632±15.3887	5.0256±2.5608		
	PDUV_F_(3,1)	42.3382±30.2457	23.1503±16.1705		
	PDUV_F_(3,2)	11.3000±14.7913	1.8346±1.1888		

Table 35: Effect of sequence information for SIDA In-Distribution (ID) and Out-of-Distribution (OOD) datasets. Error-type 2 over COM from section 4.5 is presented.

MODEL	TAG	1M		50M	
		ID	OOD	ID	OOD
UNet	PDUV_F_(1,1)	0.2325±0.2905	0.9394±0.9670	0.2235±0.3098	0.9910±0.9754
	PDUV_F_(3,1)	0.0228±0.0126	0.5918±0.4201	0.0088±0.0047	0.7818±0.7129
	PDUV_F_(3,2)	0.0566±0.0265	0.4628±0.4387	0.0251±0.0148	0.5248±0.4867
FNO	PDUV_F_(1,1)	0.2377±0.3125	1.0179±0.9760	0.2188±0.2944	0.9605±0.9621
	PDUV_F_(3,1)	0.0271±0.0130	0.2420±0.3222	0.0118±0.0078	0.2427±0.2805
	PDUV_F_(3,2)	0.0561±0.0319	0.2477±0.3338	0.0267±0.0141	0.2091±0.2934
ViT	PDUV_F_(1,1)	0.3214±0.2879	0.8025±0.8487	0.2269±0.2774	0.9255±0.9327
	PDUV_F_(3,1)	0.1844±0.1821	1.0956±0.8733	0.0326±0.0211	0.2025±0.2268
	PDUV_F_(3,2)	0.2007±0.1252	0.4172±0.3822	0.0751±0.0418	0.1544±0.1388
ScOT	PDUV_F_(1,1)	0.2393±0.3107	0.9747±0.9872	0.2238±0.2732	0.9072±0.9265
	PDUV_F_(3,1)	0.0654±0.0359	0.3114±0.3727	0.0360±0.0209	0.2175±0.2388
	PDUV_F_(3,2)	0.1993±0.0869	0.3583±0.2814	0.0623±0.0293	0.2439±0.3005
CNO	PDUV_F_(1,1)	0.4844±0.6753	0.6387±0.6294	0.2202±0.2753	0.9190±0.9273
	PDUV_F_(3,1)	0.1067±0.0623	0.5085±0.6775	0.0152±0.0097	0.2450±0.2505
	PDUV_F_(3,2)	0.1791±0.1004	0.3669±0.2622	0.0337±0.0189	0.2031±0.2339
ResNet	PDUV_F_(1,1)	0.2284±0.3093	0.9806±0.9846		
	PDUV_F_(3,1)	0.0387±0.0329	0.7315±0.6383		
	PDUV_F_(3,2)	0.0729±0.0535	0.4976±0.3697		
Transolver	PDUV_F_(1,1)	0.6920±0.4419	0.7175±0.7466		
	PDUV_F_(3,1)	2.9121±1.6738	2.3465±0.9107		
	PDUV_F_(3,2)	4.0355±2.0120	2.7159±1.0297		

Table 36: Effect of conditioning parameters for SIDA In-Distribution (ID) and Out-of-Distribution (OOD) datasets. Error-type 2 over output channels from section 4.5 is presented.

MODEL	TAG	1M		50M	
		ID	OOD	ID	OOD
UNet	PDUV_F_(3,1)	0.3383±0.2089	2.2998±1.7754	0.1356±0.0976	1.9424±1.5948
	PDUV_T_(3,1)	0.8690±0.4994	2.5683±1.8388	0.2272±0.1439	2.2561±1.7777
	PDUV[VoS]_F_(3,1)	1.4203±1.1512	2.6100±1.8673	1.2162±1.0310	2.4740±1.8269
	PDUV[VoS]_T_(3,1)	1.6310±1.2358	2.7767±1.8269	1.1111±0.9569	2.4399±1.7482
FNO	PDUV_F_(3,1)	0.5333±0.2829	2.1215±1.5319	0.2498±0.1387	2.0963±1.5242
	PDUV_T_(3,1)	0.7013±0.3424	1.8361±1.2131	0.4075±0.2168	1.7610±1.2616
	PDUV[VoS]_F_(3,1)	1.8914±1.3113	2.6203±1.7532	1.7002±1.3234	2.6674±1.8160
	PDUV[VoS]_T_(3,1)	1.8383±1.2061	2.6599±1.7452	1.6667±1.0564	2.4769±1.6513
ViT	PDUV_F_(3,1)	1.5891±0.9548	3.4253±2.4145	0.4430±0.2336	1.8428±1.3876
	PDUV_T_(3,1)	1.5949±1.0077	2.6376±1.7133	0.4249±0.2343	1.7359±1.3060
	PDUV[VoS]_F_(3,1)	2.2152±1.5536	3.2082±2.2406	1.3497±1.0659	2.3674±1.7135
	PDUV[VoS]_T_(3,1)	2.0499±1.4162	3.0158±1.9680	1.2139±0.9433	2.0682±1.4535
ScOT	PDUV_F_(3,1)	0.6884±0.4222	1.9005±1.3770	0.2059±0.1199	1.6318±1.3494
	PDUV_T_(3,1)	0.8203±0.4715	1.9132±1.2731	0.2461±0.1397	1.5425±1.1975
	PDUV[VoS]_F_(3,1)	1.5944±1.2864	2.4643±1.7766	1.2171±1.0416	2.1314±1.5666
	PDUV[VoS]_T_(3,1)	1.4401±1.0497	2.2995±1.5283	1.1764±1.0238	1.9241±1.3649
CNO	PDUV_F_(3,1)	0.6943±0.4235	2.1707±1.8099	0.1621±0.1032	1.8159±1.4794
	PDUV_T_(3,1)	0.9362±0.5384	66.4331±453.5010	0.3042±0.1905	2.3211±1.8495
	PDUV[VoS]_F_(3,1)	1.1775±0.8980	2.1291±1.4489	1.2240±0.8859	2.3550±1.6215
	PDUV[VoS]_T_(3,1)	1.3235±0.9569	7898e1±6549e2	0.9654±0.7867	2.6471±1.9216
ResNet	PDUV_F_(3,1)	0.5570±0.3461	2.3042±1.7139		
	PDUV_T_(3,1)	1.0385±0.6198	3.0052±2.1978		
	PDUV[VoS]_F_(3,1)	1.3341±1.0333	2.6392±1.8649		
	PDUV[VoS]_T_(3,1)	1.6636±1.2058	3.2900±2.3078		
Transolver	PDUV_F_(3,1)	4.7065±2.6888	4.8852±2.7289		
	PDUV_T_(3,1)	4.7696±2.5778	4.6372±2.5046		
	PDUV[VoS]_F_(3,1)	4.9803±2.8336	5.2035±2.9156		
	PDUV[VoS]_T_(3,1)	4.7139±2.5053	4.6158±2.4665		

Table 37: Effect of conditioning parameters for SIDA In-Distribution (ID) and Out-of-Distribution (OOD) datasets. Error-type 2 over KE from section 4.5 is presented.

MODEL	TAG	1M		50M	
		ID	OOD	ID	OOD
UNet	PDUV_F_(3,1)	0.5052±0.2615	2.5368±1.0710	0.1532±0.0897	1.4758±0.8257
	PDUV_T_(3,1)	1.3388±0.8539	9.7208±7.6245	0.7025±0.5759	11.4778±8.3256
	PDUV[VoS]_F_(3,1)	1.4473±1.0509	2.3929±1.6705	1.0164±0.8202	1.5336±0.9003
	PDUV[VoS]_T_(3,1)	1.6124±1.4219	13.7084±11.9033	3.1509±2.2207	19.8637±19.5043
FNO	PDUV_F_(3,1)	0.7682±0.5172	1.9919±1.3654	0.2823±0.1765	1.5754±1.9135
	PDUV_T_(3,1)	1.1989±1.1997	12.2212±8.6412	0.9527±1.0156	12.7779±10.6585
	PDUV[VoS]_F_(3,1)	8.5964±8.0247	7.1201±3.8520	4.9123±4.6565	14.2872±7.8378
	PDUV[VoS]_T_(3,1)	8.0715±11.6310	8.5574±5.6989	13.0682±10.7428	9.9693±6.6357
ViT	PDUV_F_(3,1)	6.6527±8.3450	32.5122±28.4652	0.9694±0.6501	3.3619±1.4849
	PDUV_T_(3,1)	5.3717±4.3670	10.2786±6.7211	1.0290±0.6755	5.2700±3.4986
	PDUV[VoS]_F_(3,1)	5.5548±5.2277	20.9420±21.4748	0.9345±0.7133	2.2616±0.7760
	PDUV[VoS]_T_(3,1)	7.3620±6.8146	6.6430±5.4757	1.6828±1.2214	6.3459±5.0306
ScOT	PDUV_F_(3,1)	2.6928±1.9141	2.5941±1.1618	1.0306±0.6112	2.1724±0.9115
	PDUV_T_(3,1)	3.9887±3.2842	11.9888±7.7975	1.8979±1.8130	5.5654±4.9727
	PDUV[VoS]_F_(3,1)	2.7987±2.8603	8.5151±4.4987	8.1992±5.7868	6.2404±3.3768
	PDUV[VoS]_T_(3,1)	6.5291±5.5513	5.6833±4.0009	9.0977±6.0278	22.1760±19.9296
CNO	PDUV_F_(3,1)	3.9209±2.3251	10.1072±9.3279	0.4011±0.2343	1.3602±0.6405
	PDUV_T_(3,1)	5.8777±6.1544	2.4288e8±2.9168e9	1.2505±0.9845	2.4099±2.0305
	PDUV[VoS]_F_(3,1)	4.3996±2.7430	24.1448±21.7419	6.0637±3.7637	6.9987±3.5410
	PDUV[VoS]_T_(3,1)	6.5098±6.0036	—	2.1665±2.1864	10.1886±11.2716
ResNet	PDUV_F_(3,1)	0.8521±0.5177	1.9815±0.8412		
	PDUV_T_(3,1)	1.5262±1.4191	28.0582±21.1096		
	PDUV[VoS]_F_(3,1)	1.7642±1.3131	2.4584±1.8013		
	PDUV[VoS]_T_(3,1)	2.7497±2.3888	34.0870±30.7161		
Transolver	PDUV_F_(3,1)	67.9430±41.9429	59.5887±20.7706		
	PDUV_T_(3,1)	93.0350±110.8223	258.0370±171.4161		
	PDUV[VoS]_F_(3,1)	83.0077±119.1757	35.9022±11.1758		
	PDUV[VoS]_T_(3,1)	102.3762±95.8241	162.3676±90.5726		

Table 38: Effect of conditioning parameters for SIDA In-Distribution (ID) and Out-of-Distribution (OOD) datasets. Error-type 2 over VP from section 4.5 is presented.

MODEL	TAG	1M		50M	
		ID	OOD	ID	OOD
UNet	PDUV_F_(3,1)	0.4678±0.5580	1.9011±1.4640	0.1094±0.1362	2.0724±1.6647
	PDUV_T_(3,1)	1.0717±1.8190	2.0873±2.1121	0.2973±0.2529	2.6720±2.2034
	PDUV[VoS]_F_(3,1)	1.2571±1.2591	1.2459±1.0752	0.5621±0.4353	2.3172±1.6960
	PDUV[VoS]_T_(3,1)	1.7996±1.7697	1.7940±1.4594	0.7514±1.5558	2.4527±2.0558
FNO	PDUV_F_(3,1)	0.9580±0.6336	2.1666±1.2573	0.4874±0.4576	1.7614±1.5075
	PDUV_T_(3,1)	1.3719±0.7673	2.7430±1.5973	0.6992±0.5029	1.5961±1.7109
	PDUV[VoS]_F_(3,1)	4.3073±8.5326	1.8055±1.3533	3.0148±4.1413	1.2411±0.9617
	PDUV[VoS]_T_(3,1)	1.4985±1.5211	3.7245±2.1666	1.4679±1.1389	3.9079±2.2991
ViT	PDUV_F_(3,1)	13.1278±16.1199	4.9536±5.5894	0.5882±0.9129	1.4598±2.5938
	PDUV_T_(3,1)	10.3206±10.3850	11.4467±13.3514	0.5533±0.6822	3.4015±5.2220
	PDUV[VoS]_F_(3,1)	17.3733±19.1933	5.2368±4.1392	5.3010±4.7988	2.2461±2.3365
	PDUV[VoS]_T_(3,1)	17.9269±18.2700	7.3386±7.3888	3.6743±3.3607	4.4309±5.3252
ScOT	PDUV_F_(3,1)	1.6140±2.9631	1.4442±0.6758	0.4774±0.8474	1.1108±0.9826
	PDUV_T_(3,1)	1.0985±1.9509	1.0331±0.7909	0.8093±1.4573	0.6340±0.6392
	PDUV[VoS]_F_(3,1)	2.3244±3.7987	1.2487±0.8233	2.5129±2.5532	0.7567±0.4354
	PDUV[VoS]_T_(3,1)	1.5664±2.8871	0.7565±0.4219	1.7867±3.6712	2.1391±2.2486
CNO	PDUV_F_(3,1)	1.9935±6.3802	0.9771±0.7020	0.2560±0.2127	2.0421±1.5173
	PDUV_T_(3,1)	3.3135±8.2291	8.6846e5±9.7652e6	0.4813±0.5887	1.7157±1.4923
	PDUV[VoS]_F_(3,1)	2.5010±3.3056	2.3219±1.6920	2.2471±5.3269	1.5615±1.2442
	PDUV[VoS]_T_(3,1)	2.3146±5.0735	1.3962e12±1.4557e13	0.9616±2.4379	2.9383±2.3800
ResNet	PDUV_F_(3,1)	0.5801±0.4023	1.6962±1.3323		
	PDUV_T_(3,1)	0.8478±0.6680	3.0296±2.2831		
	PDUV[VoS]_F_(3,1)	1.1306±0.5625	1.2508±1.0298		
	PDUV[VoS]_T_(3,1)	2.4775±2.0845	2.1219±1.5490		
Transolver	PDUV_F_(3,1)	42.3382±30.2457	23.1503±16.1705		
	PDUV_T_(3,1)	27.5997±22.3968	27.7379±18.3586		
	PDUV[VoS]_F_(3,1)	19.9930±27.6070	11.1969±3.1268		
	PDUV[VoS]_T_(3,1)	27.7826±22.1833	16.0020±15.6628		

Table 39: Effect of conditioning parameters for SIDA In-Distribution (ID) and Out-of-Distribution (OOD) datasets. Error-type 2 over COM from section 4.5 is presented.

MODEL	TAG	1M		50M	
		ID	OOD	ID	OOD
UNet	PDUV_F_(3,1)	0.0228±0.0126	0.5918±0.4201	0.0088±0.0047	0.7818±0.7129
	PDUV_T_(3,1)	0.0683±0.0405	1.8477±1.8043	0.0331±0.0224	0.5298±0.4377
	PDUV[VoS]_F_(3,1)	0.2094±0.3003	0.4709±0.4614	0.1798±0.2596	0.6587±0.5563
	PDUV[VoS]_T_(3,1)	0.1570±0.1729	1.0825±0.8026	0.1380±0.1897	0.9711±0.7603
FNO	PDUV_F_(3,1)	0.0271±0.0130	0.2420±0.3222	0.0118±0.0078	0.2427±0.2805
	PDUV_T_(3,1)	0.0486±0.0462	0.5155±0.4017	0.0386±0.0311	0.4851±0.4057
	PDUV[VoS]_F_(3,1)	0.2230±0.1315	0.5460±0.4013	0.1534±0.1235	0.8256±0.5094
	PDUV[VoS]_T_(3,1)	0.2803±0.1964	0.6526±0.5474	0.4330±0.2868	0.8936±0.5447
ViT	PDUV_F_(3,1)	0.1844±0.1821	1.0956±0.8733	0.0326±0.0211	0.2025±0.2268
	PDUV_T_(3,1)	0.2011±0.2260	1.3256±1.0355	0.0372±0.0299	0.2720±0.2121
	PDUV[VoS]_F_(3,1)	0.1523±0.1090	0.7958±0.7527	0.0826±0.0782	0.3130±0.3839
	PDUV[VoS]_T_(3,1)	0.1523±0.1243	0.4050±0.4486	0.0491±0.0476	0.2744±0.3014
ScOT	PDUV_F_(3,1)	0.0654±0.0360	0.3114±0.3727	0.0360±0.0209	0.2175±0.2388
	PDUV_T_(3,1)	0.1201±0.0702	0.6070±0.4590	0.0654±0.0505	0.3630±0.3077
	PDUV[VoS]_F_(3,1)	0.1470±0.1291	0.6403±0.4944	0.1550±0.1016	0.3504±0.3751
	PDUV[VoS]_T_(3,1)	0.1135±0.0753	0.5778±0.4467	0.1833±0.1173	0.4034±0.3748
CNO	PDUV_F_(3,1)	0.1067±0.0623	0.5085±0.6775	0.0152±0.0097	0.2450±0.2505
	PDUV_T_(3,1)	0.2181±0.1974	1.3132±0.9358	0.0485±0.0413	0.4230±0.3927
	PDUV[VoS]_F_(3,1)	0.0907±0.0534	0.2788±0.2190	0.0976±0.0675	0.4717±0.3578
	PDUV[VoS]_T_(3,1)	0.2610±0.1795	0.6138±0.5726	0.1189±0.1179	0.6371±0.6671
ResNet	PDUV_F_(3,1)	0.0387±0.0329	0.7315±0.6383		
	PDUV_T_(3,1)	0.0688±0.0477	1.0318±0.9240		
	PDUV[VoS]_F_(3,1)	0.1975±0.2441	0.6259±0.5556		
	PDUV[VoS]_T_(3,1)	0.1777±0.1831	0.8637±0.6592		
Transolver	PDUV_F_(3,1)	2.9121±1.6738	2.3465±0.9107		
	PDUV_T_(3,1)	3.9408±2.1468	2.5241±0.9979		
	PDUV[VoS]_F_(3,1)	3.7914±2.0321	2.4126±0.8926		
	PDUV[VoS]_T_(3,1)	3.4930±1.9160	2.3327±0.8712		

Table 40: Effect of conditioning fields for SIDA In-Distribution (ID) and Out-of-Distribution (OOD) datasets. Error-type 2 over output channels from section 4.5 is presented.

MODEL	TAG	1M		50M	
		ID	OOD	ID	OOD
UNet	PDUV_F_(1,1)	3.5661±2.4696	5.9914±3.2792	3.4983±2.5270	5.9438±3.2522
	PDUV[VoS]_F_(1,1)	3.9165±2.5452	6.1552±3.3755	3.8512±2.5096	6.0840±3.3590
	PDUV_F_(3,1)	0.3384±0.2089	2.2998±1.7754	0.1356±0.0976	1.9424±1.5948
	PDUV[VoS]_F_(3,1)	1.4203±1.1512	2.6100±1.8673	1.2162±1.0310	2.4740±1.8269
	PDUV_T_(3,1)	0.8690±0.4994	2.5683±1.8388	0.2272±0.1439	2.2561±1.7777
	PDUV[VoS]_T_(3,1)	1.6310±1.2358	2.7767±1.8269	1.1111±0.9569	2.4399±1.7482
	PDUV_F_(3,2)	0.4406±0.2437	2.1979±1.6703	0.1785±0.1080	1.8812±1.4977
	PDUV[VoS]_F_(3,2)	1.1622±0.8714	2.5568±1.8763	0.9378±0.8545	2.1892±1.6460
FNO	PDUV_F_(1,1)	3.5224±2.5529	6.0820±3.2896	3.4720±2.5577	5.9768±3.2572
	PDUV[VoS]_F_(1,1)	4.2901±3.0191	6.5170±3.5913	4.1024±2.7978	6.4133±3.4746
	PDUV_F_(3,1)	0.5333±0.2829	2.1215±1.5319	0.2498±0.1387	2.0963±1.5242
	PDUV[VoS]_F_(3,1)	1.8914±1.3113	2.6203±1.7532	1.7002±1.3234	2.6674±1.8160
	PDUV_T_(3,1)	0.7013±0.3424	1.8361±1.2131	0.4075±0.2168	1.7610±1.2616
	PDUV[VoS]_T_(3,1)	1.8383±1.2061	2.6599±1.7452	1.6667±1.0564	2.4769±1.6513
	PDUV_F_(3,2)	0.7123±0.3624	2.1449±1.5747	0.3389±0.1827	2.0990±1.5458
	PDUV[VoS]_F_(3,2)	1.8445±1.1729	2.5731±1.6426	1.5193±1.1838	2.4660±1.7004
ViT	PDUV_F_(1,1)	4.4758±2.8750	5.8219±3.1222	3.5527±2.7160	5.7645±3.1503
	PDUV[VoS]_F_(1,1)	4.6769±3.4301	5.6707±3.0938	3.9610±2.6804	5.8393±3.2097
	PDUV_F_(3,1)	1.5891±0.9548	3.4253±2.4145	0.4430±0.2336	1.8428±1.3876
	PDUV[VoS]_F_(3,1)	2.2152±1.5536	3.2082±2.2406	1.3497±1.0659	2.3674±1.7135
	PDUV_T_(3,1)	1.5949±1.0077	2.6376±1.7133	0.4249±0.2343	1.7359±1.3060
	PDUV[VoS]_T_(3,1)	2.0499±1.4162	3.0158±1.9680	1.2139±0.9433	2.0682±1.4535
	PDUV_F_(3,2)	1.3832±0.7495	2.4443±1.6647	0.5441±0.2699	1.8678±1.3767
	PDUV[VoS]_F_(3,2)	2.0047±1.2803	2.8629±1.8355	1.1189±0.8454	2.2224±1.5791
ScOT	PDUV_F_(1,1)	3.5764±2.5158	5.8985±3.2421	3.5173±2.6462	5.8306±3.1826
	PDUV[VoS]_F_(1,1)	4.7386±3.4158	5.7499±3.0977	2.0236±1.5584	4.3678±2.6511
	PDUV_F_(3,1)	0.6884±0.4222	1.9005±1.3770	0.2059±0.1199	1.6318±1.3494
	PDUV[VoS]_F_(3,1)	1.5944±1.2864	2.4643±1.7766	1.2171±1.0416	2.1314±1.5666
	PDUV_T_(3,1)	0.8203±0.4715	1.9132±1.2731	0.2461±0.1397	1.5425±1.1975
	PDUV[VoS]_T_(3,1)	1.4401±1.0497	2.2995±1.5283	1.1764±1.0238	1.9241±1.3649
	PDUV_F_(3,2)	0.7995±0.4265	1.9084±1.3867	0.2639±0.1459	1.5164±1.2414
	PDUV[VoS]_F_(3,2)	1.3294±0.9609	2.1893±1.5154	1.0655±0.9041	1.9709±1.4616
CNO	PDUV_F_(1,1)	3.9955±2.6786	5.8508±3.1777	3.5025±2.5455	5.9444±3.2344
	PDUV[VoS]_F_(1,1)	4.3438±2.7533	5.9778±3.2569	3.8389±2.5887	6.1782±3.4032
	PDUV_F_(3,1)	0.6943±0.4235	2.1707±1.8099	0.1621±0.1032	1.8159±1.4794
	PDUV[VoS]_F_(3,1)	1.1775±0.8980	2.1291±1.4489	1.2240±0.8859	2.3550±1.6215
	PDUV_T_(3,1)	0.9362±0.5384	66.43±453.50	0.3042±0.1905	2.3211±1.8495
	PDUV[VoS]_T_(3,1)	1.3235±0.9569	7898e1±6549e2	0.9654±0.7867	2.6471±1.9216
	PDUV_F_(3,2)	0.8584±0.4459	1.8360±1.3758	0.2210±0.1248	1.7634±1.3875
	PDUV[VoS]_F_(3,2)	1.2663±0.8642	1.9694±1.2874	1.0921±0.7494	2.3248±1.6283
ResNet	PDUV_F_(1,1)	3.7260±2.4574	6.0844±3.3406		
	PDUV[VoS]_F_(1,1)	4.0975±2.5778	5.9925±3.3210		
	PDUV_F_(3,1)	0.5570±0.3461	2.3042±1.7139		
	PDUV[VoS]_F_(3,1)	1.3341±1.0333	2.6392±1.8649		
	PDUV_T_(3,1)	1.0385±0.6198	3.0052±2.1978		
	PDUV[VoS]_T_(3,1)	1.6636±1.2058	3.2900±2.3078		
	PDUV_F_(3,2)	0.6356±0.3669	2.3012±1.6856		
	PDUV[VoS]_F_(3,2)	1.2118±0.9203	2.4939±1.7801		
Transolver	PDUV_F_(1,1)	5.7995±3.4502	6.9499±3.7154		
	PDUV[VoS]_F_(1,1)	5.6838±3.1902	6.6967±3.4709		
	PDUV_F_(3,1)	4.7065±2.6888	4.8852±2.7289		
	PDUV[VoS]_F_(3,1)	4.9803±2.8336	5.2035±2.9156		
	PDUV_T_(3,1)	4.7696±2.5778	4.6372±2.5046		
	PDUV[VoS]_T_(3,1)	4.7139±2.5053	4.6158±2.4665		
	PDUV_F_(3,2)	5.2026±2.7770	5.1580±2.7698		
	PDUV[VoS]_F_(3,2)	5.0919±2.7361	5.1995±2.8432		

Table 41: Effect of conditioning fields for SIDA In-Distribution (ID) and Out-of-Distribution (OOD) datasets. Error-type 2 over KE from section 4.5 is presented.

MODEL	TAG	1M		50M	
		ID	OOD	ID	OOD
UNet	PDUV_F_(1,1)	11.2017±29.5656	5.6983±3.0230	11.7372±31.0932	5.6613±2.9967
	PDUV[VoS]_F_(1,1)	13.3619±35.6175	5.5863±2.9830	12.0621±32.6814	5.6066±2.9599
	PDUV_F_(3,1)	0.5052±0.2615	2.5368±1.0710	0.1532±0.0897	1.4758±0.8257
	PDUV[VoS]_F_(3,1)	1.4473±1.0509	2.3929±1.6705	1.0164±0.8202	1.5336±0.9003
	PDUV_T_(3,1)	1.3388±0.8539	9.7208±7.6245	0.7025±0.5759	11.4778±8.3256
	PDUV[VoS]_T_(3,1)	1.6124±1.4219	13.7084±11.9033	3.1509±2.2207	19.8637±19.5043
	PDUV_F_(3,2)	0.9620±0.6433	9.6801±5.2064	0.4389±0.2677	2.2230±1.1932
	PDUV[VoS]_F_(3,2)	2.4488±1.9719	18.6904±11.8640	0.8829±0.7575	3.2323±1.6620
FNO	PDUV_F_(1,1)	10.8110±27.7074	5.7480±3.0231	10.7965±28.7023	5.6957±2.9859
	PDUV[VoS]_F_(1,1)	11.5359±30.3539	5.6379±3.0019	9.4723±24.4498	5.7736±3.0065
	PDUV_F_(3,1)	0.7682±0.5172	1.9919±1.3654	0.2823±0.1765	1.5754±1.9135
	PDUV[VoS]_F_(3,1)	8.5964±8.0247	7.1201±3.8520	4.9123±4.6565	14.2872±7.8378
	PDUV_T_(3,1)	1.1989±1.1997	12.2212±8.6412	0.9527±1.0156	12.7779±10.6585
	PDUV[VoS]_T_(3,1)	8.0715±11.6310	8.5574±5.6989	13.0682±10.7428	9.9693±6.6357
	PDUV_F_(3,2)	1.2933±0.6185	1.5242±0.8227	0.5000±0.3997	2.7004±1.5806
	PDUV[VoS]_F_(3,2)	9.4691±11.8198	5.7364±3.8886	2.9789±2.6236	9.1980±5.1366
ViT	PDUV_F_(1,1)	31.9704±87.7762	4.0911±2.0809	15.7706±44.1921	5.3135±2.7717
	PDUV[VoS]_F_(1,1)	45.4819±122.3350	3.2056±1.7203	19.0189±54.0257	4.9858±2.5512
	PDUV_F_(3,1)	6.6527±8.3450	32.5122±28.4652	0.9694±0.6501	3.3619±1.4849
	PDUV[VoS]_F_(3,1)	5.5548±5.2277	20.9420±21.4748	0.9345±0.7133	2.2616±0.7760
	PDUV_T_(3,1)	5.3717±4.3670	10.2786±6.7211	1.0290±0.6755	5.2700±3.4986
	PDUV[VoS]_T_(3,1)	7.3620±6.8146	6.6430±5.4757	1.6828±1.2214	6.3459±5.0306
	PDUV_F_(3,2)	5.3889±3.2322	5.4872±2.9669	1.9649±1.1585	2.7149±1.9905
	PDUV[VoS]_F_(3,2)	8.3093±6.0799	19.7742±12.6920	2.3528±1.3365	5.9363±2.9190
ScOT	PDUV_F_(1,1)	16.2807±44.8844	5.3495±2.8561	15.2877±42.6846	5.3579±2.8067
	PDUV[VoS]_F_(1,1)	32.4834±90.6835	3.9399±1.8714	6.1295±7.5593	1.8328±1.4427
	PDUV_F_(3,1)	2.6928±1.9141	2.5941±1.1618	1.0306±0.6112	2.1724±0.9115
	PDUV[VoS]_F_(3,1)	2.7987±2.8603	8.5151±4.4987	8.1992±5.7868	6.2404±3.3768
	PDUV_T_(3,1)	3.9887±3.2842	11.9888±7.7975	1.8979±1.8130	5.5654±4.9727
	PDUV[VoS]_T_(3,1)	6.5291±5.5513	5.6833±4.0009	9.0977±6.0278	22.1760±19.9296
	PDUV_F_(3,2)	4.2225±2.2977	9.6165±5.0281	1.7483±0.9528	5.3631±2.7718
	PDUV[VoS]_F_(3,2)	3.7081±2.5449	6.3008±2.9780	2.3370±1.6511	4.1953±1.7958
CNO	PDUV_F_(1,1)	17.6490±49.1966	5.0935±2.5799	12.7633±35.2539	5.5010±2.8628
	PDUV[VoS]_F_(1,1)	34.8635±91.4468	4.3743±2.4571	11.2465±26.6401	5.8412±3.1259
	PDUV_F_(3,1)	3.9209±2.3251	10.1072±9.3279	0.4011±0.2343	1.3602±0.6405
	PDUV[VoS]_F_(3,1)	4.3996±2.7430	24.1448±21.7419	6.0637±3.7637	6.9987±3.5410
	PDUV_T_(3,1)	5.8777±6.1544	2428e5±2916e5	1.2505±0.9845	2.4099±2.0305
	PDUV[VoS]_T_(3,1)	6.5098±6.0036	–	2.1665±2.1864	10.1886±11.2716
	PDUV_F_(3,2)	4.9192±3.6170	20.5139±13.7615	0.8113±0.5196	1.3482±0.7874
	PDUV[VoS]_F_(3,2)	8.8186±4.5825	15.8403±6.7297	7.7326±4.5056	7.9407±4.5767
ResNet	PDUV_F_(1,1)	10.9262±28.4670	5.7403±3.0356		
	PDUV[VoS]_F_(1,1)	27.4023±76.4492	4.4619±2.2558		
	PDUV_F_(3,1)	0.8521±0.5177	1.9815±0.8412		
	PDUV[VoS]_F_(3,1)	1.7642±1.3131	2.4584±1.8013		
	PDUV_T_(3,1)	1.5262±1.4191	28.0582±21.1096		
	PDUV[VoS]_T_(3,1)	2.7497±2.3888	34.0870±30.7161		
	PDUV_F_(3,2)	1.4069±0.6998	5.6830±3.2346		
	PDUV[VoS]_F_(3,2)	3.2122±2.2595	9.1524±3.6021		
Transolver	PDUV_F_(1,1)	21.6155±58.9766	5.0188±2.6784		
	PDUV[VoS]_F_(1,1)	69.0841±195.2310	4.1611±2.9672		
	PDUV_F_(3,1)	67.9430±41.9429	59.5887±20.7706		
	PDUV[VoS]_F_(3,1)	83.0077±119.1757	35.9022±11.1758		
	PDUV_T_(3,1)	93.0350±110.8223	258.0369±171.4161		
	PDUV[VoS]_T_(3,1)	102.3762±95.8241	162.3676±90.5726		
	PDUV_F_(3,2)	181.1406±151.2849	96.0656±48.8018		
	PDUV[VoS]_F_(3,2)	113.5771±105.2289	77.0457±28.0248		

Table 42: Effect of conditioning fields for SIDA In-Distribution (ID) and Out-of-Distribution (OOD) datasets. Error-type 2 over VP from section 4.5 is presented.

MODEL	TAG	1M		50M	
		ID	OOD	ID	OOD
UNet	PDUV_F_(1,1)	4.8548±9.7684	5.1872±2.8746	5.1272±10.2187	5.1860±2.8710
	PDUV[VoS]_F_(1,1)	4.7080±9.0211	5.3153±2.9026	4.6359±5.0888	5.5856±3.1400
	PDUV_F_(3,1)	0.4678±0.5580	1.9011±1.4640	0.1094±0.1362	2.0724±1.6647
	PDUV[VoS]_F_(3,1)	1.2571±1.2591	1.2459±1.0752	0.5621±0.4353	2.3172±1.6960
	PDUV_T_(3,1)	1.0717±1.8190	2.0873±2.1121	0.2973±0.2529	2.6720±2.2034
	PDUV[VoS]_T_(3,1)	1.7996±1.7697	1.7940±1.4594	0.7514±1.5558	2.4527±2.0558
	PDUV_F_(3,2)	0.7461±1.0477	2.4576±1.7732	0.3118±0.3532	2.1101±1.7997
	PDUV[VoS]_F_(3,2)	2.0485±2.9920	1.5854±1.0366	0.6229±0.4991	2.2803±1.6937
FNO	PDUV_F_(1,1)	4.6886±8.4082	5.4445±2.9026	4.7255±9.1404	5.3154±2.8825
	PDUV[VoS]_F_(1,1)	4.7356±3.4140	5.9386±3.2272	5.5056±12.1875	5.2449±2.7262
	PDUV_F_(3,1)	0.9580±0.6336	2.1666±1.2573	0.4874±0.4576	1.7614±1.5075
	PDUV[VoS]_F_(3,1)	4.3073±8.5326	1.8055±1.3533	3.0148±4.1413	1.2411±0.9617
	PDUV_T_(3,1)	1.3719±0.7673	2.7430±1.5973	0.6992±0.5029	1.5961±1.7109
	PDUV[VoS]_T_(3,1)	1.4985±1.5211	3.7245±2.1666	1.4679±1.1389	3.9079±2.2991
	PDUV_F_(3,2)	1.1520±0.7034	2.7981±1.6515	0.6015±0.4159	1.3866±0.9442
	PDUV[VoS]_F_(3,2)	6.4856±9.7679	2.6203±1.6912	1.9468±2.0439	0.9703±0.8280
ViT	PDUV_F_(1,1)	28.3750±59.3870	2.6103±1.1959	5.4192±11.6520	5.0160±2.7830
	PDUV[VoS]_F_(1,1)	78.3286±188.0569	6.6896±6.4194	10.8812±26.3883	4.0604±2.1094
	PDUV_F_(3,1)	13.1278±16.1199	4.9536±5.5894	0.5882±0.9129	1.4598±2.5938
	PDUV[VoS]_F_(3,1)	17.3733±19.1933	5.2368±4.1392	5.3010±4.7988	2.2461±2.3365
	PDUV_T_(3,1)	10.3206±10.3850	11.4467±13.3514	0.5533±0.6822	3.4015±5.2220
	PDUV[VoS]_T_(3,1)	17.9269±18.2700	7.3386±7.3888	3.6743±3.3607	4.4309±5.3252
	PDUV_F_(3,2)	4.1804±4.5308	2.1003±1.7241	0.8756±1.1214	1.7605±2.6311
	PDUV[VoS]_F_(3,2)	10.2143±10.9571	3.9340±3.2964	2.1356±2.0161	1.3421±1.2843
ScOT	PDUV_F_(1,1)	5.0246±10.1023	5.1421±2.8596	5.4551±12.0375	4.9934±2.7667
	PDUV[VoS]_F_(1,1)	9.3970±23.3038	4.3577±2.2503	1.6456±3.2854	3.6278±2.1986
	PDUV_F_(3,1)	1.6140±2.9631	1.4442±0.6758	0.4774±0.8474	1.1108±0.9826
	PDUV[VoS]_F_(3,1)	2.3244±3.7987	1.2487±0.8233	2.5129±2.5532	0.7567±0.4354
	PDUV_T_(3,1)	1.0985±1.9509	1.0331±0.7909	0.8093±1.4573	0.6340±0.6392
	PDUV[VoS]_T_(3,1)	1.5664±2.8871	0.7565±0.4219	1.7867±3.6712	2.1391±2.2486
	PDUV_F_(3,2)	1.3736±2.0323	0.7779±0.5431	0.8046±1.0890	0.7494±0.6484
	PDUV[VoS]_F_(3,2)	1.1559±1.8917	1.0690±0.8675	2.3292±3.2330	1.0448±0.4318
CNO	PDUV_F_(1,1)	5.0839±10.2831	5.0351±2.8432	5.0165±10.3994	5.0809±2.8365
	PDUV[VoS]_F_(1,1)	4.8944±10.2847	5.1612±2.8534	4.4769±6.0270	5.4406±3.0542
	PDUV_F_(3,1)	1.9935±6.3802	0.9771±0.7020	0.2560±0.2127	2.0421±1.5173
	PDUV[VoS]_F_(3,1)	2.5010±3.3056	2.3219±1.6920	2.2471±5.3269	1.5615±1.2442
	PDUV_T_(3,1)	3.3135±8.2291	8684e2±9765e3	0.4813±0.5887	1.7157±1.4923
	PDUV[VoS]_T_(3,1)	2.3146±5.0735	1396e9±1455e10	0.9616±2.4379	2.9383±2.3800
	PDUV_F_(3,2)	3.4611±6.6855	2.8181±1.6026	0.5898±0.4428	2.1937±1.6745
	PDUV[VoS]_F_(3,2)	3.0088±6.6812	1.0182±0.8092	3.0996±5.7459	1.5902±1.2229
ResNet	PDUV_F_(1,1)	5.1266±10.6196	5.1755±2.8330		
	PDUV[VoS]_F_(1,1)	6.0033±14.0618	4.9715±2.6616		
	PDUV_F_(3,1)	0.5801±0.4023	1.6962±1.3323		
	PDUV[VoS]_F_(3,1)	1.1306±0.5625	1.2508±1.0298		
	PDUV_T_(3,1)	0.8478±0.6680	3.0296±2.2831		
	PDUV[VoS]_T_(3,1)	2.4775±2.0845	2.1219±1.5490		
	PDUV_F_(3,2)	0.6297±0.4655	2.2821±1.5949		
	PDUV[VoS]_F_(3,2)	0.7945±0.6044	1.8356±1.2950		
Transolver	PDUV_F_(1,1)	6.9632±15.3887	5.0256±2.5608		
	PDUV[VoS]_F_(1,1)	9.8138±26.7480	4.8703±2.2493		
	PDUV_F_(3,1)	42.3382±30.2457	23.1503±16.1705		
	PDUV[VoS]_F_(3,1)	19.9930±27.6070	11.1969±3.1268		
	PDUV_T_(3,1)	27.5997±22.3968	27.7379±18.3586		
	PDUV[VoS]_T_(3,1)	27.7826±22.1833	16.0020±15.6628		
	PDUV_F_(3,2)	11.3000±14.7913	1.8346±1.1888		
	PDUV[VoS]_F_(3,2)	9.2376±12.2430	2.5793±1.7156		

Table 43: Effect of conditioning fields for SIDA In-Distribution (ID) and Out-of-Distribution (OOD) datasets. Error-type 2 over COM from section 4.5 is presented.

MODEL	TAG	1M		50M	
		ID	OOD	ID	OOD
UNet	PDUV_F_(1,1)	0.2325±0.2905	0.9394±0.9670	0.2235±0.3098	0.9910±0.9754
	PDUV[VoS]_F_(1,1)	0.2669±0.3680	1.0355±1.0419	0.2547±0.3429	1.0036±1.0209
	PDUV_F_(3,1)	0.0228±0.0126	0.5918±0.4201	0.0088±0.0047	0.7818±0.7129
	PDUV[VoS]_F_(3,1)	0.2094±0.3003	0.4709±0.4614	0.1798±0.2596	0.6587±0.5563
	PDUV_T_(3,1)	0.0683±0.0405	1.8477±1.8043	0.0331±0.0224	0.5298±0.4377
	PDUV[VoS]_T_(3,1)	0.1570±0.1729	1.0825±0.8026	0.1380±0.1897	0.9711±0.7603
	PDUV_F_(3,2)	0.0566±0.0265	0.4628±0.4387	0.0251±0.0148	0.5248±0.4867
	PDUV[VoS]_F_(3,2)	0.1600±0.1434	1.0387±0.6696	0.1552±0.1965	0.7248±0.6708
FNO	PDUV_F_(1,1)	0.2377±0.3125	1.0179±0.9760	0.2188±0.2944	0.9605±0.9621
	PDUV[VoS]_F_(1,1)	0.2766±0.3603	1.0277±1.0291	0.2747±0.3434	0.9904±1.0263
	PDUV_F_(3,1)	0.0271±0.0130	0.2420±0.3222	0.0118±0.0078	0.2427±0.2805
	PDUV[VoS]_F_(3,1)	0.2230±0.1315	0.5460±0.4013	0.1534±0.1235	0.8256±0.5094
	PDUV_T_(3,1)	0.0486±0.0462	0.5155±0.4017	0.0386±0.0311	0.4851±0.4057
	PDUV[VoS]_T_(3,1)	0.2803±0.1964	0.6526±0.5474	0.4330±0.2868	0.8936±0.5447
	PDUV_F_(3,2)	0.0561±0.0319	0.2477±0.3338	0.0267±0.0141	0.2091±0.2934
	PDUV[VoS]_F_(3,2)	0.4183±0.1414	0.5852±0.4017	0.1546±0.1802	0.7524±0.5978
ViT	PDUV_F_(1,1)	0.3214±0.2879	0.8025±0.8487	0.2269±0.2774	0.9255±0.9327
	PDUV[VoS]_F_(1,1)	0.3038±0.2661	0.8288±0.8959	0.2590±0.3339	0.9899±1.0103
	PDUV_F_(3,1)	0.1844±0.1821	1.0956±0.8733	0.0326±0.0211	0.2025±0.2268
	PDUV[VoS]_F_(3,1)	0.1523±0.1090	0.7958±0.7527	0.0826±0.0782	0.3130±0.3839
	PDUV_T_(3,1)	0.2011±0.2260	1.3256±1.0355	0.0372±0.0299	0.2720±0.2121
	PDUV[VoS]_T_(3,1)	0.1523±0.1243	0.4050±0.4486	0.0491±0.0476	0.2744±0.3014
	PDUV_F_(3,2)	0.2007±0.1252	0.4172±0.3822	0.0751±0.0418	0.1544±0.1388
	PDUV[VoS]_F_(3,2)	0.1785±0.1410	0.9977±0.6339	0.0679±0.0424	0.3529±0.3592
ScOT	PDUV_F_(1,1)	0.2393±0.3107	0.9747±0.9872	0.2238±0.2732	0.9072±0.9265
	PDUV[VoS]_F_(1,1)	0.2696±0.2834	0.7985±0.8553	0.1273±0.1445	0.6410±0.7542
	PDUV_F_(3,1)	0.0654±0.0359	0.3114±0.3727	0.0360±0.0209	0.2175±0.2388
	PDUV[VoS]_F_(3,1)	0.1470±0.1291	0.6403±0.4944	0.1550±0.1016	0.3504±0.3751
	PDUV_T_(3,1)	0.1201±0.0702	0.6070±0.4590	0.0654±0.0505	0.3630±0.3077
	PDUV[VoS]_T_(3,1)	0.1135±0.0753	0.5778±0.4467	0.1833±0.1173	0.4034±0.3748
	PDUV_F_(3,2)	0.1993±0.0869	0.3583±0.2814	0.0623±0.0293	0.2439±0.3005
	PDUV[VoS]_F_(3,2)	0.1407±0.1018	0.4966±0.3738	0.1141±0.1122	0.4051±0.3803
CNO	PDUV_F_(1,1)	0.4844±0.6753	0.6387±0.6294	0.2202±0.2753	0.9190±0.9273
	PDUV[VoS]_F_(1,1)	0.3139±0.3389	0.7298±0.8015	0.2666±0.3817	1.0782±1.0407
	PDUV_F_(3,1)	0.1067±0.0623	0.5085±0.6775	0.0152±0.0097	0.2450±0.2505
	PDUV[VoS]_F_(3,1)	0.0907±0.0534	0.2788±0.2190	0.0976±0.0675	0.4717±0.3578
	PDUV_T_(3,1)	0.2181±0.1974	1.3132±0.9358	0.0485±0.0413	0.4230±0.3927
	PDUV[VoS]_T_(3,1)	0.2610±0.1795	0.6138±0.5726	0.1189±0.1179	0.6371±0.6671
	PDUV_F_(3,2)	0.1791±0.1004	0.3669±0.2622	0.0337±0.0189	0.2031±0.2339
	PDUV[VoS]_F_(3,2)	0.3016±0.1480	0.6484±0.3145	0.2154±0.0912	0.6700±0.4355
ResNet	PDUV_F_(1,1)	0.2284±0.3093	0.9806±0.9846		
	PDUV[VoS]_F_(1,1)	0.2574±0.2885	0.9271±0.9708		
	PDUV_F_(3,1)	0.0387±0.0329	0.7315±0.6383		
	PDUV[VoS]_F_(3,1)	0.1975±0.2441	0.6259±0.5556		
	PDUV_T_(3,1)	0.0688±0.0477	1.0318±0.9240		
	PDUV[VoS]_T_(3,1)	0.1777±0.1831	0.8637±0.6592		
	PDUV_F_(3,2)	0.0729±0.0535	0.4976±0.3697		
	PDUV[VoS]_F_(3,2)	0.1063±0.0724	0.8453±0.5704		
Transolver	PDUV_F_(1,1)	0.6920±0.4419	0.7175±0.7466		
	PDUV[VoS]_F_(1,1)	1.4407±1.0233	0.7835±0.5373		
	PDUV_F_(3,1)	2.9121±1.6738	2.3465±0.9107		
	PDUV[VoS]_F_(3,1)	3.7914±2.0321	2.4126±0.8926		
	PDUV_T_(3,1)	3.9408±2.1468	2.5241±0.9979		
	PDUV[VoS]_T_(3,1)	3.4930±1.9160	2.3327±0.8712		
	PDUV_F_(3,2)	4.0355±2.0120	2.7159±1.0297		
	PDUV[VoS]_F_(3,2)	4.1446±2.1033	2.6625±1.0178		

D ERROR ROLLOUT OVER TIMESTEPS

D.1 ERROR ROLLOUT OVER TIMESTEPS FOR THE LIDE DATASET

The evolution of cumulative nRMSE is studied in a cumulative fashion over timesteps for 1M and 50M models on the test trajectories of both In-Distribution (ID) and Out-of-Distribution (OOD) LIDE datasets.

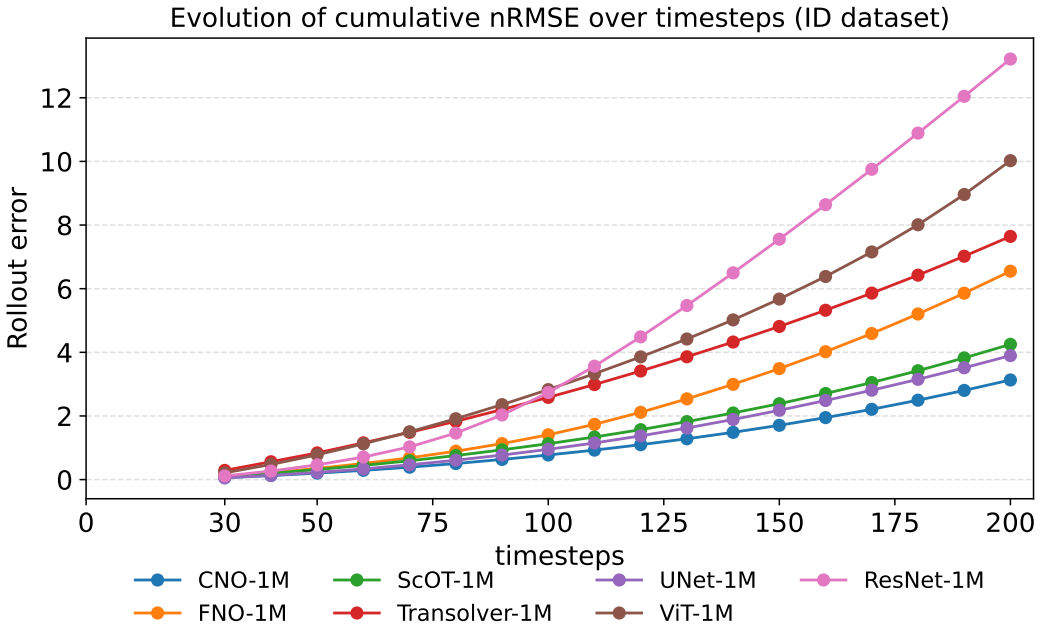

Figure 9: Temporal rollout of cumulative nRMSE over output channels for the LIDE-ID-Experiment PDUV_F_(3,1) for all 1M models.

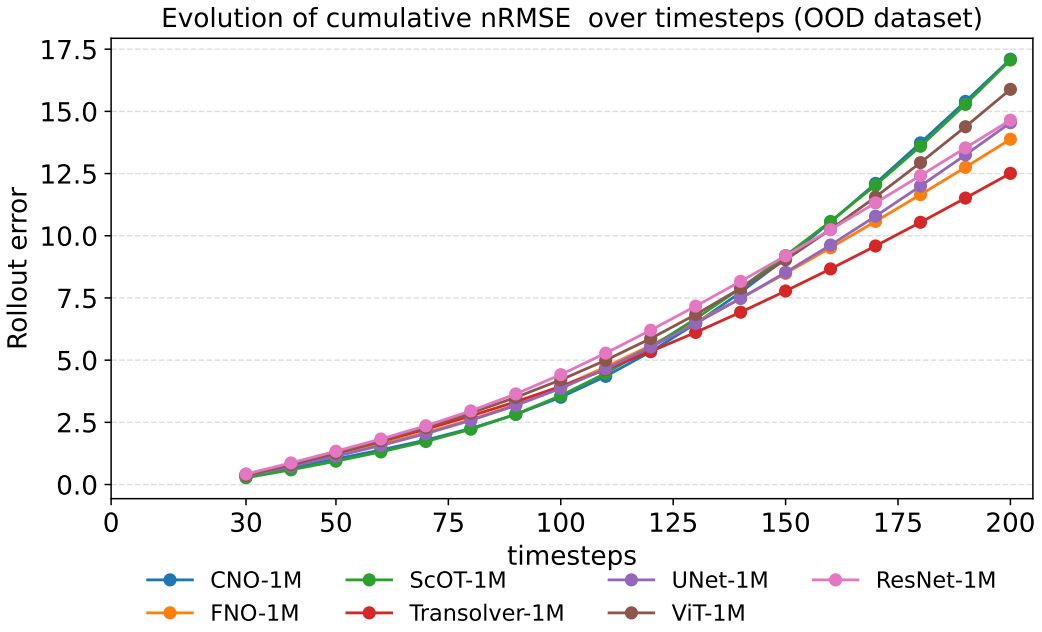

Figure 10: Temporal rollout of cumulative nRMSE over output channels for the LIDE-OOD-Experiment PDUV_F_(3,1) for all 1M models.

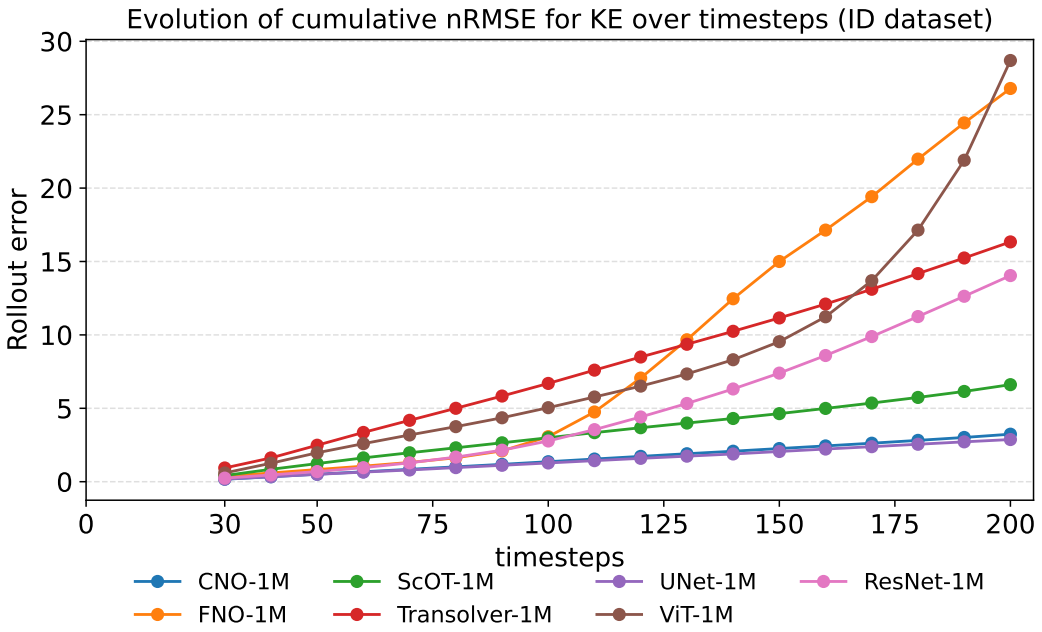

Figure 11: Temporal rollout of cumulative nRMSE over KE for the LIDE-ID-Experiment PDUV_F_(3,1) for all 1M models.

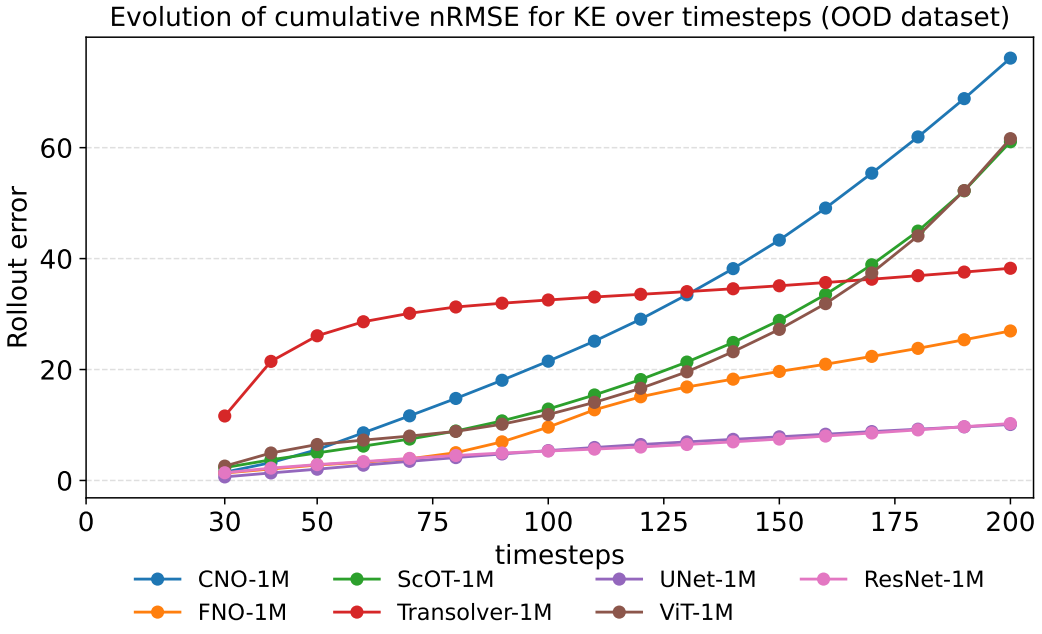

Figure 12: Temporal rollout of cumulative nRMSE over KE for the LIDE-OOD-Experiment PDUV_F_(3,1) for all 1M models.

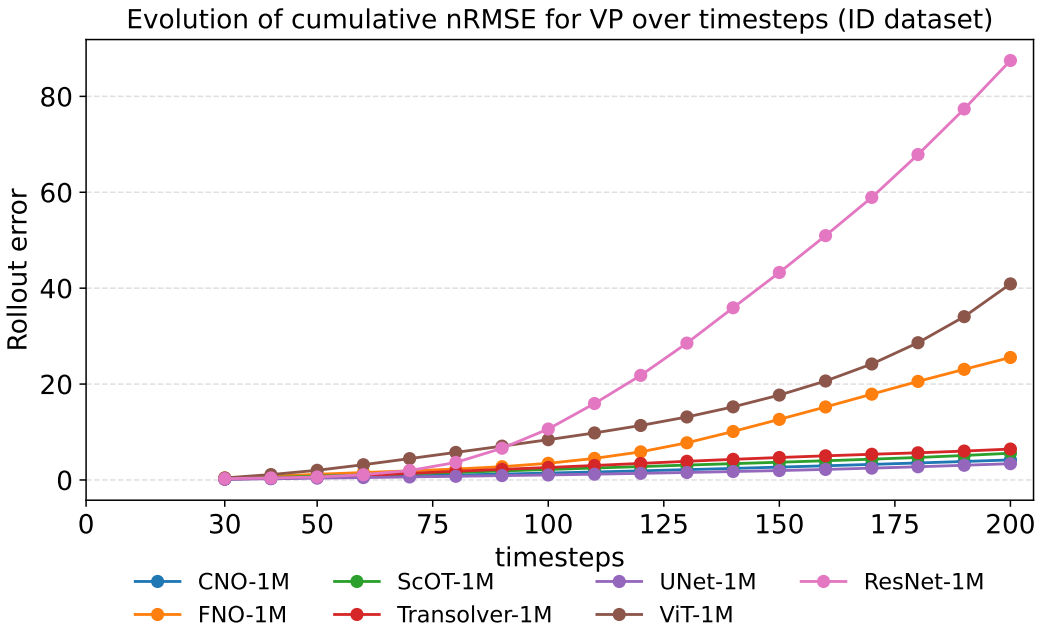

Figure 13: Temporal rollout of cumulative nRMSE over VP for the LIDE-ID-Experiment PDUV_F_(3,1) for all 1M models.

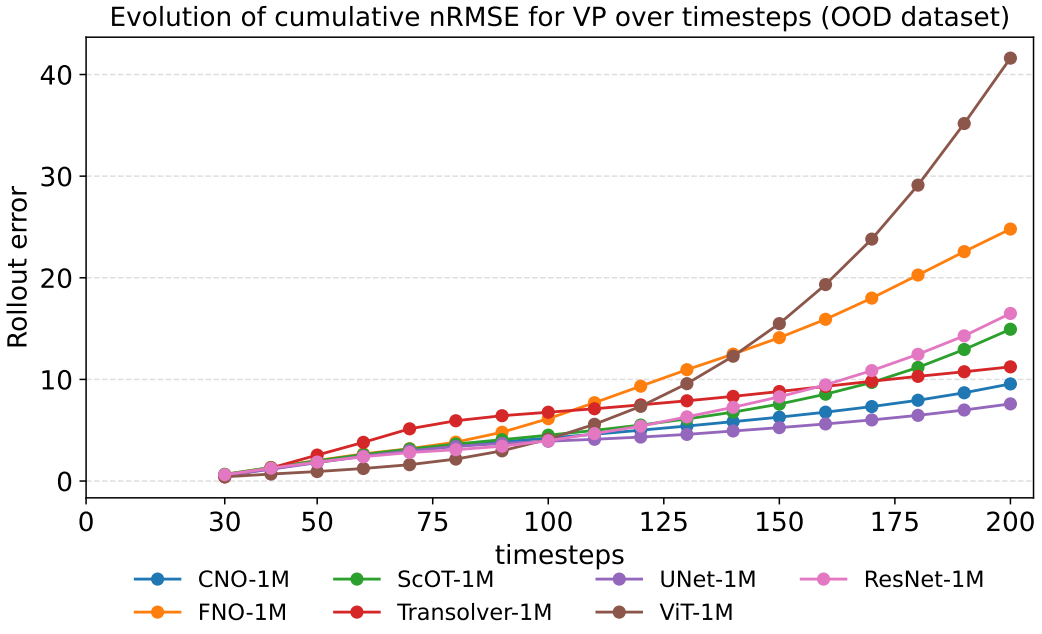

Figure 14: Temporal rollout of cumulative nRMSE over VP for the LIDE-OOD-Experiment PDUV_F_(3,1) for all 1M models.

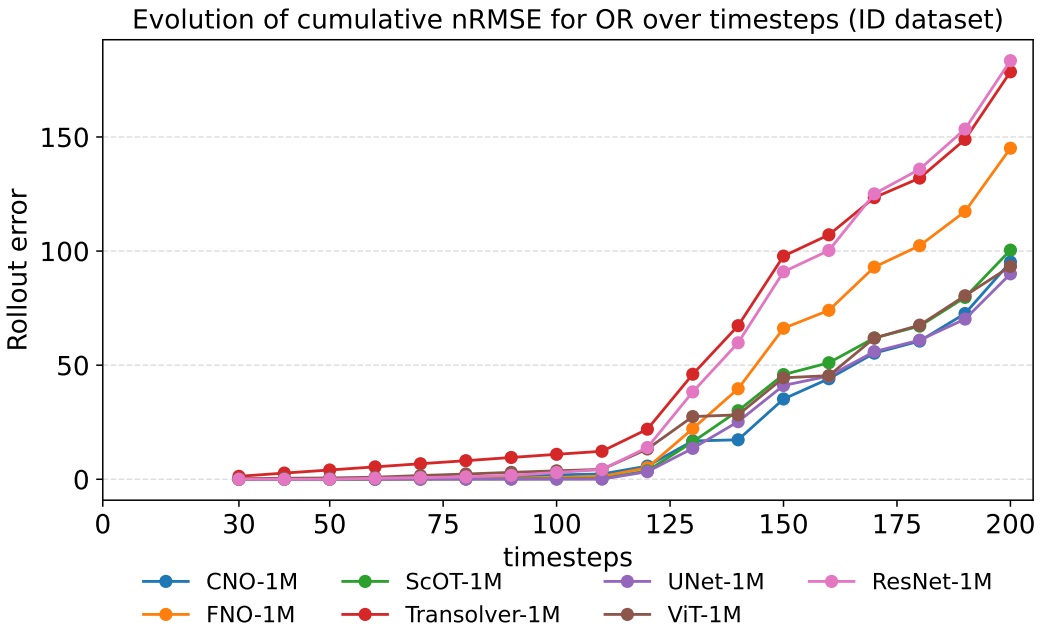

Figure 15: Temporal rollout of cumulative nRMSE over OR for the LIDE-ID-Experiment PDUV_F_(3,1) for all 1M models.

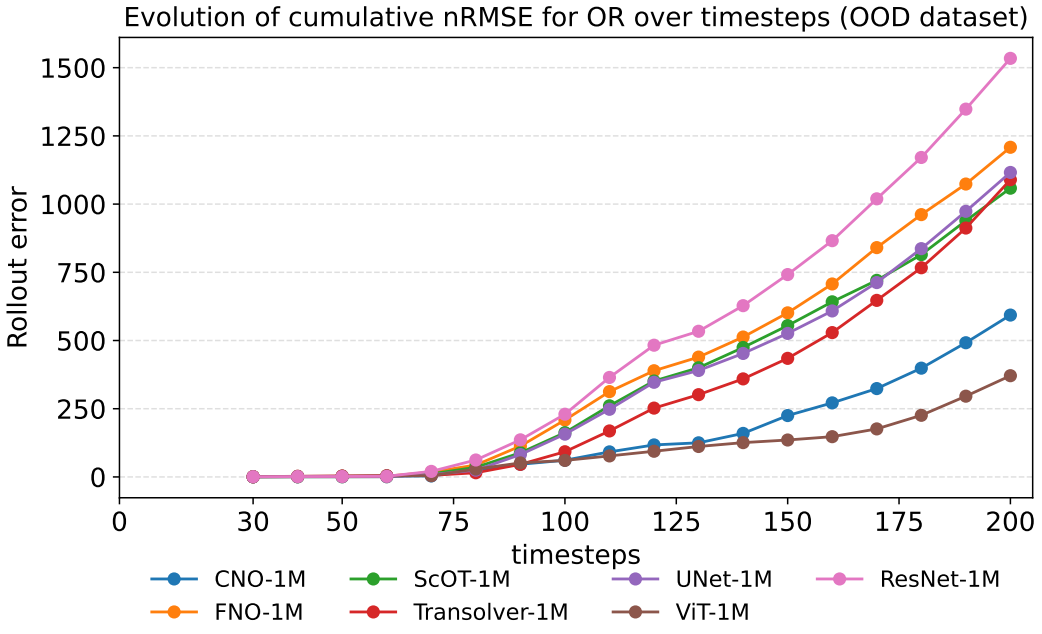

Figure 16: Temporal rollout of cumulative nRMSE over OR for the LIDE-OOD-Experiment PDUV_F_(3,1) for all 1M models.

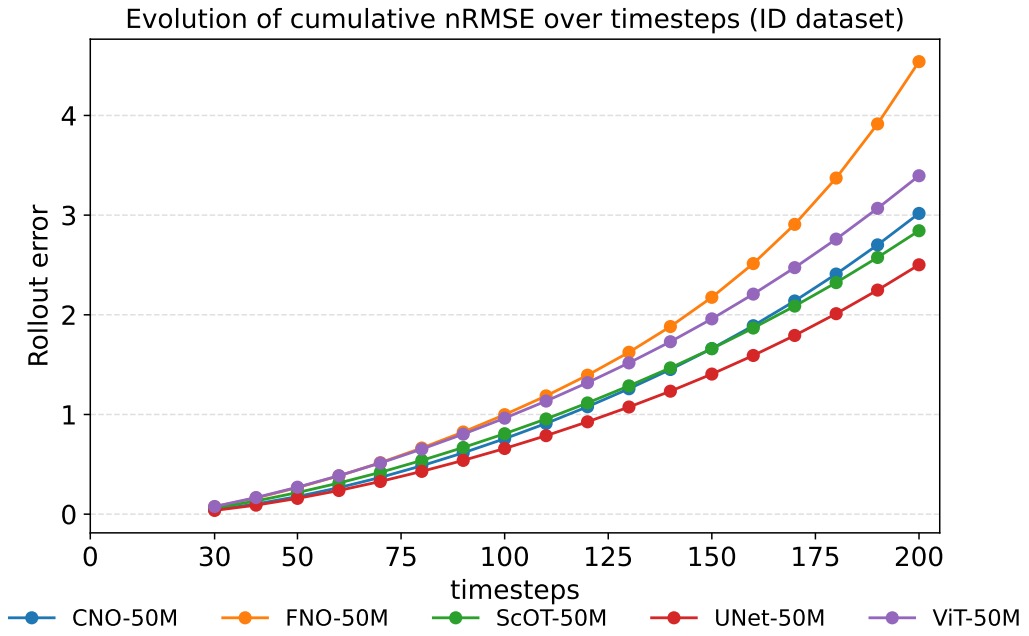

Figure 17: Temporal rollout of cumulative nRMSE over output channels for the LIDE-ID-Experiment PDUV_F_(3,1) for all 50M models.

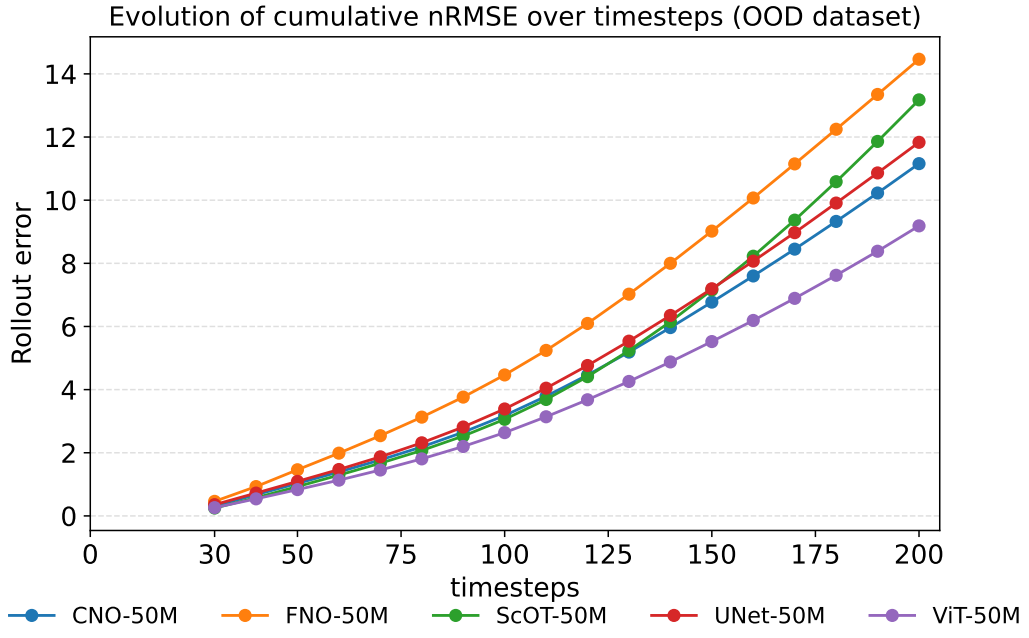

Figure 18: Temporal rollout of cumulative nRMSE over output channels for the LIDE-OOD-Experiment PDUV_F_(3,1) for all 50M models.

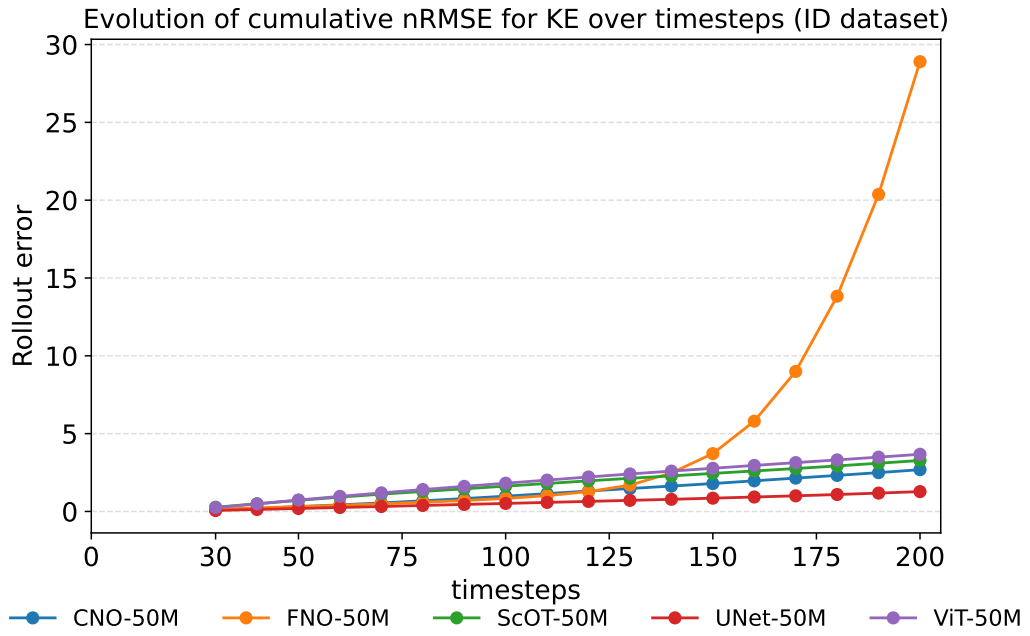

Figure 19: Temporal rollout of cumulative nRMSE over KE for the LIDE-ID-Experiment PDUV_F_(3,1) for all 50M models.

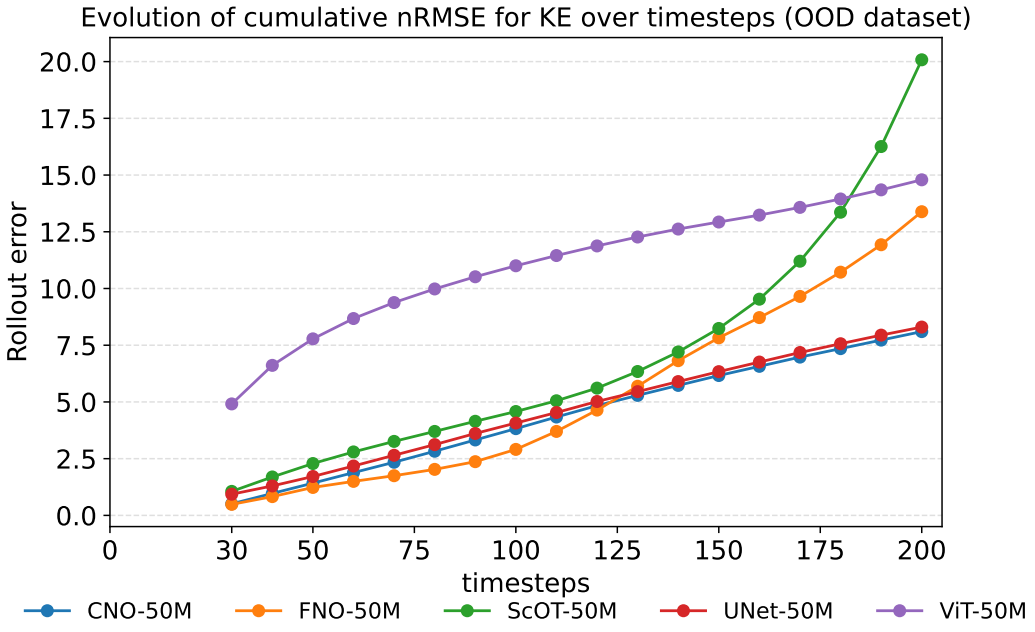

Figure 20: Temporal rollout of cumulative nRMSE over KE for the LIDE-OOD-Experiment PDUV_F_(3,1) for all 50M models.

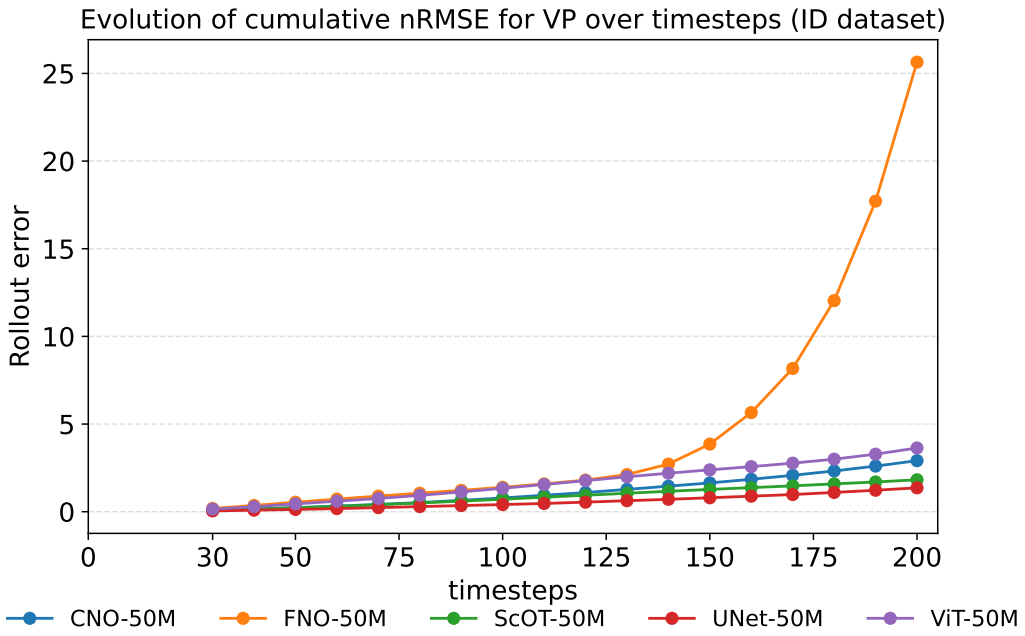

Figure 21: Temporal rollout of cumulative nRMSE over VP for the LIDE-ID-Experiment PDUV_F_(3,1) for all 50M models.

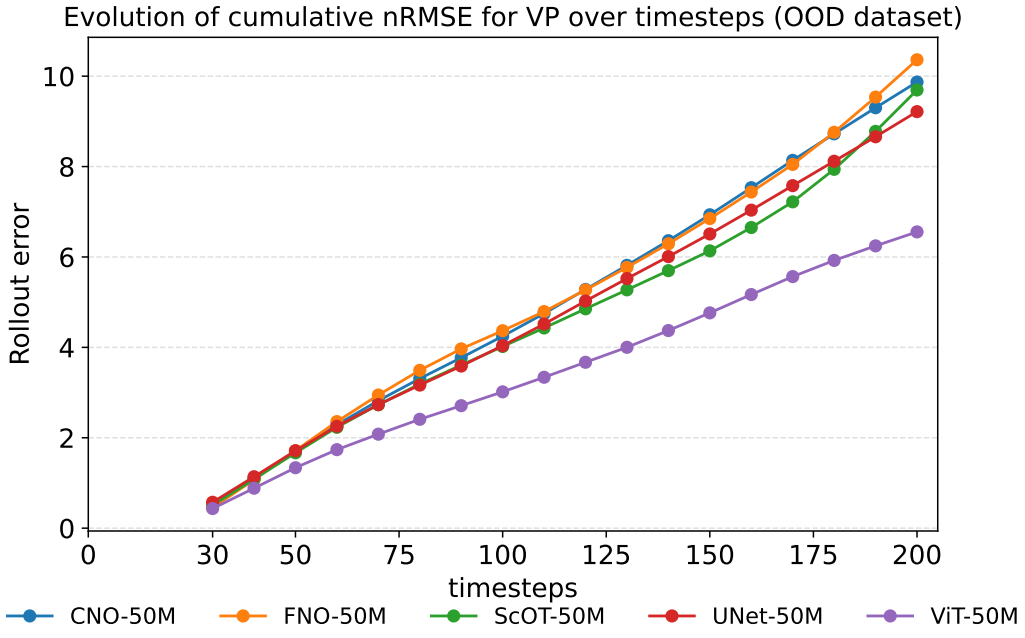

Figure 22: Temporal rollout of cumulative nRMSE over VP for the LIDE-OOD-Experiment PDUV_F_(3,1) for all 50M models.

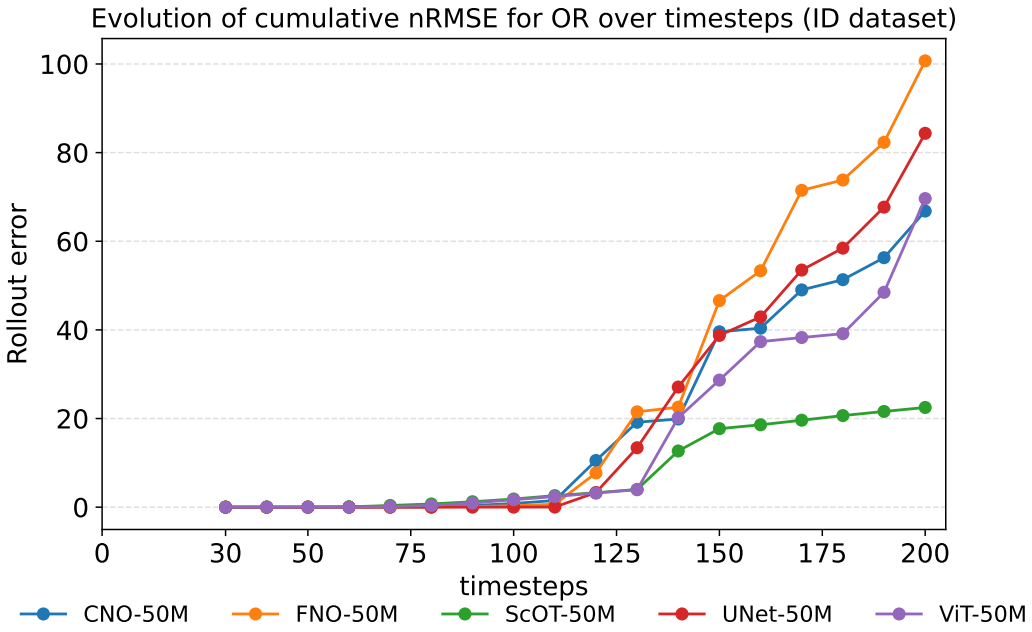

Figure 23: Temporal rollout of cumulative nRMSE over OR for the LIDE-ID-Experiment PDUV_F_(3,1) for all 50M models.

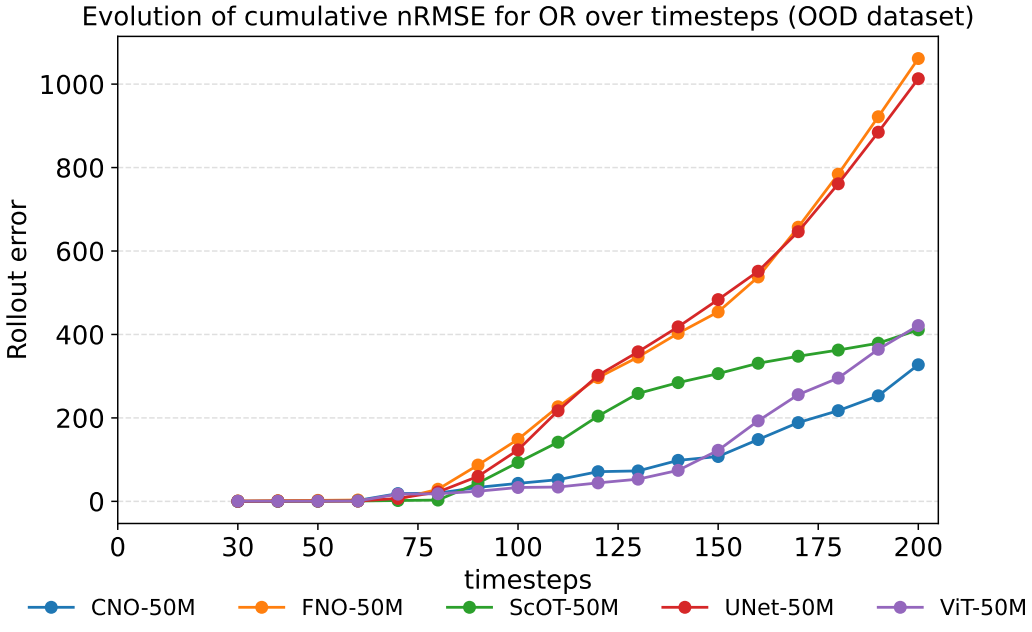

Figure 24: Temporal rollout of cumulative nRMSE over OR for the LIDE-OOD-Experiment PDUV_F_(3,1) for all 50M models.

D.2 Error rollout over timesteps for the SIDA dataset

The evolution of nRMSE is studied in a cumulative fashion over timesteps for 1M and 50M models on the test trajectories of both In-Distribution (ID) and Out-of-Distribution (OOD) SIDA datasets.

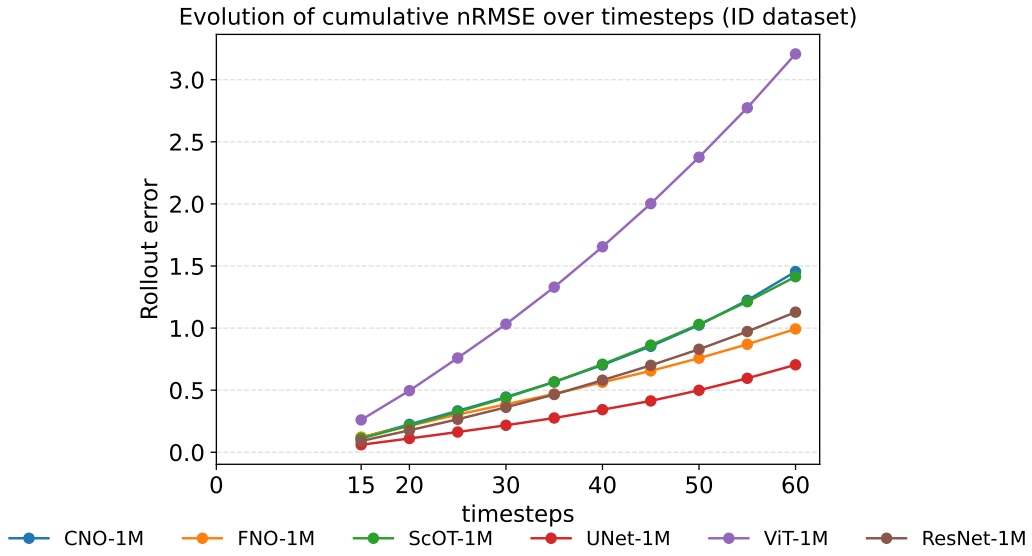

Figure 25: Temporal rollout of cumulative nRMSE over output channels for the SIDA-ID-Experiment PDUV_F_(3,1) for all 1M models.

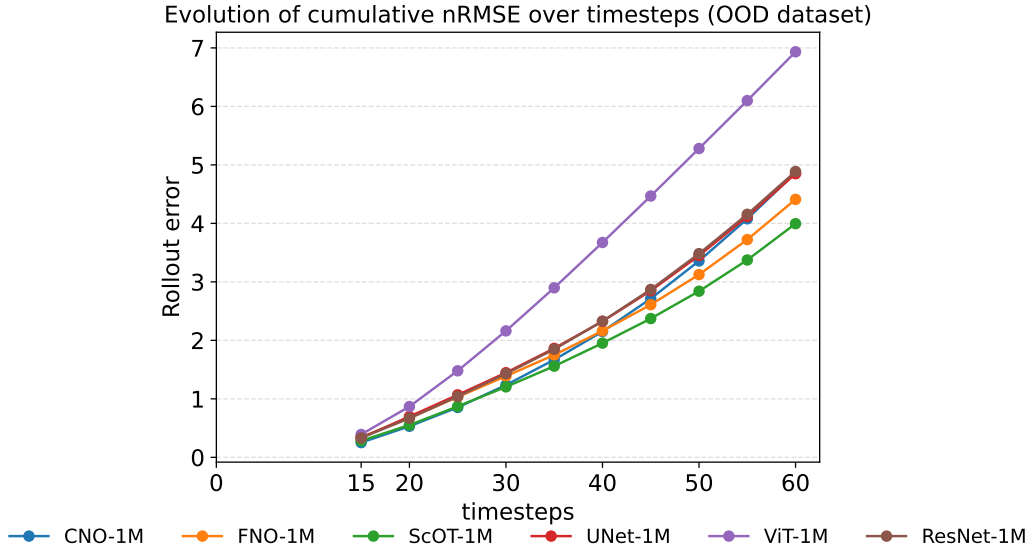

Figure 26: Temporal rollout of cumulative nRMSE over output channels for the SIDA-OOD-Experiment PDUV_F_(3,1) for all 1M models.

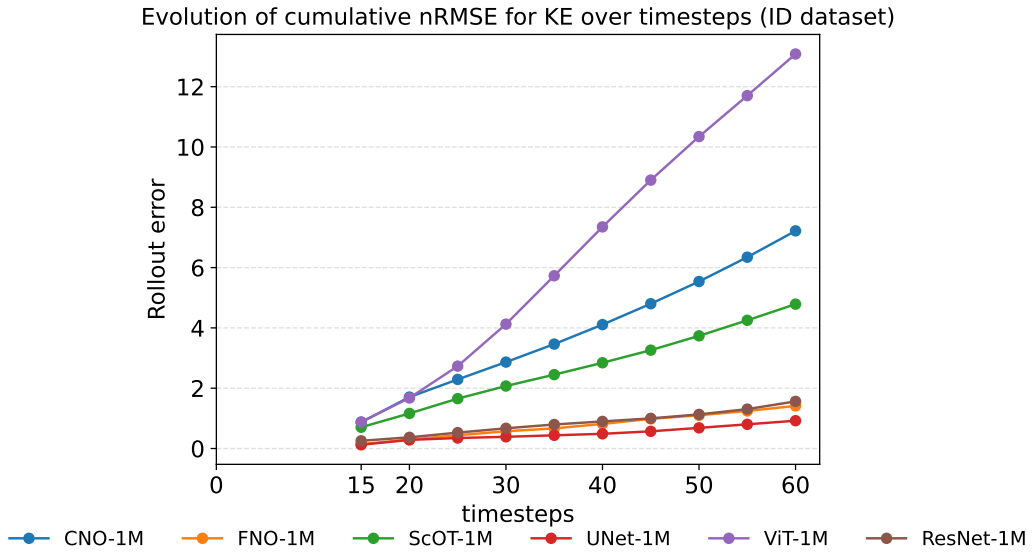

Figure 27: Temporal rollout of cumulative nRMSE over KE for the SIDA-ID-Experiment PDUV_F_(3,1) for all 1M models.

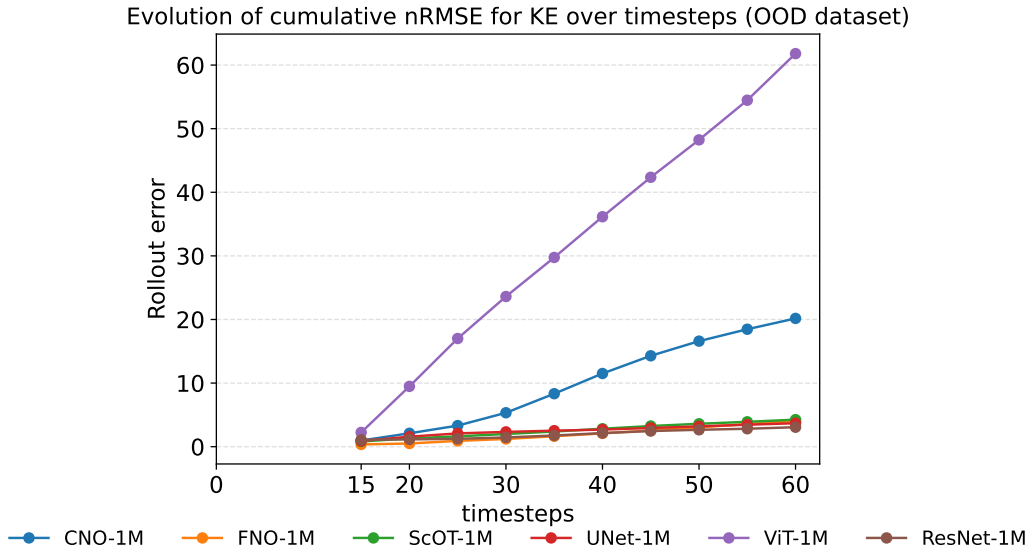

Figure 28: Temporal rollout of cumulative nRMSE over KE for the SIDA-OOD-Experiment PDUV_F_(3,1) for all 1M models.

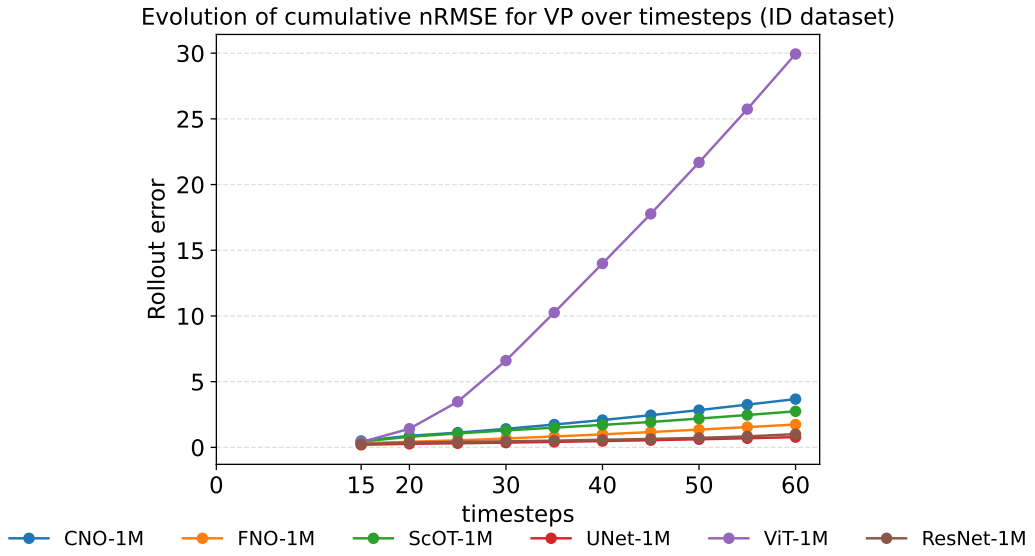

Figure 29: Temporal rollout of cumulative nRMSE over VP for the SIDA-ID-Experiment PDUV_F_(3,1) for all 1M models.

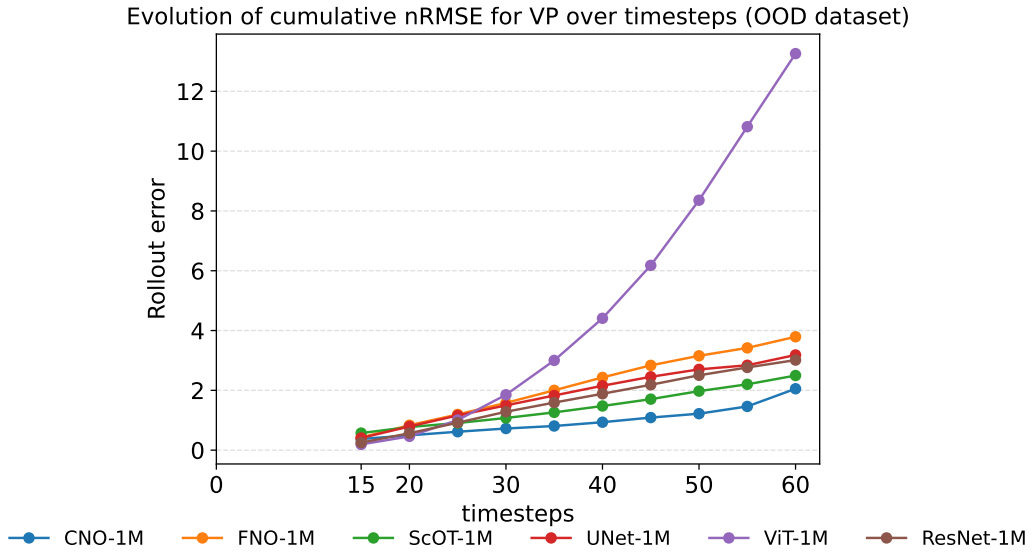

Figure 30: Temporal rollout of cumulative nRMSE over VP for the SIDA-OOD-Experiment PDUV_F_(3,1) for all 1M models.

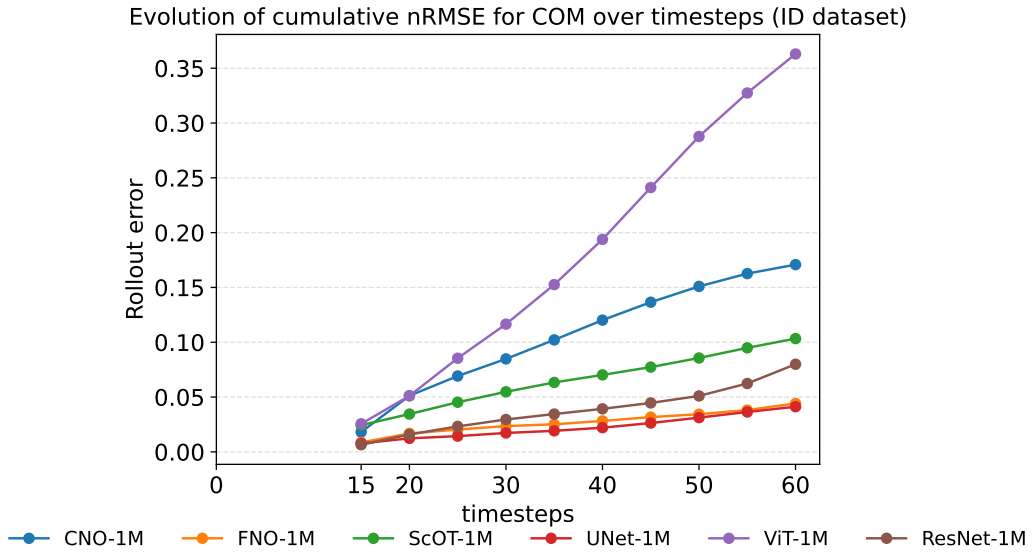

Figure 31: Temporal rollout of cumulative nRMSE over COM for the SIDA-ID-Experiment PDUV_F_(3,1) for all 1M models.

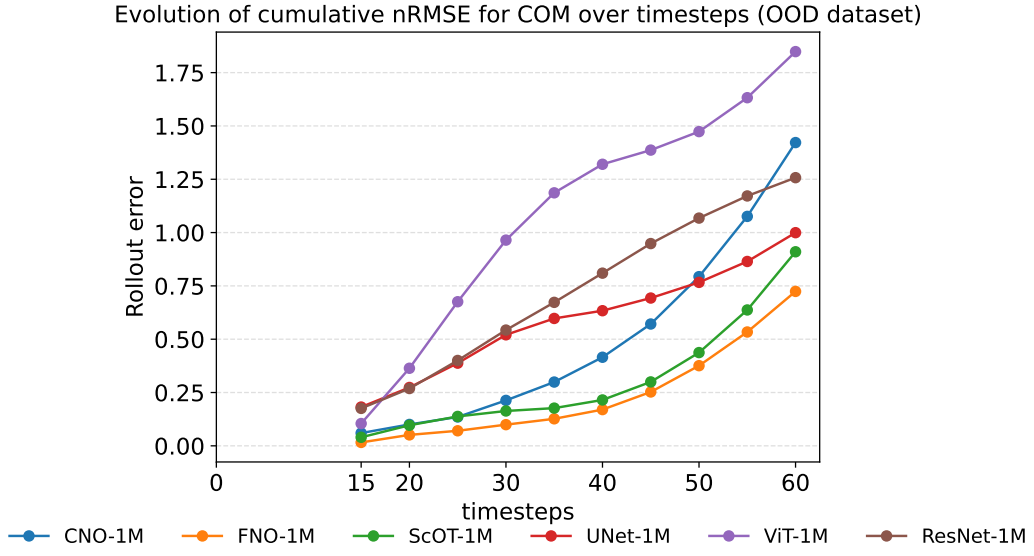

Figure 32: Temporal rollout of cumulative nRMSE over COM for the SIDA-OOD-Experiment PDUV_F_(3,1) for all 1M models.

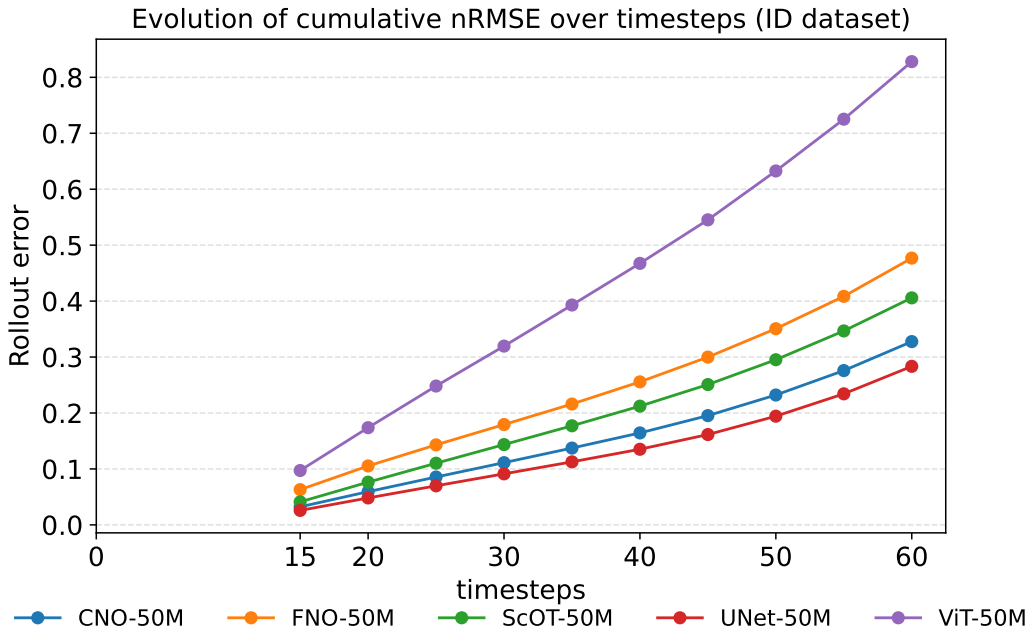

Figure 33: Temporal rollout of cumulative nRMSE over output channels for the SIDA-ID-Experiment PDUV_F_(3,1) for all 50M models.

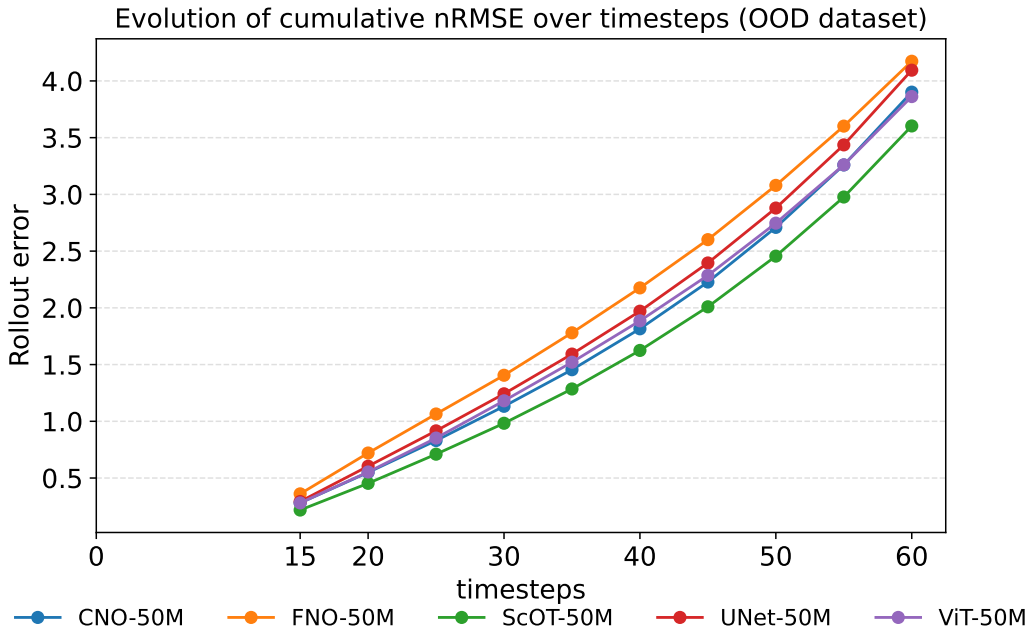

Figure 34: Temporal rollout of cumulative nRMSE over output channels for the SIDA-OOD-Experiment PDUV_F_(3,1) for all 50M models.

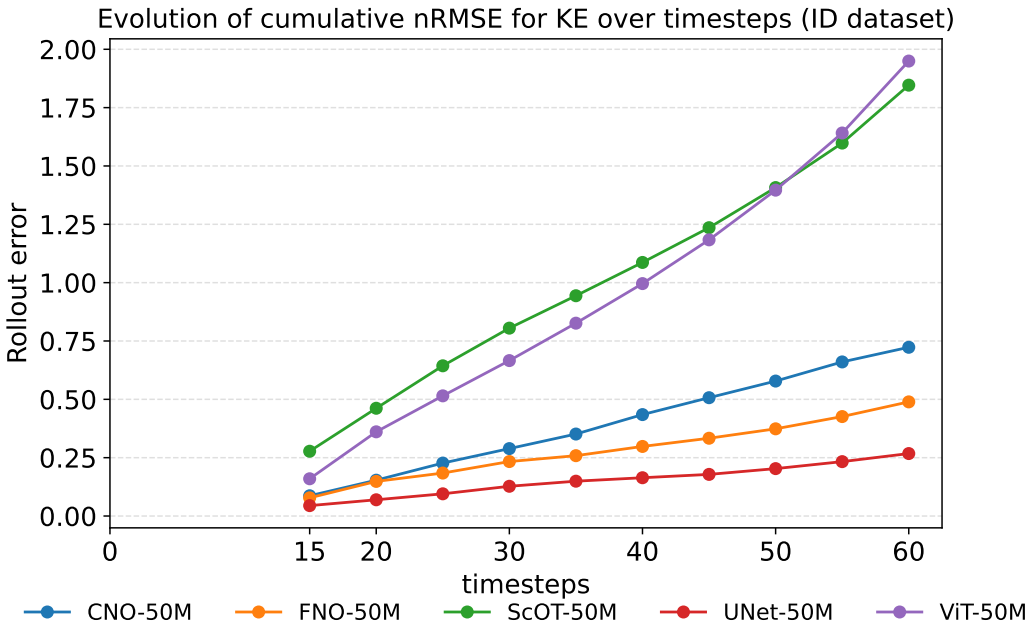

Figure 35: Temporal rollout of cumulative nRMSE over KE for the SIDA-ID-Experiment PDUV_F_(3,1) for all 50M models.

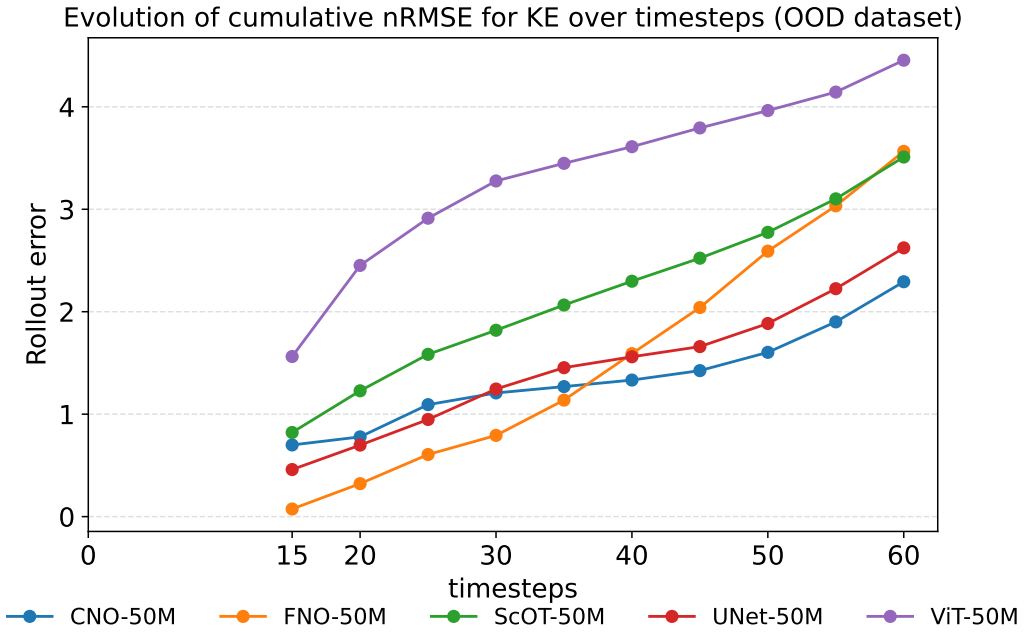

Figure 36: Temporal rollout of cumulative nRMSE over KE for the SIDA-OOD-Experiment PDUV_F_(3,1) for all 50M models.

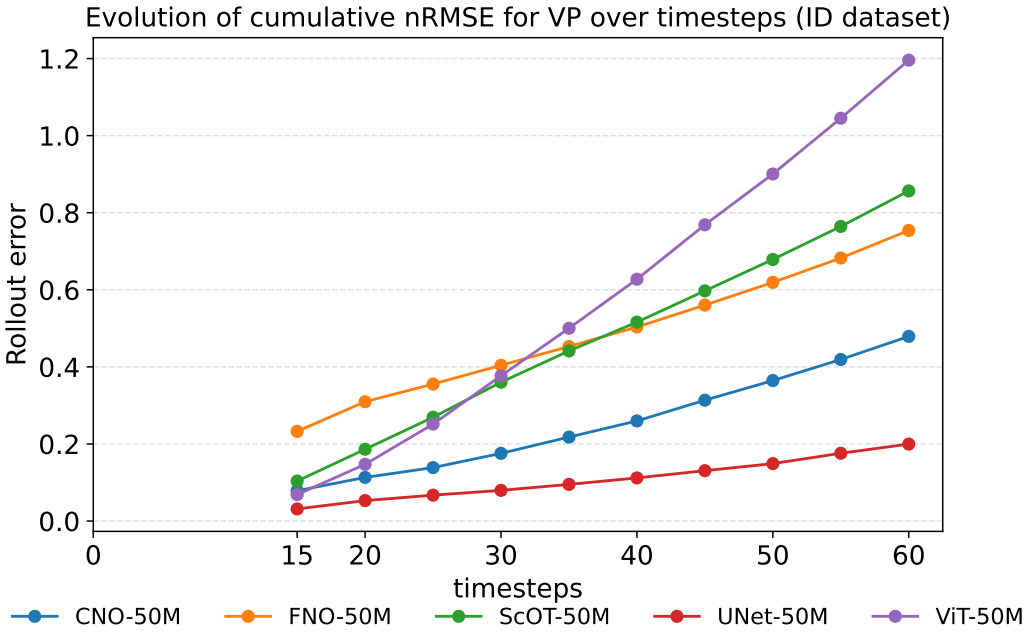

Figure 37: Temporal rollout of cumulative nRMSE over VP for the SIDA-ID-Experiment PDUV_F_(3,1) for all 50M models.

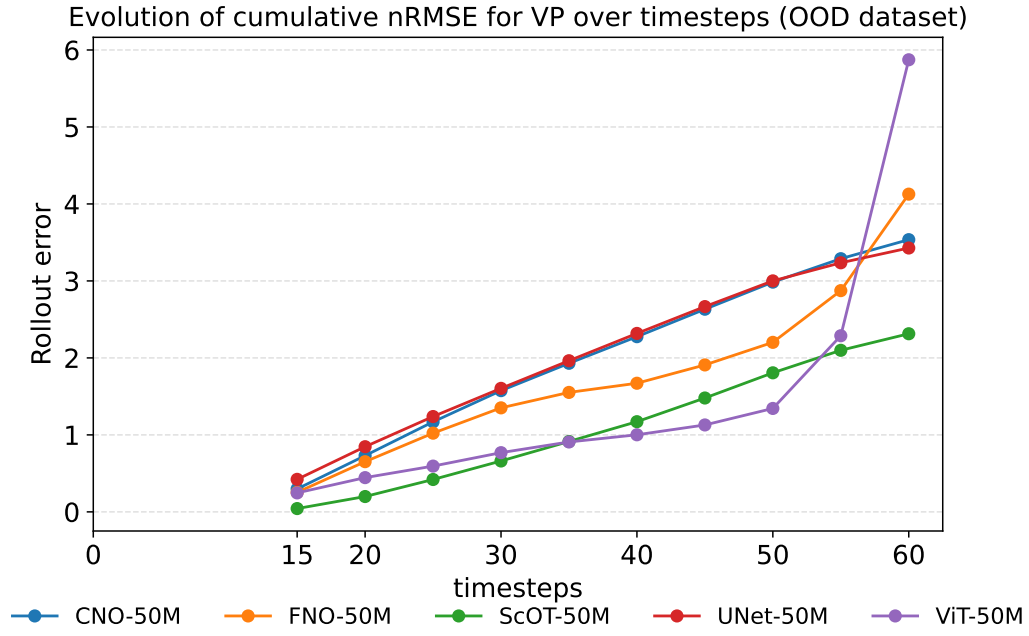

Figure 38: Temporal rollout of cumulative nRMSE over VP for the SIDA-OOD-Experiment PDUV_F_(3,1) for all 50M models.

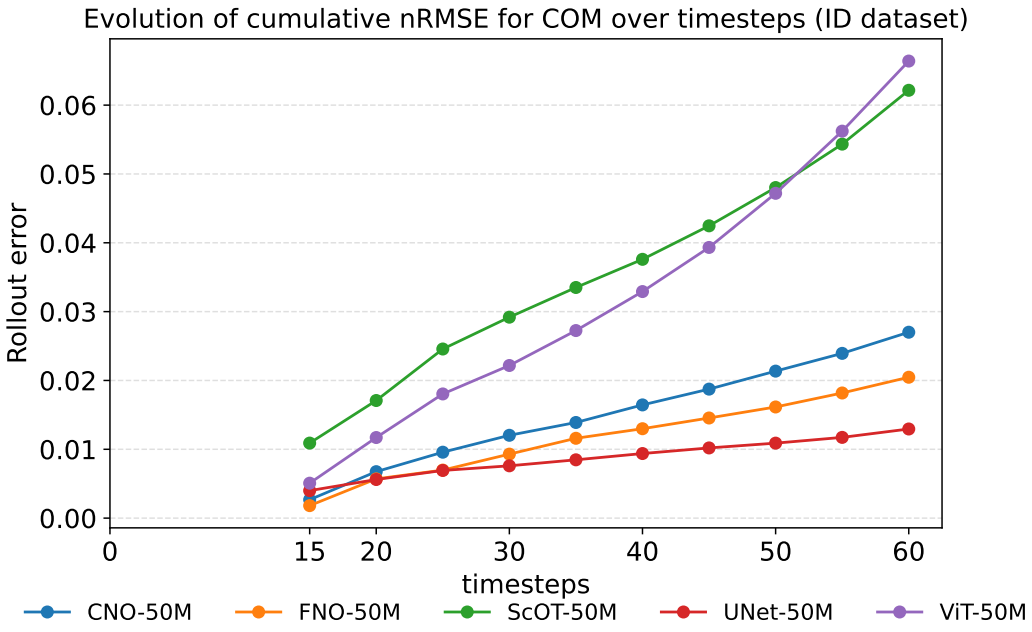

Figure 39: Temporal rollout of cumulative nRMSE over COM for the SIDA-ID-Experiment PDUV_F_(3,1) for all 50M models.

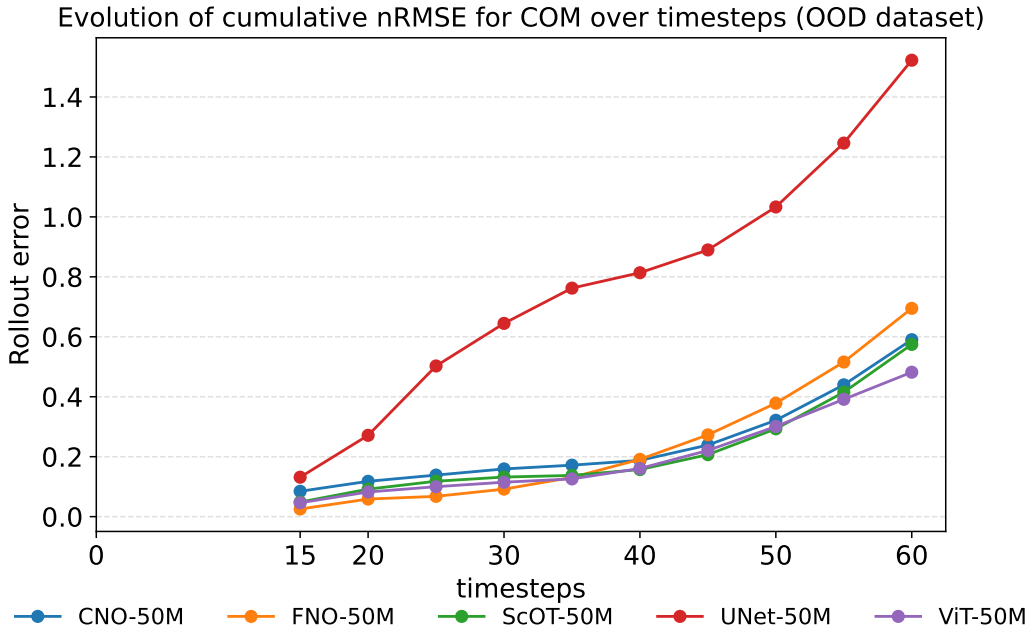

Figure 40: Temporal rollout of cumulative nRMSE over COM for the SIDA-OOD-Experiment PDUV_F_(3,1) for all 50M models.

E TABLES

E.1 ERROR-TYPE 1 METRICS FOR THE LIDE DATASET

In this section, we present the nRMSE of Type 1 **from section 4.5** for all experiments on the LIDE In- and Out of Distribution dataset. The error is represented over four quantities of interest. The output channels column represents the relative RMSE across all output channels and test trajectories, considering the maximum allowable rollout steps. OR represents the error over the outer radius of the droplet. KE and VP represent the error over the kinetic energy and vorticity production of the whole system.

Table 44: Error-type 1 for experiment P_F_(1,1) for the LIDE dataset across all 1M models.

MODEL	ID				OOD			
	output channels	OR	KE	VP	output channels	OR	KE	VP
CNO	0.5036	-	-	-	1.4540	-	-	-
FNO	0.4514	-	-	-	0.8434	-	-	-
ResNet	0.8425	-	-	-	0.9781	-	-	-
ScOT	0.6704	-	-	-	0.8929	-	-	-
Transolver	0.5548	-	-	-	0.8193	-	-	-
UNet	0.6122	-	-	-	0.9712	-	-	-
ViT	0.6313	-	-	-	0.8377	-	-	-

Table 45: Error-type 1 for experiment P_F_(1,1) for the LIDE dataset across all 50M models.

MODEL	ID				OOD			
	output channels	OR	KE	VP	output channels	OR	KE	VP
CNO	0.4558	-	-	-	1.6325	-	-	-
FNO	0.4377	-	-	-	0.8540	-	-	-
ScOT	0.4835	-	-	-	0.8752	-	-	-
UNet	0.5040	-	-	-	0.9437	-	-	-
ViT	0.5079	-	-	-	0.8232	-	-	-

Table 46: Error-type 1 for experiment P_F_(3,1) for the LIDE dataset across all 1M models.

MODEL	ID				OOD			
	output channels	OR	KE	VP	output channels	OR	KE	VP
CNO	0.2824	-	-	-	0.9684	-	-	-
FNO	0.6141	-	-	-	0.9833	-	-	-
ResNet	0.8883	-	-	-	1.0743	-	-	-
ScOT	0.6511	-	-	-	0.7819	-	-	-
Transolver	0.4400	-	-	-	0.7585	-	-	-
UNet	0.3964	-	-	-	0.9759	-	-	-
ViT	0.8650	-	-	-	1.0220	-	-	-

Table 47: Error-type 1 for experiment P_F_(3,1) for the LIDE dataset across all 50M models.

MODEL	ID				OOD			
	output channels	OR	KE	VP	output channels	OR	KE	VP
CNO	0.3665	-	-	-	0.8253	-	-	-
FNO	0.4943	-	-	-	0.9420	-	-	-
ScOT	0.4988	-	-	-	0.7273	-	-	-
UNet	0.3230	-	-	-	0.9112	-	-	-
ViT	0.5398	-	-	-	0.8904	-	-	-

Table 48: Error-type 1 for experiment P_T_(1,1) for the LIDE dataset across all 1M models.

MODEL	ID				OOD			
	output channels	OR	KE	VP	output channels	OR	KE	VP
CNO	0.3746	-	-	-	1.0632	-	-	-
FNO	0.4191	-	-	-	0.8097	-	-	-
ResNet	0.5210	-	-	-	1.1980	-	-	-
ScOT	0.5417	-	-	-	3.2936	-	-	-
Transolver	0.2742	-	-	-	0.7994	-	-	-
UNet	0.3959	-	-	-	1.0804	-	-	-
ViT	0.4802	-	-	-	0.8444	-	-	-

Table 49: Error-type 1 for experiment P_T_(1,1) for the LIDE dataset across all 50M models.

MODEL	ID				OOD			
	output channels	OR	KE	VP	output channels	OR	KE	VP
CNO	0.3518	-	-	-	0.9494	-	-	-
FNO	0.3365	-	-	-	1.0315	-	-	-
ScOT	0.1841	-	-	-	0.8564	-	-	-
UNet	0.1689	-	-	-	0.8466	-	-	-
ViT	0.1382	-	-	-	0.6708	-	-	-

Table 50: Error-type 1 for experiment P_T_(3,1) for the LIDE dataset across all 1M models.

MODEL	ID				OOD			
	output channels	OR	KE	VP	output channels	OR	KE	VP
CNO	0.4647	-	-	-	1.0615	-	-	-
FNO	0.4439	-	-	-	0.9360	-	-	-
ResNet	0.7218	-	-	-	1.8583	-	-	-
ScOT	0.5154	-	-	-	3.9418	-	-	-
Transolver	0.3271	-	-	-	0.8181	-	-	-
UNet	0.4858	-	-	-	1.2237	-	-	-
ViT	0.5381	-	-	-	1.0488	-	-	-

Table 51: Error-type 1 for experiment P_T_(3,1) for the LIDE dataset across all 50M models.

MODEL	ID				OOD			
	output channels	OR	KE	VP	output channels	OR	KE	VP
CNO	0.3652	-	-	-	0.9529	-	-	-
FNO	0.3219	-	-	-	0.9391	-	-	-
ScOT	0.2252	-	-	-	2.5944	-	-	-
UNet	0.1979	-	-	-	0.8472	-	-	-
ViT	0.1912	-	-	-	0.8504	-	-	-

Table 52: Error-type 1 for experiment PDUV_F_(1,1) for the LIDE dataset across all 1M models.

MODEL	ID				OOD			
	output channels	OR	KE	VP	output channels	OR	KE	VP
CNO	0.2629	0.3114	0.2102	0.2316	0.8049	1.9745	0.7422	0.7015
FNO	0.4939	0.7593	1.4189	1.6107	0.8035	1.7849	0.8039	0.8758
ResNet	0.8566	1.1304	2.5096	1.1816	0.9591	2.0483	1.7894	0.7860
ScOT	0.3322	0.3044	0.3134	0.3627	0.7746	0.9406	0.5202	0.8277
Transolver	0.5692	1.2263	0.7104	0.5402	0.8377	2.2660	0.7232	0.7507
UNet	0.3817	0.4428	0.2472	0.2280	0.9356	1.3699	0.7342	0.9043
ViT	0.7592	0.4418	1.1000	2.5903	0.8513	1.3258	0.6202	0.6930

Table 53: Error-type 1 for experiment PDUV_F_(1,1) for the LIDE dataset across all 50M models.

MODEL	ID				OOD			
	output channels	OR	KE	VP	output channels	OR	KE	VP
CNO	0.2647	0.3075	0.1199	0.1540	0.6902	1.2532	0.5474	0.7395
FNO	0.3472	0.6953	0.7417	1.1417	0.7403	1.8706	1.3258	1.0421
ScOT	0.2806	0.6725	0.1422	0.1706	0.7444	1.7365	0.5360	0.7541
UNet	0.2673	0.4714	0.0647	0.1123	0.8562	1.5476	0.9008	0.8546
ViT	0.2625	0.7581	0.1653	0.2395	0.6853	1.1653	0.4153	0.7482

Table 54: Error-type 1 for experiment PDUV_F_(3,1) for the LIDE dataset across all 1M models.

MODEL	ID				OOD			
	output channels	OR	KE	VP	output channels	OR	KE	VP
CNO	0.1641	0.7208	0.1182	0.2360	0.7965	1.3917	2.6376	0.7217
FNO	0.3814	0.7405	1.5689	2.0840	0.6766	1.9568	1.2789	1.0530
ResNet	0.7244	1.0878	0.2947	1.4805	0.6969	2.2930	0.6900	0.7133
ScOT	0.2234	0.4091	0.3476	0.3303	0.9286	1.7081	4.6177	0.8089
Transolver	0.4091	1.2833	0.7547	0.4055	0.6324	2.0543	14.7765	1.3631
UNet	0.2140	0.3373	0.1471	0.1766	0.6814	1.6791	0.5000	0.6830
ViT	0.5237	0.8853	1.5604	1.3256	0.7154	1.3003	2.6848	1.6023

Table 55: Error-type 1 for experiment PDUV_F_(3,1) for the LIDE dataset across all 50M models.

MODEL	ID				OOD			
	output channels	OR	KE	VP	output channels	OR	KE	VP
CNO	0.1658	0.7696	0.0995	0.1413	0.5502	1.2733	0.5196	0.7047
FNO	0.2538	0.7069	0.7270	0.9354	0.7913	1.8454	0.7272	0.6834
ScOT	0.1570	0.8316	0.1831	0.1294	0.7089	1.3724	1.9937	0.6623
UNet	0.1383	0.3408	0.0601	0.0677	0.5854	1.5623	0.5511	0.7349
ViT	0.1792	0.8206	0.2179	0.1896	0.4485	1.2850	2.7728	0.4836

Table 56: Error-type 1 for experiment P[ES]_F_(1,1) for the LIDE dataset across all 1M models.

MODEL	ID				OOD			
	output channels	OR	KE	VP	output channels	OR	KE	VP
CNO	1.6851	-	-	-	1.6036	-	-	-
FNO	1.6562	-	-	-	1.1943	-	-	-
ResNet	1.3139	-	-	-	1.4039	-	-	-
ScOT	1.3833	-	-	-	1.1345	-	-	-
Transolver	1.0443	-	-	-	0.9856	-	-	-
UNet	1.2778	-	-	-	1.0259	-	-	-
ViT	1.3596	-	-	-	1.0713	-	-	-

Table 57: Error-type 1 for experiment P[ES]_F_(1,1) for the LIDE dataset across all 50M models.

MODEL	ID				OOD			
	output channels	OR	KE	VP	output channels	OR	KE	VP
CNO	1.7389	-	-	-	1.4028	-	-	-
FNO	1.8858	-	-	-	1.2497	-	-	-
ScOT	0.9373	-	-	-	0.9780	-	-	-
UNet	1.8593	-	-	-	1.5409	-	-	-
ViT	0.9180	-	-	-	0.9606	-	-	-

Table 58: Error-type 1 for experiment P[ES]_F_(3,1) for the LIDE dataset across all 1M models.

MODEL	ID				OOD			
	output channels	OR	KE	VP	output channels	OR	KE	VP
CNO	1.0090	-	-	-	1.0005	-	-	-
FNO	1.1216	-	-	-	1.2849	-	-	-
ResNet	1.0200	-	-	-	1.3084	-	-	-
ScOT	0.7419	-	-	-	0.8235	-	-	-
Transolver	1.0213	-	-	-	1.0578	-	-	-
UNet	1.6746	-	-	-	1.7769	-	-	-
ViT	1.0429	-	-	-	1.1444	-	-	-

Table 59: Error-type 1 for experiment P[ES]_F_(3,1) for the LIDE dataset across all 50M models.

MODEL	ID				OOD			
	output channels	OR	KE	VP	output channels	OR	KE	VP
CNO	0.9660	-	-	-	1.4007	-	-	-
FNO	1.4601	-	-	-	1.3018	-	-	-
ScOT	0.6965	-	-	-	0.8378	-	-	-
UNet	1.3407	-	-	-	1.6829	-	-	-
ViT	0.8213	-	-	-	1.0365	-	-	-

Table 60: Error-type 1 for experiment PDUV[ES]_F_(1,1) for the LIDE dataset across all 1M models.

MODEL	ID				OOD			
	output channels	OR	KE	VP	output channels	OR	KE	VP
CNO	1.2229	0.6435	4.6978	0.7810	1.2592	1.5198	7.5844	0.6541
FNO	1.0630	0.9357	2.0852	0.6448	1.1524	2.1351	1.1364	0.8400
ResNet	0.7373	0.9818	2.1267	4.0487	0.9972	0.9069	3.2353	1.4468
ScOT	1.2051	0.7292	3.7019	0.6542	0.9178	1.5549	1.7931	0.8171
Transolver	1.1740	1.0733	3.4391	6.1363	0.9761	1.8676	1.2208	1.4010
UNet	0.9590	0.9442	1.0926	0.5010	1.0156	0.9468	0.7576	0.7147
ViT	1.6079	0.7157	84.3898	19.0520	1.2845	1.3337	25.3722	3.6711

Table 61: Error-type 1 for experiment PDUV[ES]_F_(1,1) for the LIDE dataset across all 50M models.

MODEL	ID				OOD			
	output channels	OR	KE	VP	output channels	OR	KE	VP
CNO	1.0375	0.3462	2.2243	0.6907	1.1061	0.7104	4.1761	0.6623
FNO	1.1017	0.3970	1.1027	0.8632	1.0473	0.8639	0.6317	0.7118
ScOT	1.0842	0.3138	5.1516	1.2275	1.0623	0.9669	2.0632	0.8507
UNet	1.2581	0.3212	10.1976	0.9566	1.0858	0.8798	8.4109	1.0080
ViT	0.5288	0.3013	1.1427	0.4881	0.7361	0.9410	0.4628	0.6720

Table 62: Error-type 1 for experiment PDUV[ES]_F_(3,1) for the LIDE dataset across all 1M models.

MODEL	ID				OOD			
	output channels	OR	KE	VP	output channels	OR	KE	VP
CNO	0.8496	0.8761	2.3398	0.3785	0.8293	1.0048	1.9510	0.6839
FNO	0.9314	0.5236	1.5661	0.5155	1.0127	1.1182	0.5089	0.6728
ResNet	0.8098	0.8470	2.2236	1.9128	0.9036	0.9456	1.2876	0.8280
ScOT	0.7853	0.5273	2.4910	0.6505	1.3457	1.6916	6.7820	0.8291
Transolver	0.7752	1.1435	8.5083	1.1835	0.8184	1.9053	12.2341	1.2247
UNet	0.8315	0.3880	1.5762	0.5594	1.0015	0.8827	9.4459	1.4276
ViT	0.7199	0.7572	1.7756	3.1967	0.8519	1.0887	2.0591	2.0040

Table 63: Error-type 1 for experiment PDUV[ES]_F_(3,1) for the LIDE dataset across all 50M models.

MODEL	ID				OOD			
	output channels	OR	KE	VP	output channels	OR	KE	VP
CNO	0.7444	0.3423	0.4881	0.4047	0.8804	0.8859	0.5464	0.7090
FNO	0.7419	0.3347	0.6132	0.3902	0.9423	1.3608	1.0011	1.4644
ScOT	0.7998	0.3195	3.1428	0.5878	1.1444	1.1325	3.7367	0.6780
UNet	0.6749	0.3143	1.3913	0.4287	0.9349	0.9718	2.6840	0.8234
ViT	0.5741	0.8446	0.6115	0.5772	0.6063	1.1230	2.0634	0.4701

Table 64: Error-type 1 for experiment P_F_(3,2) for the LIDE dataset across all 1M models.

MODEL	ID				OOD			
	output channels	OR	KE	VP	output channels	OR	KE	VP
CNO	0.3370	-	-	-	0.8082	-	-	-
FNO	0.5785	-	-	-	0.9104	-	-	-
ResNet	0.7244	-	-	-	0.9998	-	-	-
ScOT	0.5407	-	-	-	0.7937	-	-	-
Transolver	0.5719	-	-	-	0.8974	-	-	-
UNet	0.4697	-	-	-	0.9480	-	-	-
ViT	0.8045	-	-	-	1.0514	-	-	-

Table 65: Error-type 1 for experiment P_F_(3,2) for the LIDE dataset across all 50M models.

MODEL	ID				OOD			
	output channels	OR	KE	VP	output channels	OR	KE	VP
CNO	0.3623	-	-	-	1.0601	-	-	-
FNO	0.4481	-	-	-	0.8793	-	-	-
ScOT	0.5479	-	-	-	0.7460	-	-	-
UNet	0.3347	-	-	-	0.8520	-	-	-
ViT	0.5914	-	-	-	0.8713	-	-	-

Table 66: Error-type 1 for experiment PDUV_F_(3,2) for the LIDE dataset across all 1M models.

MODEL	ID				OOD			
	output channels	OR	KE	VP	output channels	OR	KE	VP
CNO	0.1681	0.5961	0.2427	0.3172	0.4908	1.3585	0.5875	0.7162
FNO	0.2659	0.6912	0.4239	0.5619	0.6846	1.8140	0.7110	0.8241
ResNet	0.3439	0.7605	0.2512	1.1572	0.6110	1.4525	0.9998	0.7292
ScOT	0.1991	0.4183	0.5548	0.4106	0.5261	1.6937	2.0553	0.7480
Transolver	0.6848	0.9282	3.3758	1.9064	0.7317	1.4803	5.4101	2.4985
UNet	0.2602	0.3964	0.1902	0.3175	0.5980	1.4825	0.6453	0.6684
ViT	0.4009	0.7294	0.6847	0.2659	0.8038	1.9366	17.3108	0.7356

Table 67: Error-type 1 for experiment PDUV_F_(3,2) for the LIDE dataset across all 50M models.

MODEL	ID				OOD			
	output channels	OR	KE	VP	output channels	OR	KE	VP
CNO	0.1772	0.7030	0.1803	0.1979	0.5377	1.9170	0.4089	0.6949
FNO	0.2015	0.5992	0.1149	0.2680	0.7814	1.7143	0.6559	0.6455
ScOT	0.1596	0.6556	0.2521	0.1761	0.5054	1.5690	0.6536	0.6506
UNet	0.1398	0.5207	0.1052	0.1055	0.6313	1.2962	0.4841	0.6589
ViT	0.1584	0.8388	0.3299	0.2562	0.4713	1.8939	3.1967	0.5349

Table 68: Error-type 1 for experiment PDUV_T_(1,1) for the LIDE dataset across all 1M models.

MODEL	ID				OOD			
	output channels	OR	KE	VP	output channels	OR	KE	VP
CNO	0.3308	0.3259	1.2956	0.3905	1.0250	1.3658	15.1482	0.8278
FNO	0.3758	0.7462	0.2703	0.7034	0.9118	2.0678	0.6794	1.4235
ResNet	0.5823	0.8530	0.7443	3.0600	0.8987	1.2044	2.1359	0.9952
ScOT	0.2423	0.8981	0.6786	0.4264	1.6251	1.2974	6.4974	0.7815
Transolver	0.8041	1.0787	2.6660	3.2419	0.8448	1.6026	0.8981	1.5772
UNet	0.3366	0.3787	0.2565	0.2655	0.9788	1.1754	2.3093	0.7987
ViT	0.5406	0.5891	1.7829	1.0861	1.3901	1.0735	27.0802	5.5687

Table 69: Error-type 1 for experiment PDUV_T_(1,1) for the LIDE dataset across all 50M models.

MODEL	ID				OOD			
	output channels	OR	KE	VP	output channels	OR	KE	VP
CNO	0.2563	0.5913	0.3306	0.2356	0.9424	0.9781	2.7716	0.9026
FNO	0.2186	0.5734	0.1571	0.3101	0.8777	1.9468	2.2576	2.1369
ScOT	0.1154	0.5328	0.1918	0.1369	1.1404	2.2448	46.2113	2.1308
UNet	0.1541	0.4554	0.1905	0.1161	0.8473	1.1420	0.9216	0.9274
ViT	0.1190	0.6870	0.1765	0.1727	0.6476	1.8988	0.8740	0.6958

Table 70: Error-type 1 for experiment PDUV_T_(3,1) for the LIDE dataset across all 1M models.

MODEL	ID				OOD			
	output channels	OR	KE	VP	output channels	OR	KE	VP
CNO	0.3545	0.3782	0.5048	0.3388	0.9964	1.3516	1.8233	0.7798
FNO	0.3364	0.7212	0.6183	1.0469	0.7403	1.9948	2.2181	1.0348
ResNet	0.4386	0.6767	0.6628	1.5547	0.9144	1.0341	0.6918	0.9492
ScOT	0.2259	0.4166	0.5126	0.3882	0.9113	1.3358	19.9497	0.7177
Transolver	0.5447	1.0129	2.8613	1.0453	0.9236	0.9998	3.6309	0.9388
UNet	0.3723	0.4363	0.5094	0.2309	1.0128	1.0576	10.6509	0.8182
ViT	0.4118	0.6382	0.7999	0.9934	1.3428	1.9946	7.8630	9.3536

Table 71: Error-type 1 for experiment PDUV_T_(3,1) for the LIDE dataset across all 50M models.

MODEL	ID				OOD			
	output channels	OR	KE	VP	output channels	OR	KE	VP
CNO	0.2463	0.7879	0.2353	0.2650	0.8835	1.4789	2.2330	0.7969
FNO	0.1969	0.6082	0.0841	0.2513	0.8324	1.5054	1.0485	1.0591
ScOT	0.1111	0.8634	0.2411	0.1482	0.9309	1.4528	6.9306	0.8574
UNet	0.1407	0.5266	0.1017	0.1425	0.7480	0.8901	3.6310	0.8814
ViT	0.1293	0.6679	0.2070	0.1606	0.5036	1.4336	1.1170	0.3788

E.2 Error-type 1 metrics for the SIDA Dataset

In this section, we present the nRMSE **as defined in section 4.5** of Type 1 for all experiments on the SIDA In-and Out of Distribution dataset. The error is represented over four quantities of interest. The output channels column represents the relative RMSE across all output channels and test trajectories, considering the maximum allowable rollout steps. COM represents the error over displacement of the droplet's Center of Mass. KE and VP represent the error over the kinetic energy and vorticity production of the whole system, respectively.

Table 72: Error-type 1 for experiment PDUV_F_(1,1) for the SIDA dataset across all 1M models.

MODEL	ID				OOD			
	output channels	COM	KE	VP	output channels	COM	KE	VP
CNO	0.7350	0.2510	0.6356	0.7034	0.9400	0.2304	0.8165	0.8690
FNO	0.6937	0.1068	0.7125	0.7587	0.9734	0.4068	0.9016	0.8879
ResNet	0.7199	0.1097	0.7132	0.6845	0.9816	0.4103	0.9046	0.8655
ScOT	0.6814	0.1124	0.6331	0.6905	0.9582	0.4134	0.8645	0.8727
Transolver	1.0046	0.1246	0.6115	0.7339	1.0749	0.3686	0.8160	0.8206
UNet	0.6883	0.1082	0.7101	0.6913	0.9673	0.4082	0.9035	0.8727
ViT	0.7152	0.0942	0.9125	1.7978	0.9308	0.3674	0.6793	0.5404

Table 73: Error-type 1 for experiment PDUV_F_(1,1) for the SIDA dataset across all 50M models.

MODEL	ID				OOD			
	output channels	COM	KE	VP	output channels	COM	KE	VP
CNO	0.6693	0.0987	0.6471	0.6852	0.9580	0.3944	0.8728	0.8692
FNO	0.6768	0.1045	0.6949	0.7280	0.9636	0.4038	0.8974	0.8805
ScOT	0.6544	0.0965	0.6185	0.6560	0.9448	0.3904	0.8513	0.8509
UNet	0.6760	0.1068	0.7001	0.6774	0.9608	0.4068	0.8997	0.8687
ViT	0.6479	0.0972	0.6126	0.6634	0.9373	0.3921	0.8444	0.8565

Table 74: Error-type 1 for experiment PDUV_F_(3,1) for the SIDA dataset across all 1M models.

MODEL	ID				OOD			
	output channels	COM	KE	VP	output channels	COM	KE	VP
CNO	0.1589	0.0208	0.7489	0.2001	0.6232	0.3265	2.7838	0.2841
FNO	0.1081	0.0058	0.1871	0.2550	0.5309	0.1788	0.4071	0.4372
ResNet	0.1366	0.0160	0.2594	0.1918	0.5838	0.1536	0.4090	0.4080
ScOT	0.1479	0.0125	0.4926	0.2315	0.4771	0.2262	0.4276	0.3090
Transolver	0.9153	0.5274	10.8694	8.2858	0.9343	0.3303	8.9317	3.5904
UNet	0.0855	0.0051	0.1208	0.1086	0.5933	0.1555	0.4710	0.4239
ViT	0.3440	0.0522	1.0397	3.3843	0.7788	0.2326	7.8675	1.7382

Table 75: Error-type 1 for experiment PDUV_F_(3,1) for the SIDA dataset across all 50M models.

MODEL	ID				OOD			
	output channels	COM	KE	VP	output channels	COM	KE	VP
CNO	0.0432	0.0036	0.1054	0.0694	0.4912	0.1246	0.4211	0.4616
FNO	0.0580	0.0028	0.0483	0.1251	0.5014	0.1479	0.6771	0.6162
ScOT	0.0486	0.0076	0.2135	0.0509	0.4607	0.1329	0.4149	0.3405
UNet	0.0427	0.0020	0.0375	0.0290	0.5261	0.2744	0.3688	0.4780
ViT	0.0910	0.0081	0.2439	0.1242	0.4739	0.0995	0.7688	1.2988

Table 76: Error-type 1 for experiment PDUV_T_(3,1) for the SIDA dataset across all 1M models.

MODEL	ID				OOD			
	output channels	COM	KE	VP	output channels	COM	KE	VP
CNO	0.1897	0.0560	1.2485	0.4213	329.3752	0.2660	inf	inf
FNO	0.1344	0.0115	0.3637	0.3582	0.4198	0.1680	2.5206	0.5613
ResNet	0.2266	0.0148	0.4769	0.3163	0.7322	0.2278	6.4481	0.7256
ScOT	0.1694	0.0241	0.7422	0.1666	0.4334	0.1210	2.3970	0.3141
Transolver	0.8795	0.6770	17.3106	6.8722	0.8577	0.3341	54.9306	4.7863
UNet	0.1842	0.0170	0.3507	0.1606	0.6009	0.3724	2.0907	0.6366
ViT	0.4162	0.0823	1.2424	3.5928	0.5955	0.2493	2.0887	5.7141

Table 77: Error-type 1 for experiment PDUV_T_(3,1) for the SIDA dataset across all 50M models.

MODEL	ID				OOD			
	output channels	COM	KE	VP	output channels	COM	KE	VP
CNO	0.0780	0.0125	0.2857	0.1107	0.5859	0.1692	0.5093	0.4618
FNO	0.0864	0.0089	0.1515	0.1579	0.4269	0.1612	3.0881	0.7062
ScOT	0.0577	0.0137	0.3477	0.0736	0.3840	0.0814	1.4028	0.2192
UNet	0.0628	0.0075	0.1949	0.0766	0.5529	0.1964	2.2313	0.7016
ViT	0.0928	0.0103	0.2557	0.1125	0.4577	0.0799	1.0613	2.0527

Table 78: Error-type 1 for experiment PDUV[VoS]_F_(1,1) for the SIDA dataset across all 1M models.

MODEL	ID				OOD			
	output channels	COM	KE	VP	output channels	COM	KE	VP
CNO	0.7918	0.0992	0.6924	0.6835	0.9571	0.3585	0.7551	0.8626
FNO	0.9003	0.1372	0.7275	0.8660	1.0429	0.4379	0.9090	0.9489
ResNet	0.7620	0.1160	0.7873	0.6619	0.9709	0.4164	0.7139	0.8288
ScOT	0.8163	0.0923	1.2445	0.7049	0.9180	0.3643	0.6217	0.7423
Transolver	0.9367	0.2609	5.0196	1.0873	1.0140	0.2702	0.8002	0.7441
UNet	0.7622	0.1353	0.6859	0.7230	0.9877	0.4363	0.8919	0.8820
ViT	0.7847	0.0958	1.4725	6.4234	0.9272	0.3799	0.5464	1.6108

Table 79: Error-type 1 for experiment PDUV[VoS]_F_(1,1) for the SIDA dataset across all 50M models.

MODEL	ID				OOD			
	output channels	COM	KE	VP	output channels	COM	KE	VP
CNO	0.7827	0.1344	0.7758	0.7839	0.9983	0.4357	0.9271	0.9184
FNO	0.8233	0.1310	0.7085	0.7276	1.0158	0.4319	0.9013	0.8486
ScOT	0.4879	0.0623	0.6491	0.3016	0.7900	0.3329	0.4133	0.6805
UNet	0.7603	0.1319	0.6798	0.7842	0.9836	0.4330	0.8903	0.9261
ViT	0.7295	0.1276	0.6112	0.7436	0.9490	0.4290	0.7976	0.7233

Table 80: Error-type 1 for experiment PDUV[VoS]_F_(3,1) for the SIDA dataset across all 1M models.

MODEL	ID				OOD			
	output channels	COM	KE	VP	output channels	COM	KE	VP
CNO	0.3491	0.0248	0.9291	0.2643	0.4978	0.1225	6.7419	0.5641
FNO	0.4655	0.0601	1.8175	0.4452	0.6241	0.2448	1.1234	0.4679
ResNet	0.3957	0.1040	0.4972	0.2219	0.6470	0.2972	0.4464	0.3036
ScOT	0.5083	0.0586	1.1911	0.4072	0.6315	0.2591	1.4353	0.2242
Transolver	0.9821	0.6493	10.1858	2.2680	0.9961	0.3362	6.9883	1.6341
UNet	0.4399	0.1227	0.3030	0.1796	0.6513	0.2596	0.4430	0.3453
ViT	0.5564	0.0612	0.8397	3.2743	0.7827	0.3364	5.5856	1.5554

Table 81: Error-type 1 for experiment PDUV[VoS]_F_(3,1) for the SIDA dataset across all 50M models.

MODEL	ID				OOD			
	output channels	COM	KE	VP	output channels	COM	KE	VP
CNO	0.3364	0.0352	1.2159	0.2618	0.5647	0.2030	1.1491	0.4548
FNO	0.4698	0.0548	2.0420	0.3363	0.6415	0.2331	2.4405	0.3442
ScOT	0.4151	0.0514	1.6202	0.3146	0.5552	0.2223	1.0314	0.1890
UNet	0.4064	0.1086	0.2991	0.1905	0.6389	0.2908	0.3951	0.5494
ViT	0.4062	0.0389	0.2410	1.5262	0.6021	0.2244	0.4503	0.9361

Table 82: Error-type 1 for experiment PDUV[VoS]_T_(3,1) for the SIDA dataset across all 1M models.

MODEL	ID				OOD			
	output channels	COM	KE	VP	output channels	COM	KE	VP
CNO	0.3917	0.0611	1.1840	0.3466	64.7e4	0.2348	inf	inf
FNO	0.4649	0.0819	1.7223	0.4595	0.6151	0.3043	1.3698	0.7637
ResNet	0.4587	0.0798	0.9467	0.5002	0.7801	0.2378	9.0898	0.4642
ScOT	0.3974	0.0290	1.7939	0.1907	0.5321	0.1693	1.1423	0.1948
Transolver	0.8631	0.5943	16.2865	7.1293	0.8508	0.3161	29.8996	2.7680
UNet	0.4721	0.0715	0.6354	0.4156	0.6236	0.2490	3.3039	0.4502
ViT	0.5181	0.0432	1.6658	3.9481	0.6729	0.2653	1.5476	2.4982

Table 83: Error-type 1 for experiment PDUV[VoS]_T_(3,1) for the SIDA dataset across all 50M models.

MODEL	ID				OOD			
	output channels	COM	KE	VP	output channels	COM	KE	VP
CNO	0.3125	0.0498	0.6993	0.1445	0.6209	0.2689	3.0228	0.7119
FNO	0.4128	0.0980	2.5765	0.4931	0.5936	0.2335	1.5842	0.8104
ScOT	0.4188	0.0556	1.9811	0.1534	0.4735	0.2147	6.3644	0.6552
UNet	0.3896	0.0904	0.6386	0.1623	0.5941	0.2198	5.5796	0.6366
ViT	0.3560	0.0232	0.4724	1.1887	0.5107	0.1515	1.6572	2.1826

Table 84: Error-type 1 for experiment PDUV_F_(3,2) for the SIDA dataset across all 1M models.

MODEL	ID				OOD			
	output channels	COM	KE	VP	output channels	COM	KE	VP
CNO	0.1575	0.0388	1.4388	0.4546	0.5050	0.1514	5.1212	0.6247
FNO	0.1338	0.0107	0.2739	0.3349	0.5554	0.1943	0.3353	0.5985
ResNet	0.1472	0.0233	0.2932	0.1528	0.5761	0.1077	1.1428	0.5209
ScOT	0.1532	0.0393	0.9001	0.1925	0.4968	0.2138	1.7578	0.2268
Transolver	0.9577	0.6721	28.9895	1.3517	0.9609	0.3576	13.6453	0.3941
UNet	0.0955	0.0120	0.3596	0.1350	0.5663	0.1878	1.8528	0.5861
ViT	0.2780	0.0439	1.0290	0.6201	0.5849	0.1939	1.0244	0.6553

Table 85: Error-type 1 for experiment PDUV_F_(3,2) for the SIDA dataset across all 50M models.

MODEL	ID				OOD			
	output channels	COM	KE	VP	output channels	COM	KE	VP
CNO	0.0513	0.0070	0.2164	0.1403	0.4681	0.1316	0.2591	0.5476
FNO	0.0737	0.0063	0.1264	0.1556	0.5289	0.1629	0.5149	0.3155
ScOT	0.0571	0.0113	0.3775	0.0879	0.4410	0.1673	0.9820	0.2451
UNet	0.0463	0.0054	0.1301	0.0561	0.4909	0.1693	0.3850	0.5484
ViT	0.1081	0.0172	0.4534	0.1510	0.4738	0.0835	0.8493	1.2346

Table 86: Error-type 1 for experiment PDUV[VoS]_F_(3,2) for the SIDA dataset across all 1M models.

MODEL	ID				OOD			
	output channels	COM	KE	VP	output channels	COM	KE	VP
CNO	0.3466	0.0682	1.6896	0.3208	0.4629	0.1822	2.9526	0.3537
FNO	0.4198	0.0780	1.5123	0.5962	0.5853	0.2031	1.1691	0.5967
ResNet	0.3530	0.0344	0.9827	0.1911	0.6241	0.1701	1.7610	0.4161
ScOT	0.3796	0.0512	0.7868	0.1669	0.5444	0.1718	1.1167	0.3058
Transolver	0.9507	0.6911	18.3170	1.1671	0.9841	0.3493	12.6450	0.5056
UNet	0.3325	0.0638	0.8743	0.2758	0.6513	0.2507	3.5701	0.3652
ViT	0.4556	0.0487	1.2767	1.7015	0.6301	0.2489	3.8598	0.9421

Table 87: Error-type 1 for experiment PDUV[VoS]_F_(3,2) for the SIDA dataset across all 50M models.

MODEL	ID				OOD			
	output channels	COM	KE	VP	output channels	COM	KE	VP
CNO	0.2647	0.0412	1.8487	0.3474	0.5649	0.1785	1.2554	0.4279
FNO	0.4295	0.0724	1.3556	0.2476	0.6063	0.2797	1.6246	0.2670
ScOT	0.3694	0.0557	0.6053	0.2316	0.5262	0.2207	0.6769	0.2067
UNet	0.3423	0.0871	0.3185	0.2050	0.5732	0.3279	0.7159	0.5444
ViT	0.3239	0.0240	0.4701	0.4947	0.5605	0.1965	1.2653	0.5427

F INFERNCE ROLLOUT PLOTS

F.1 ROLLOUT PREDICTIONS FROM INITIAL CONDITIONS FOR THE LIDE IN-DISTRIBUTION (ID) DATASET

In the following, we present rollout predictions for various models—each with 50M parameters, except for ResNet and Transolver, which have only 1M parameter count. The trajectories are shown in the Figures 41, 42, 43, 44, 45, 46, and 47. It corresponds to the following simulation parameters: filament pressure 9.3886×10^9 [Pa], ambient pressure 1.0382×10^5 [Pa], laser half-width 1.1727×10^{-6} [m], and droplet radii 1.5966×10^{-5} [m] and 1.2139×10^{-5} [m] along z- and r-axis, respectively. In all figures, the time frames are presented in order from top to bottom.

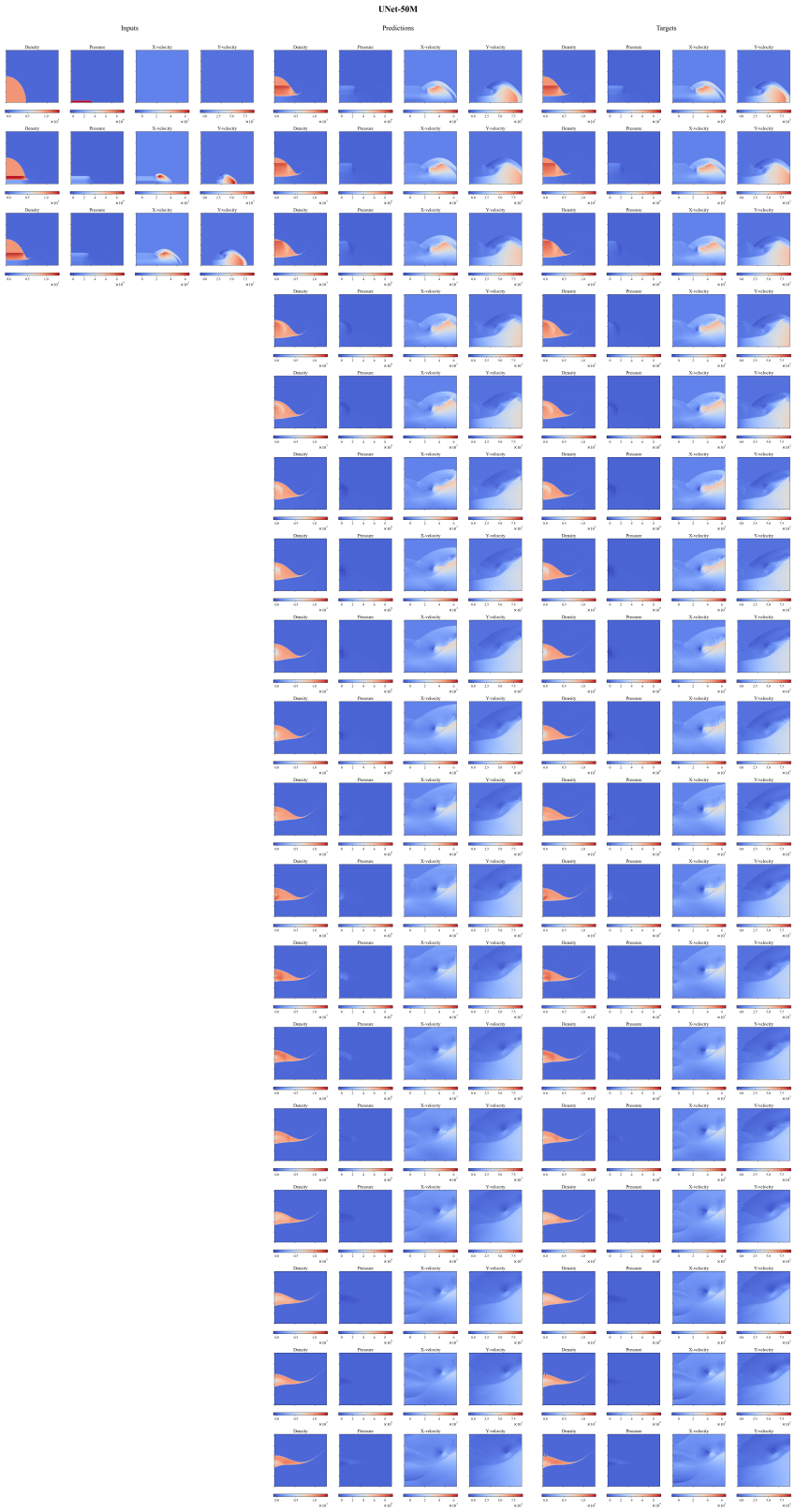

Figure 41: Rollout predictions for the LIDE-ID-Experiment PDUV_F_(3,1) with UNet-50M.

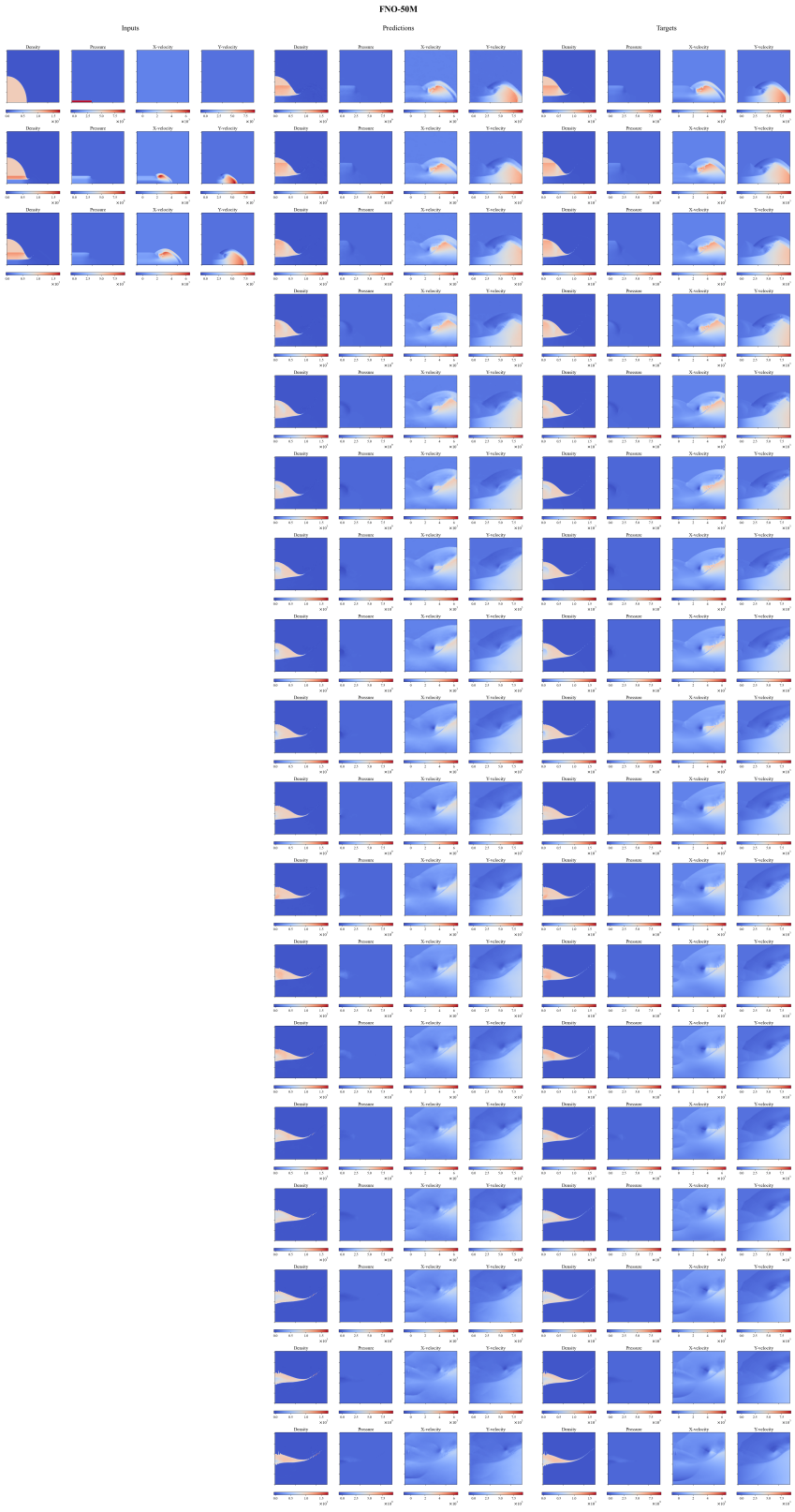

Figure 42: Rollout predictions for the LIDE-ID-Experiment PDUV_F_(3,1) with FNO-50M.

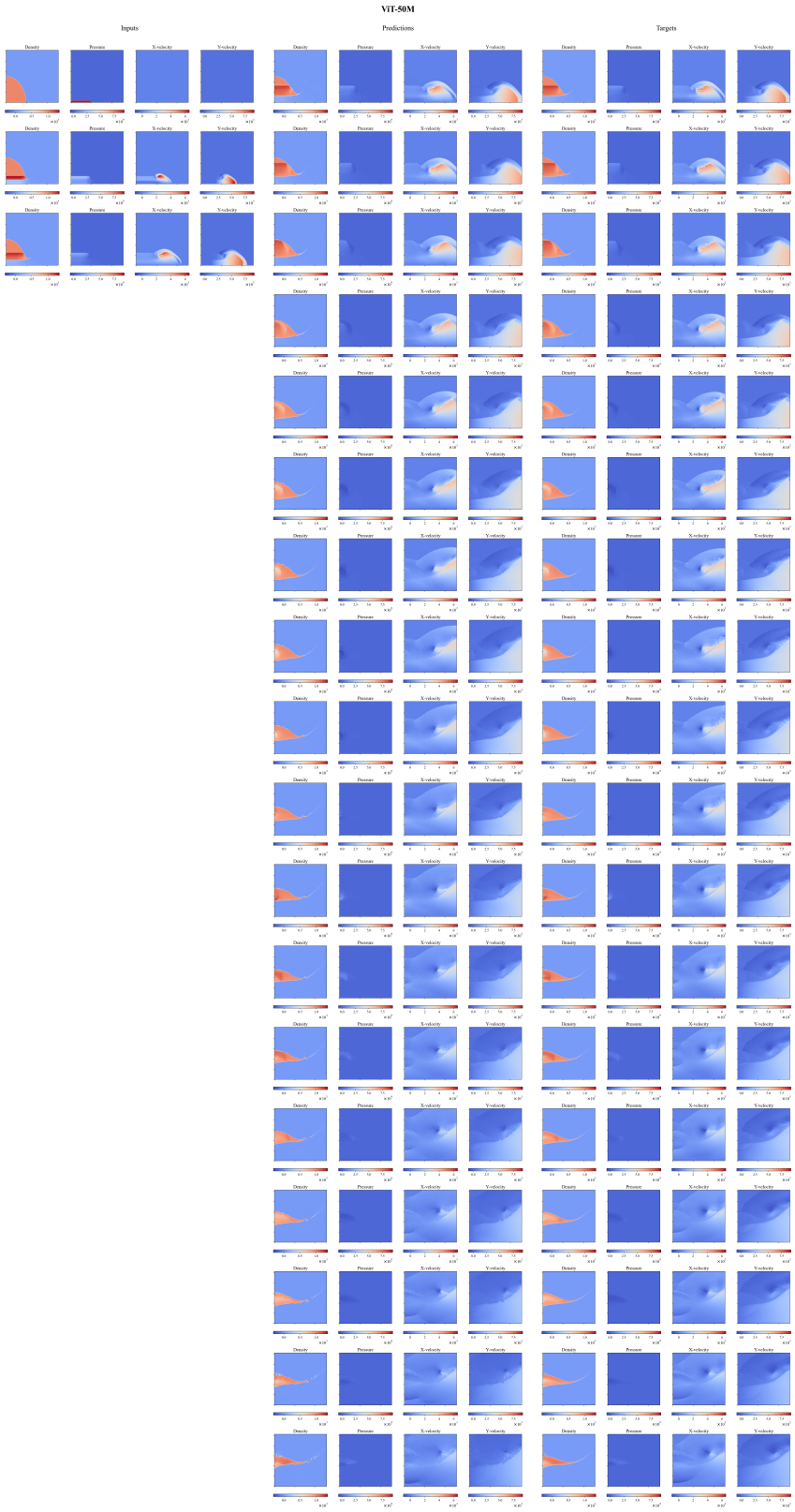

Figure 43: Rollout predictions for the LIDE-ID-Experiment PDUV_F_(3,1) with ViT-50M.

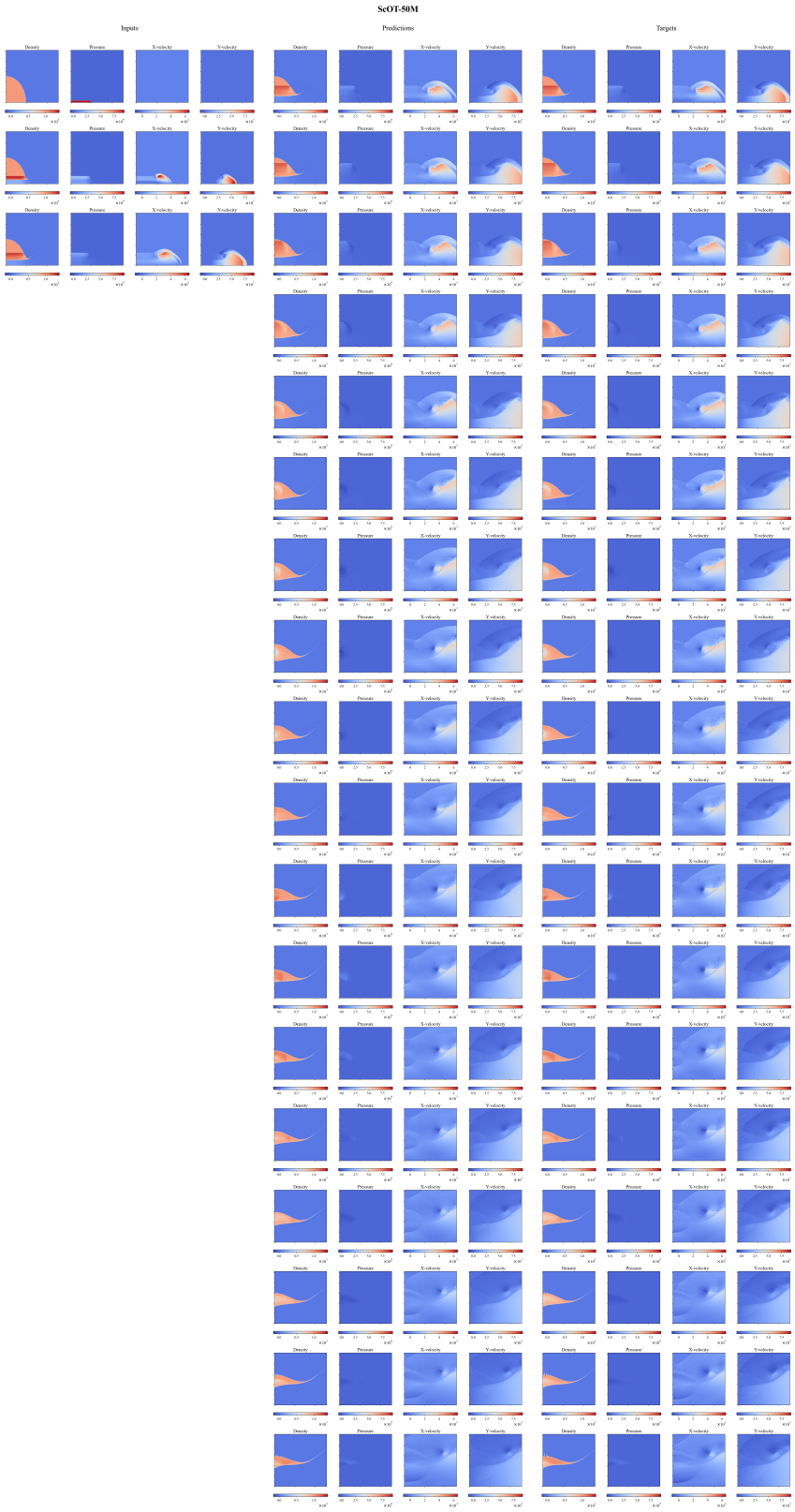

Figure 44: Rollout predictions for the LIDE-ID-Experiment PDUV_F_(3,1) with ScOT-50M.

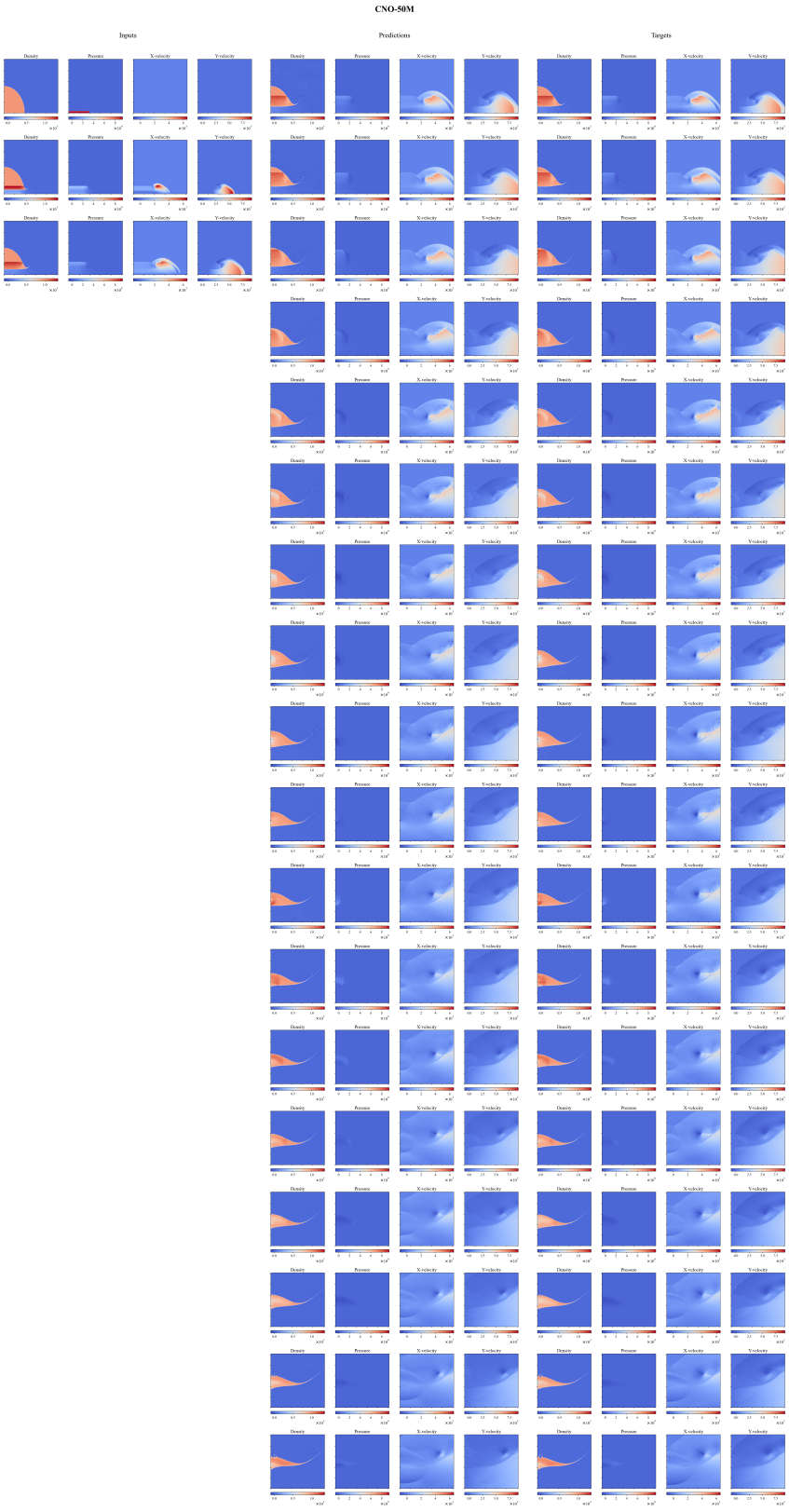

Figure 45: Rollout predictions for the LIDE-ID-Experiment PDUV_F_(3,1) with CNO-50M.

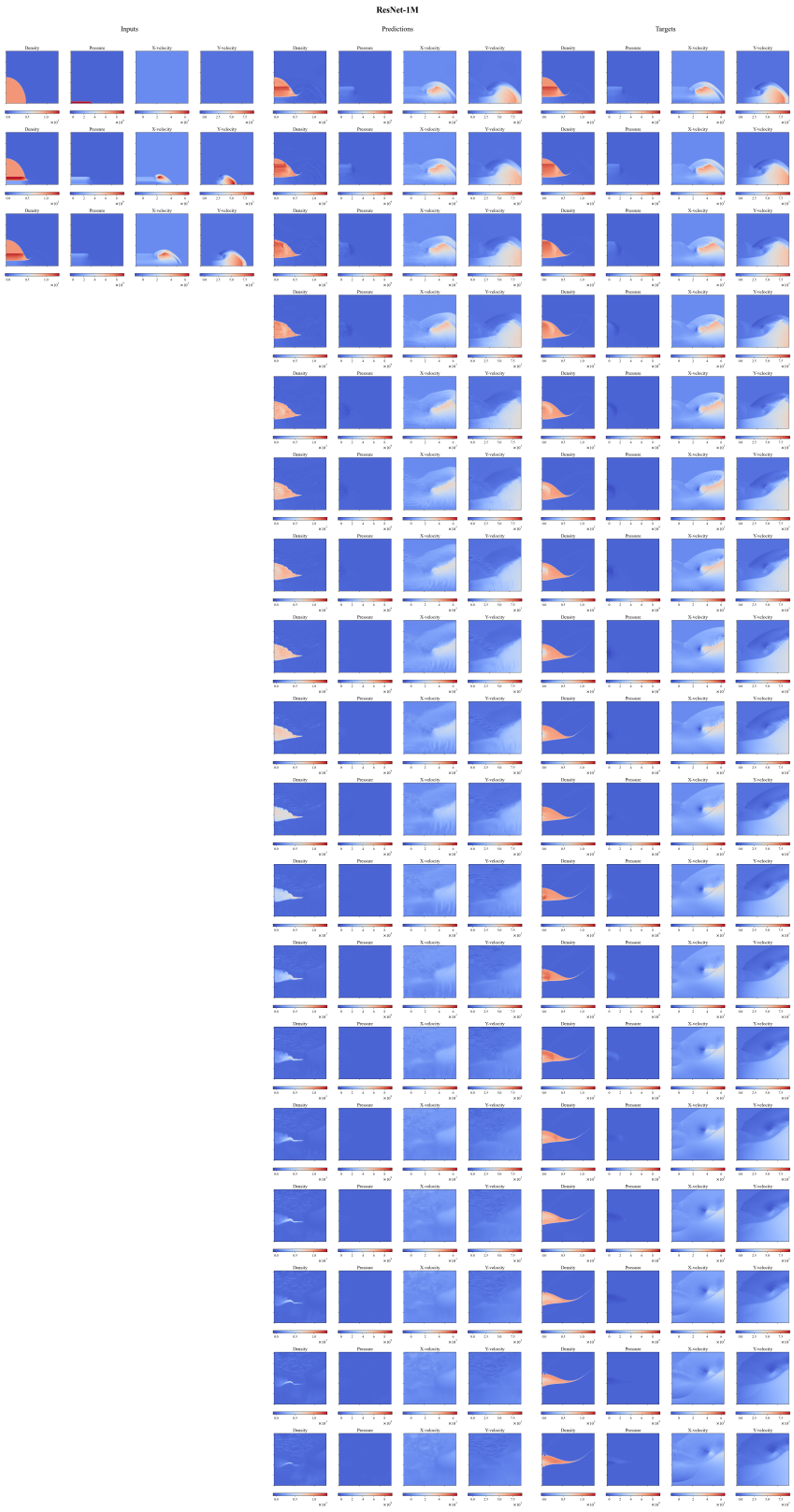

Figure 46: Rollout predictions for the LIDE-ID-Experiment PDUV_F_(3,1) with ResNet-1M.

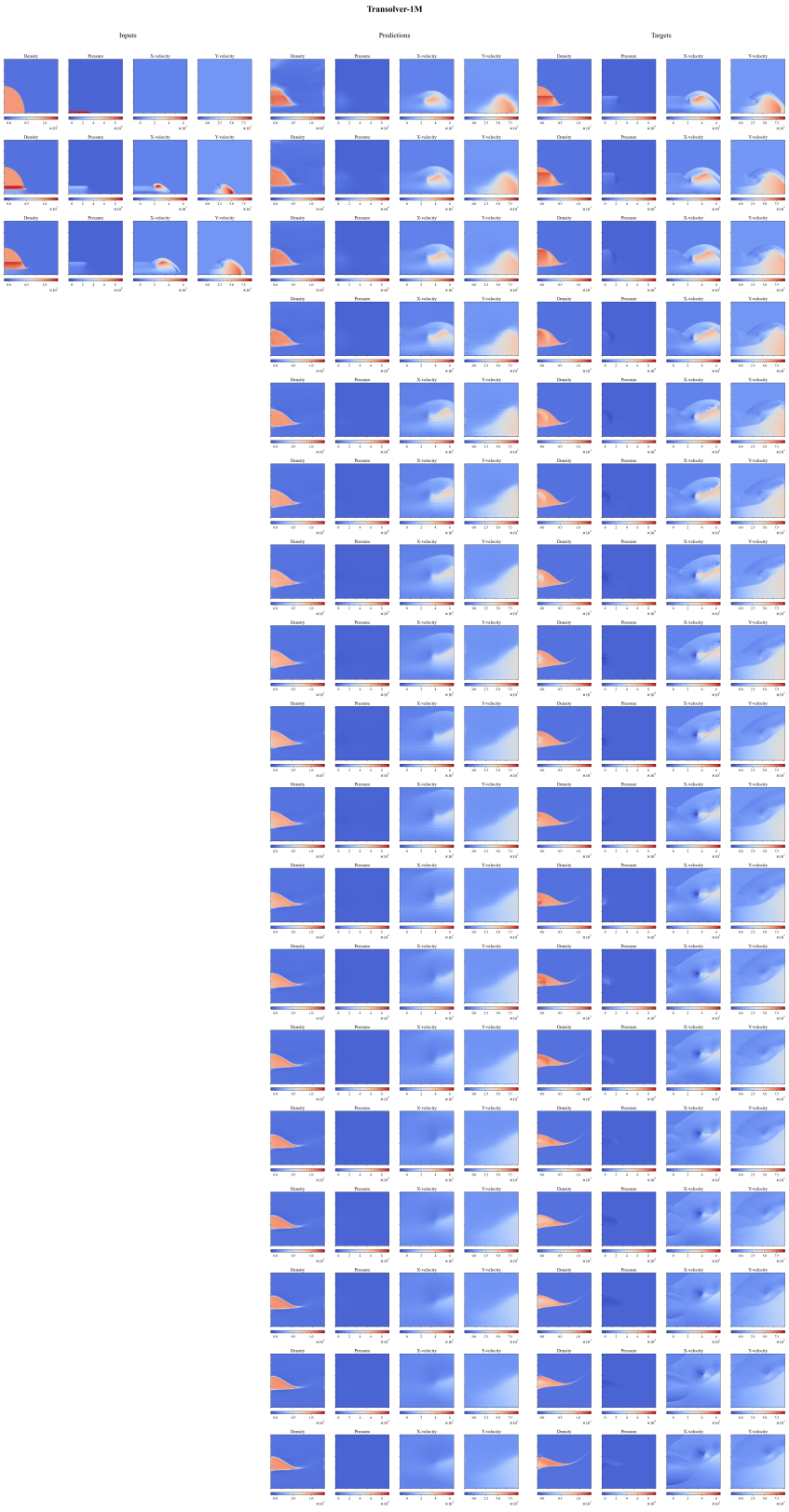

Figure 47: Rollout predictions for the LIDE-ID-Experiment PDUV_F_(3,1) with Transolver-1M.

F.2 ROLLOUT PREDICTIONS FROM INITIAL CONDITIONS FOR THE SIDA IN-DISTRIBUTION (ID) DATASET

Here, we present rollout predictions for various models—each with 50M parameters, except for ResNet, which has only 1M parameter count. The trajectory shown in the Figures 48, 49, 50, 51, 52, and 53 corresponds to the following simulation parameters: The shock Mach number 3.26, the flow Mach number 1.42, and the Weber number 13820. In all figures, the time frames are presented in order from top to bottom.

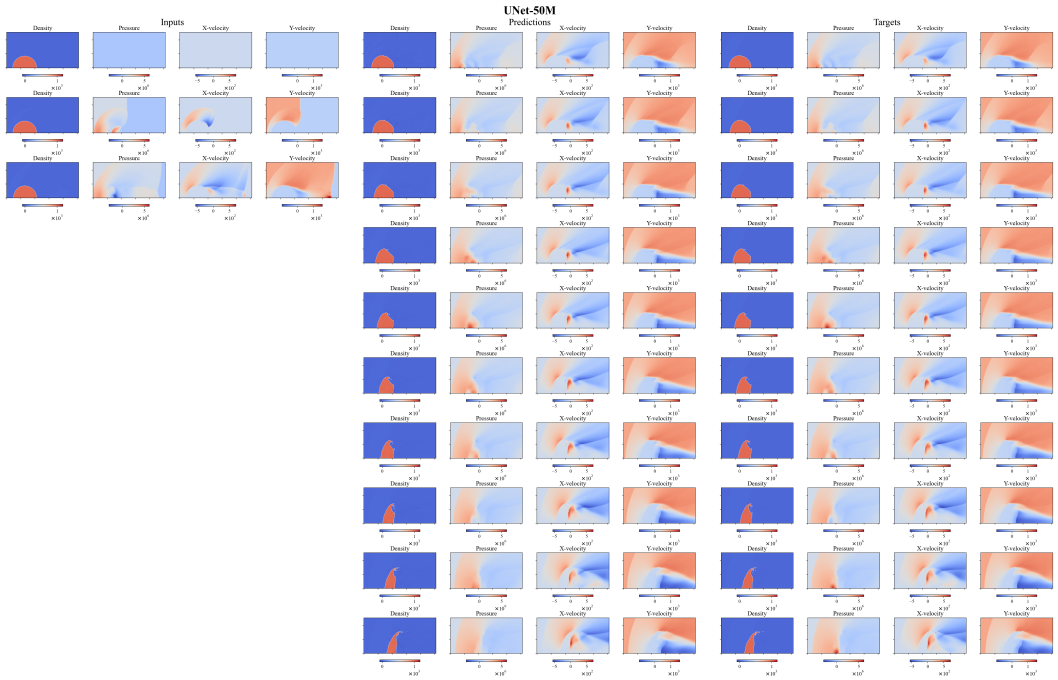

Figure 48: Rollout predictions for the SIDA-ID-Experiment PDUV_F_(3,1) with UNet-50M.

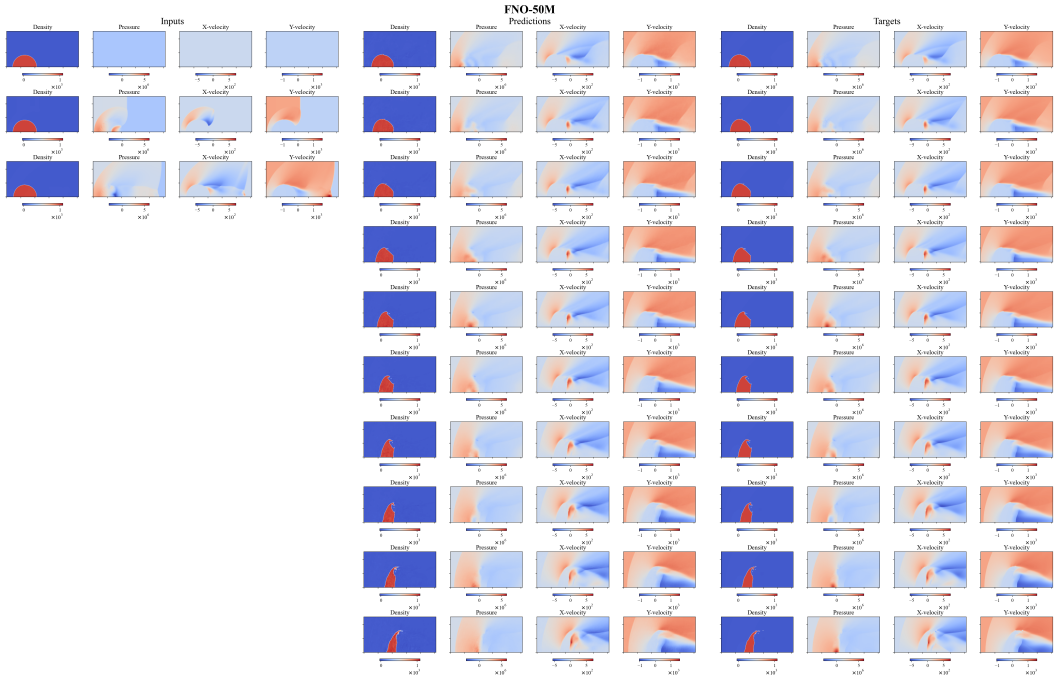

Figure 49: Rollout predictions for the SIDA-ID-Experiment PDUV_F_(3,1) with FNO-50M.

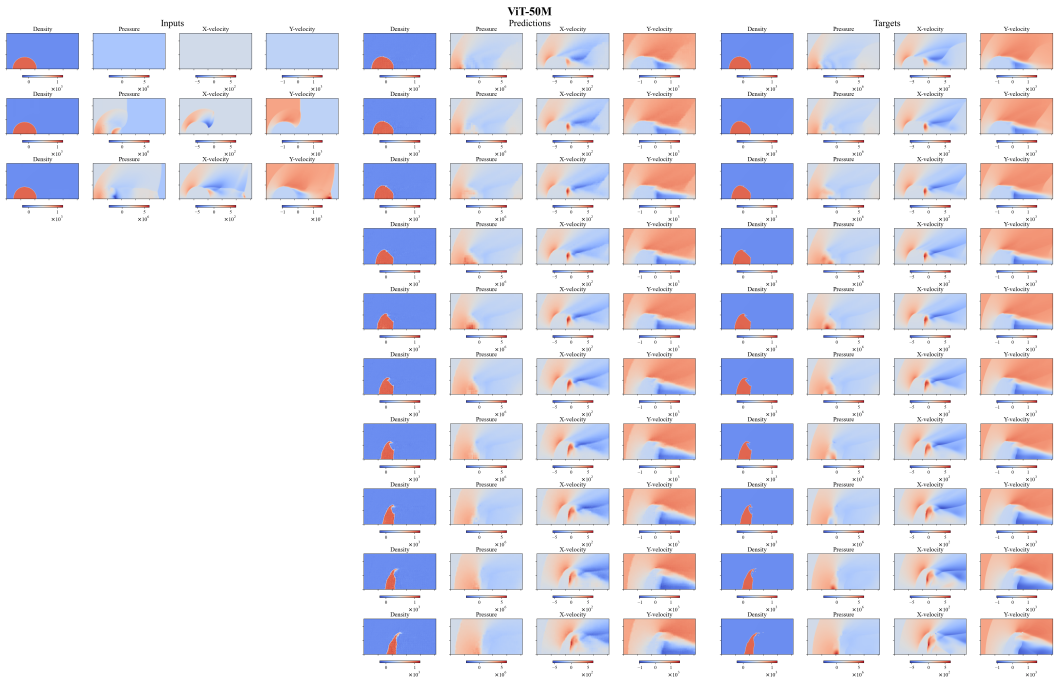

Figure 50: Rollout predictions for the SIDA-ID-Experiment PDUV_F_(3,1) with ViT-50M.

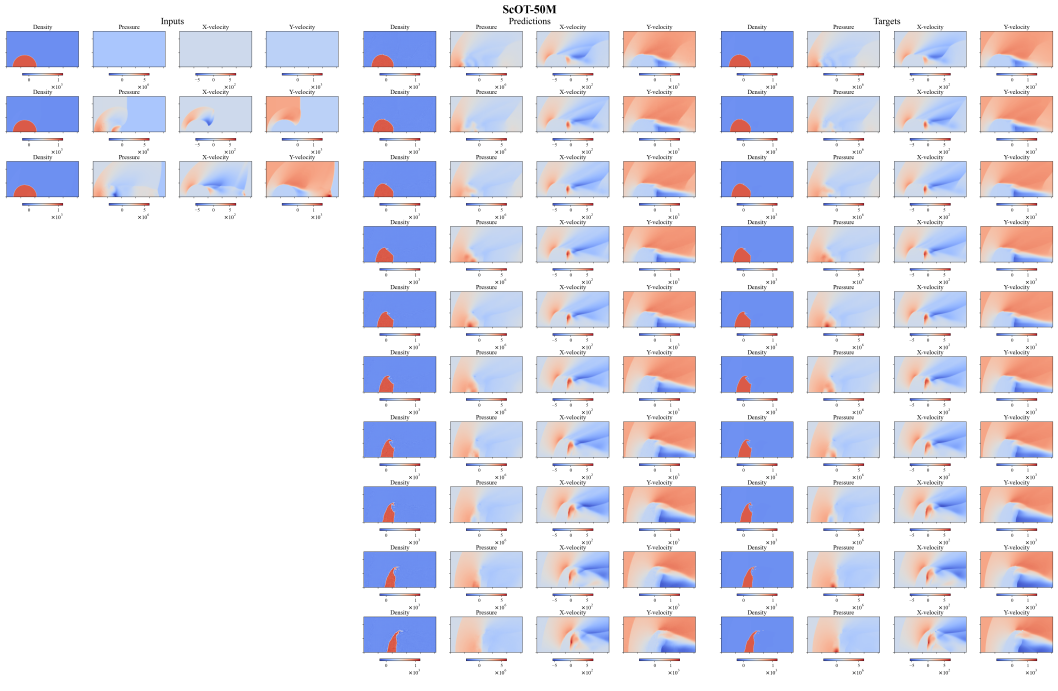

Figure 51: Rollout predictions for the SIDA-ID-Experiment PDUV_F_(3,1) with ScOT-50M.

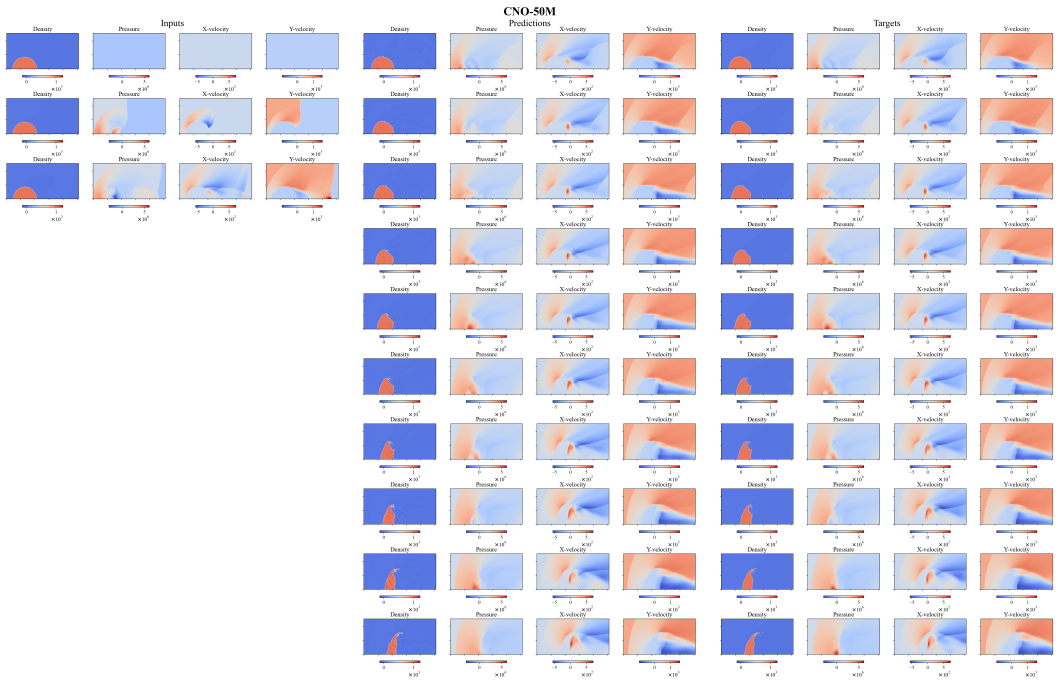

Figure 52: Rollout predictions for the SIDA-ID-Experiment PDUV_F_(3,1) with CNO-50M.

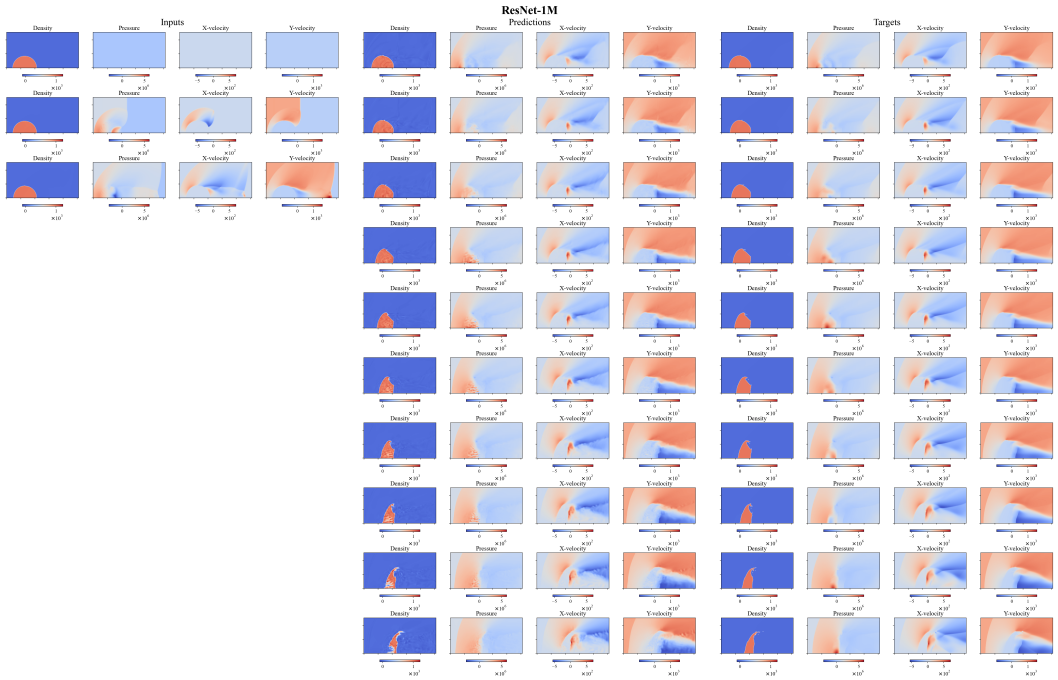

Figure 53: Rollout predictions for the SIDA-ID-Experiment PDUV_F_(3,1) with ResNet-1M.

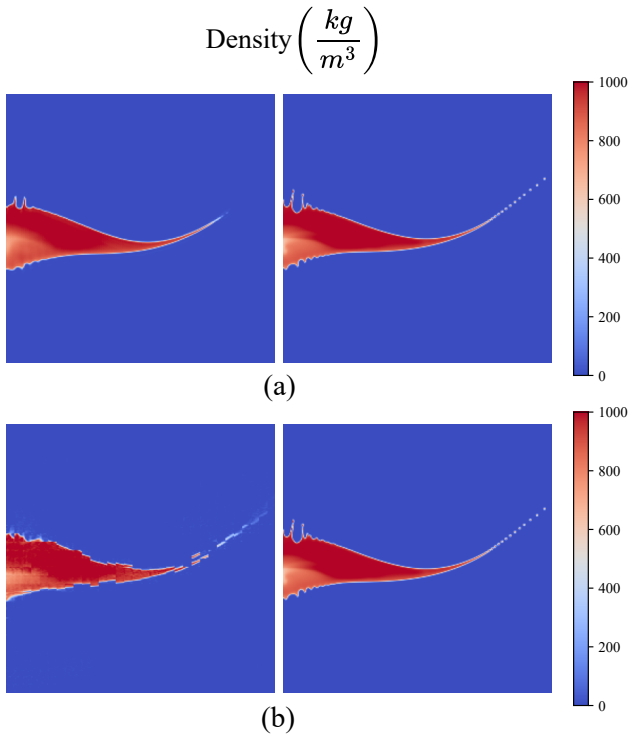

Figure 54: Comparison between UNet 50-M (a) and ViT 50-M (b) with target (for both at right) at the last rollout step for experiment PDUV_T_(3,1).

G LARGE LANGUAGE MODEL (LLM) USAGE

Large Language Models (LLMs) were utilized to polish the writing and find suitable words in some scenarios.